GROWTH OF BORON DOPED DIAMOND BY VAPOR DEPOSITION

by

DAVID J. POFERL

Submitted in partial fulfillment of the requirements

for the Degree of Doctor of Philosophy

Thesis Advisor: Dr. John C. Angus

Department of Chemistry

CASE WESTERN RESERVE UNIVERSITY

June, 1971

(157 pages)

GROWTH OF BORON DOPED DIAMOND
BY VAPOR DEPOSITION

Abstract

by

DAVID J. POFERL

The production of p-type semiconducting diamond by vapor phase deposition of a methane-diborane gas mixture at 1050° C and 0.2 Torr in the presence of natural Type 1 diamond seed crystals has been achieved.

Evidence showing boron doped diamond was grown included; chemical etching, X-ray and electron diffraction, density measurements, Seebeck and resistivity measurements, chemical analysis, optical measurements, induced electron emission spectroscopy, scanning electron microscopy, and electron spin resonance experiments. Blank runs using hydrogen-diborane mixtures showed no weight gains, doping, or evidence of the formation of boron carbide.

Cumulative weight increases during the boron doping experiments were as high as 9.86 percent after six doping runs. A distinct change in color of the diamond seed crystals from an off-white or gray before doping to light blue after doping was observed. Results of chemical

analysis indicate that the concentration of boron in the diamond sample after a 9.86 percent cumulative weight increase was between 100 and 1010 ppm depending on whether the increase in boron content during doping was considered uniformly distributed through the seed crystals or limited solely to the region of new diamond growth. The relative Seebeck coefficient for the boron doped diamond was approximately 296 $\mu V/^{o}C$ after a 4.57 percent weight gain and 120 $\mu V/^{o}C$ after a cumulative weight increase of 9.86 percent. The sign of the Seebeck voltage after doping was indicative of a p-type semiconductor. The approximate carrier concentration deduced from the Seebeck measurements is consistent with the increase in boron content determined by chemical analysis.

A striking feature of the boron doping experiments was the marked decrease in new diamond growth with each successive run on the same sample. This is suggestive that active sites such as edges and kinks are being filled.

ACKNOWLEDGEMENTS

The author wishes to express his appreciation to Dr. John C. Angus for his insight, guidance and assistance throughout the course of this study. He is also indebted to Dr. H. Will for the basic design and assembly of the initial vapor deposition test facility, to Mr. Thomas J. Dyble for his assistance in modifying the vapor deposition test facility design to provide for safe handling of diborane during boron doping experiments, to Dr. Wayne Stanko for developing the density measurement technique, and to Dr. John Helmer of Varian Associates for the induced electron emission spectroscopy measurements.

The author is also grateful to the Lewis Research Center of NASA for the continuing assistance and support provided during the course of this work. Without the extensive support provided by the Lewis Research Center, the completion of my graduate program would not have been possible.

TABLE OF CONTENTS

LIST OF FIGURES

LIST OF TABLES

CHAPTER I

INTRODUCTION AND BACKGROUND

1.1 Introduction

The purpose of this investigation was to determine if p-type semiconducting diamond can be grown by vapor phase deposition using a methane-diborane doping gas mixture in the presence of diamond seed crystals.

It has been shown previously that diamond can be grown at low pressures where it is actually metastable.[1,2,3] When diamond seed crystals were exposed to methane at 1050° C and pressures from 0.1 to 1.0 Torr, new diamond growth was obtained.[1,2] Both new diamond and graphite were produced during the vapor deposition growth process. The graphite formed during deposition was selectively removed by reaction with hydrogen at approximately 1033° C and 50 atm. Cumulative weight increases as high as 23.7 percent were obtained by H. Will[2] after nine deposition and hydrogen cleaning cycles.

Diamond is an insulator at room temperature due to the relatively large intrinsic conduction energy gap of approximately 5.6 eV between the valence and conduction bands.[4] Semiconducting diamond can be obtained by introducing appropriate impurities, e.g., boron, into the diamond lattice. The doped diamond will then exhibit

semiconducting properties similar to doped germanium or silicon. the impurity could be introduced during the epitaxial growth of diamond by vapor deposition, it should be possible to produce "controlled impurity" semiconducting diamond.

Since diamond growth by vapor phase deposition had been demonstrated, the incorporation of the desired dopant in the reacting gas mixture above the bed of diamond seed crystals at the conditions known to favor diamond growth appeared to be the most direct method of obtaining semiconducting diamond by vapor deposition. As was the case for epitaxial diamond growth,[1,2] the spontaneous heterogeneous nucleation of graphite on the diamond seed crystals from the supersaturated vapor phase will occur during boron doping experiments using methane-diborane mixtures. However, if both the carbon atoms and the boron atoms on the diamond surface have high mobilities, they may be incorporated as new diamond growth before nuclei at stable phases are formed. Eventually, all active sites on the diamond seed crystals may be exhausted and new growth may terminate.

Since the energy gap of diamond is relatively large, semiconducting diamond produced by boron doping may be used to develop high temperature devices. The applications for devices capable of high temperature operation are numerous. The incorporation of semiconducting diamond devices in spacecraft or missile electronics, for instance, could result in increased payload and reliability.

1.2 Classification of Diamonds

Diamonds are usually classified as type I or type II based on differences in their ultraviolet and infrared absorption spectra.[5] Type I diamonds exhibit an absorption edge at 3300 Å with absorption increasing rapidly at smaller wavelengths. Type I diamonds are also characterized by an absorption peak at 7.8 μ corresponding to the presence of nitrogen present as an impurity in concentrations up to 0.23 percent.[6] Type II diamonds exhibit a sharp absorption edge at 2200 Å and do not show the nitrogen absorption peak at 7.8 μ. Type II diamonds are classified further as type IIa and IIb.[7] The type IIa diamonds are non-conducting, whereas the type IIb diamonds show conductivity and phosphorescence effects not found in type IIa diamonds. It is the type IIb diamonds that are of primary interest with regard to this investigation, especially those that have been produced by boron doping.

Synthesis and Properties of Type IIb Diamond

Naturally occurring semiconducting diamonds, type IIb, were first described by Custers.[7] They are p-type semiconductors with conduction activation energies from 0.29 to 0.38 eV, carrier concentrations of approximately $2X10^{13}/cm^3$, and carrier mobilities from 1000 to 1600 $cm^2V^{-1}sec^{-1}$.[8,9,10] In contrast to non-conducting diamonds having resistivities of approximately 10^{11} to 10^{14} ohm-cm, type IIb diamonds exhibit resistivities from 25 to 10^{10} ohm-cm. The existence of natural type IIb diamonds generated a considerable amount of interest in

artificial production of semiconducting diamond. Several methods[11-15] have been used previously to produce man-made semiconducting diamonds including: the introduction of the desired dopant during the growth of diamond at high pressure and high temperature; diffusion of the dopant into an existing, non-conductive diamond crystal; and ion bombardment.

Measurements made by E. Lightowlers and A. Collins[16] on aluminum doped and boron doped synthetic semiconducting diamonds initially indicated that aluminum was the acceptor center responsible for the semiconducting properties in both aluminum and boron doped diamonds. However, a subsequent investigation by A. Collins and A. Williams[17] has shown that the acceptor in the semiconducting diamonds investigated is not aluminum since the aluminum concentrations were shown to be much less than the concentration of acceptor centers. It was therefore concluded that boron was the acceptor center responsible for the semiconducting properties of all natural and synthetic diamond available at the present time. Presumably, the boron is incorporated substitutionally into the diamond lattice and since it has only three valence electrons, it results in a hole (acceptor site). Aluminum is currently thought to be a "getter" for nitrogen in synthetic semiconducting diamonds and once the nitrogen is removed traces of acceptor impurity will result in semiconducting diamond. The aluminum does not appear to be electrically or optically active and is probably present as inclusions or in interstitial lattice positions.

In view of the recent study by A. Collins and A. Williams,[17] the reported production of semiconducting diamonds with active aluminum acceptor centers by the methods described below appears questionable.

A. Growth Method[11,12]

This method of incorporating a dopant material into the diamond lattice is somewhat similar to the doping procedures used in the preparation of conventional silicon or germanium semiconductors with the primary difference being that diamond is grown from a molten transition metal catalyst system. The production of semiconducting diamond by the growth method is accomplished by incorporating the desired impurity in the graphite and catalyst mixture. The graphite charge is then heated to temperatures from 1400° to 1600° C at approximately 57,000 atm. The temperature and pressure used are varied slightly to account for the particular composition of the catalyst system.

In 1962, Wentorf and Bovenkerk[11] reported the growth of p-type semiconducting diamonds at high temperatures and pressures. Small quantities of the aluminum, beryllium, or boron impurity were incorporated in a mixture of graphite and a suitable catalyst and them exposed to diamond forming temperatures and pressures. The resulting diamond crystals were found to have low resistivities and the crystals were verified as p-type by thermoelectric power measurements. Electrical resistivity for boron doped diamond was inversely related to the concentration of boron with resistivities varying from 10^2 to 10^5 ohm-cm. The color of the boron doped diamonds was also a function

of the boron concentration. Those diamonds containing 0.1 percent boron were deep blue, while lower boron concentrations resulted in less intense color or even colorless diamonds. Diamonds grown incorporating aluminum or beryllium as the impurity in the graphite charge resulted in colorless or pale yellow-green crystals. Conduction activation energy for boron doped diamond crystals was 0.17 to 0.18 eV. The aluminum doped diamond showed an activation energy of 0.32 eV while the activation energy of beryllium doped diamonds ranged between 0.2 and 0.35 eV. Hall effect, carrier mobilities, and absorption spectra were not determined due to the small crystal size and electrical contact problems.

Huggins and Cannon[12] also report the introduction of boron and aluminum impurities into diamond during the growth process by incorporating the dopant in the graphite/transition metal catalyst reaction mixture. The diamonds grown during the high temperature and high pressure process were recovered by acid etching. The boron and aluminum doped diamonds were electrical conductors with resistivities from 50 to $5X10^9$ ohm-cm. Electron spin resonance measurements made on the boron doped diamonds resulted in spectra for which no explanation could be given. It was postulated that an electronic interaction between boron and nickel from the catalyst mixture resulted in a complex system which influenced the electron spin resonance spectra obtained.

B. Diffusion Method[11,12]

The diffusion method of producing p-type semiconducting diamond crystals is similar to the incorporation of impurities in the silicon or germanium lattice by diffusion. In this process, the required impurity is placed in contact with diamonds and the mixture is then subjected to high temperature and pressure.

Wentorf and Bovenkerk[11] determined that semiconducting diamonds could be produced by exposing diamond to boron carbide for ten minutes at a pressure of 60,000 atm and temperatures from 1300° to 2000° C. Resistivity of doped diamonds produced in this manner was reduced by six orders of magnitude. The doped diamonds were p-type semiconductors with resistivities of approximately 10^4 ohm-cm and conduction activation energies from 0.02 to 0.05 eV. Diamonds that were initially colorless before boron diffusion doping appeared gray or bluish-gray after treatment. Huggins and Cannon[12] prepared both boron and aluminum doped diamonds by the diffusion process. Boron and aluminum concentrations in the doped diamond were as high as 10^{21} atoms/cm^3. The doping achieved in this process is limited to a thin external layer. The electron spin resonance curve for the boron doped diamond showed no unpaired spins resulting from the diffusion process.

C. Ion Bombardment[13,14,15]

The success in forming n- and p-type semiconductors by ion implantation of phosphorous, arsenic, boron, and gallium in silicon

indicates that the ion implantation process might be also applied successfully to diamond. In this process the crystal to be doped is usually subjected to bombardment by a high energy stream of impurity ions.

Wentorf and Darrow[13] produced semiconducting surface layers on synthetic diamond crystals by ionic bombardment in an ionized gas flow discharge stream between electrodes maintained at a potential difference of 1500 to 2800 V. The type of ionized gas environment, rather than the electrode metal, appears to determine whether n- or p-type diamond layers are formed. Nitrogen or argon environment resulted in n-type semiconducting layers, while those exposed to a hydrogen environment during ion bombardment produced p-type layers. The average resistances of the diamond crystals decreased from approximately 10^{11} ohms before bombardment to about 10^{5} to 10^{10} ohms after treatment. In all cases the color of surface layer after bombardment was gray-brown. In most cases the thermoelectric power of the diamonds after ion bombardment was approximately 10 $\mu V/^{o}C$ except for helium or oxygen which resulted in thermoelectric power too small for sign determination. Electron diffraction patterns indicate that the affected surface layers are somewhat amorphous and these surface layers are partly destroyed by heat treatment for about one hour at 300^{o} to 400^{o} C in air.

Vavilov[14] et al doped natural diamonds with boron and lithium using the ion bombardment technique. The lithium doped diamond exhibited n-type conductivity, while diamond doped with boron resulted

in p-type conductivity. Activation energies varied from 0.25 eV for the boron doped diamond to 0.29 eV for lithium doped diamond. Electrical resistivities were reduced from 10^{12} to 10^{15} ohm-cm before ion bombardment to $5X10^{4}$ ohm-cm after doping.

Ion implantation of phosphorous and boron in non-conducting diamond macles has been recently described by Carlson.[15] The implantation ions were produced by r-f discharge in phosphine or boron triflouride. Annealing of the samples after ion bombardment had essentially no affect on the electrical properties of the diamonds. Activation energies of 0.17 to 0.34 eV were determined from the slope of the resistance versus reciprocal temperature curves. However, it was not possible to determine carrier mobilities since the Hall voltages were too small to be measured (less than 10 μV) on any of the implanted macles. Mobilities were estimated at less than 10 $cm^{2}V^{-1}sec^{-1}$ in contrast to normal values of approximately 1500 $cm^{2}V^{-1}sec^{-1}$ for natural type IIb semiconducting diamonds. The thermoelectric power measurements indicated that an n-type diamond surface layer having a Seebeck coefficient of about 10 $\mu V/^{o}C$ was produced by ion bombardment experiments using phosphorous, while no thermoelectric power could be detected from the boron implantation studies.

CHAPTER II

CHEMICAL EQUILIBRIUM CALCULATIONS

2.1 Chemical Equilibrium Computer Program

Chemical equilibrium compositions for the C-H-B system were calculated in order to determine the conditions of temperature, pressure, and initial reaction mixture composition that would favor boron doping during epitaxial diamond growth. Equilibrium compositions were determined by minimizing the total Gibbs free energy of the reacting systems. The computer program[18-21] used for these calculations was obtained from NASA and is described in Appendix A. Equilibrium calculations were made over a wide range of pressure and temperatures for several initial concentrations of B_2H_6 in CH_4. These data are presented in Tables A-2 through A-14 of Appendix A.

2.2 Analysis of Equilibrium Data

An analysis of the equilibrium compositions in Tables A-2 through A-14 indicated that except at high temperatures and very low initial concentrations of B_2H_6 in CH_4, both boron and diamond solid phases were always present. Graphite was excluded from the set of allowed

species. It was decided to make the initial doping runs under conditions of temperature and pressure that were known to produce epitaxial diamond growth. In this manner it would be theoretically possible to introduce boron into the diamond lattice during epitaxial growth of the diamond seed crystals rather than relying solely on the deposition of boron or a boron species on the diamond surface followed by diffusion of the surface boron into the diamond lattice. By attempting to dope the diamond seed crystals with boron concurrent with epitaxial diamond growth, it was postulated that the new diamond growth could possibly be uniformly doped.

As can be seen from the data in Appendix A, the initial concentration of B_2H_6 in CH_4 was not critical since two solid phases were present at equilibrium in most cases. The gas used in the boron doping experiments contained 0.83 percent B_2H_6 by volume in CH_4. Although the experimental doping apparatus was designed such that the dopant gas could be diluted with other gases, it was decided to make initial doping runs with the undiluted B_2H_6-CH_4 mixture. The gas phase composition for the initial doping runs is given in Table A-4. Although the concentration of B_2H_6 in CH_4 in the dopant gas mixture is considerably higher than the B_2H_6 concentration to which the data in Table A-4 correspond, the gas phase composition still applies since two solid phases will also be present at the higher B_2H_6 concentration. As discussed in Appendix A, the system has, therefore, only two degrees of freedom and for a given temperature and pressure the equilibrium gas phase composition is fixed.

CHAPTER III

PREPARATION OF DIAMOND FOR DOPING

3.1 Acid Cleaning

The first step in preparing the diamond sample for boron doping was to clean the diamond in aqua regia at 90° C for one hour, after which the acid was decanted and discarded. Aqua regia was again added to the diamond and the sample remained in the acid for an additional 24 hours at room temperature. The aqua regia was again decanted and a mixture of 50 percent HNO_3 and 50 percent HF was added to the sample. The diamond remained in the HNO_3/HF mixture for 24 hours at room temperature. The acid was then discarded and replaced with aqua regia. After an additional 24 hours, the aqua regia was decanted and the diamond was rinsed three times with distilled water. The sample was centrifuged between rinsings to insure removal of most of the distilled water. Three acetone rinses followed in order to facilitate drying of the sample. This cleaning procedure was used to remove metallic and oxide impurities present in the original diamond sample as provided by the diamond vendor.

3.2 Hydrogen Cleaning

The acid cleaning described above was followed by hydrogen cleaning. Although the hydrogen cleaning was performed on all diamond samples prior to doping runs, its primary use was to remove graphite deposited on the diamond during each doping run. In order to clean the diamond, the sample was exposed to hydrogen at 52 atmospheres and 1040° C for 7 hours.

The reaction rates of diamond and graphite with hydrogen have been determined by W. Stanko.[22,23] The following equations define these rates:

$$Rg = \frac{7.31X10^{12}}{T} \exp\ [-85,000/RT]P \qquad (3.1)$$

$$Rd = 1.26X10^{9}\ \exp[-115,800/RT]P^{2.343} \qquad (3.2)$$

where:

Rg = reaction rate of graphite with hydrogen, g moles/g minute

Rd = reaction rate of diamond with hydrogen, g moles/g minute

R = universal gas constant, cal/g mole, °K

T = temperature, °K

P = pressure, atm

At the conditions used for hydrogen cleaning the diamond, the reaction rate of hydrogen with diamond is approximately three orders of magnitude less than the reaction rate of hydrogen with graphite. It is this large difference in reaction rates that permits selective removal of graphite from diamond with very small loss of the diamond sample.

The combinations of temperature, pressure, and reaction time which result in removal of 99.99 percent of the graphite present on the diamond are given in Figure 3.1. From this figure, it can be seen that under the conditions used for hydrogen cleaning the diamond samples for the doping runs; i.e., 52 atmospheres and 1040° C approximately six hours are required for 99.99 percent graphite removal. During the time required for removing this graphite from the diamond sample, approximately 0.3 percent of the diamond is lost.

A schematic of the apparatus used for hydrogen cleaning is shown in Figure 3.2. This is basically the same apparatus as was used by H. Will[2] and W. Stanko.[22,23] The detailed H_2 cleaning procedure is given in Appendix B. The procedure consisted basically of placing the sample to be cleaned inside the Hastelloy-X tube portion of the resistance furnace, evacuating the system to 10 microns, pressurizing the system with hydrogen to 750 psig and maintaining the furnace at 1040° C for 7 hours while supplying a hydrogen flow of approximately 6 cm^3 per minute during the cleaning period. The Hastelloy-X tube was designed to operate at pressures up to 100 atm and temperatures as high as 1100° C. Although it was operated at less severe conditions during these hydrogen cleanings, the oxidation problem at these temperatures reduced the wall thickness to such an extent that the tube had to be replaced during the course of this study. The details of the Hastelloy-X

tube reaction chamber, as installed in the resistance furnace, are shown in Figure 33. The tube was a three-foot section of two-inch diameter Hastelloy-X rod in which a 11/16-inch hole had been bored axially. The sample test tube was placed in the middle of the central cavity in the tube. High pressure stainless steel hose connections were made at each end of the tube, and a thermocouple fitting was provided at the downstream end of the tube. The thermocouple was positioned such that it was approximately one centimeter downstream of the sample.

3.3 Weighing

After acid and hydrogen cleaning, the diamond sample was weighed. Since moisture is adsorbed readily on the diamond powder and since the surface area of the powder was large, approximately 12 square meters per gram, it was necessary to weigh the sample in a controlled atmosphere. The sample to be weighed was placed in a sample chamber and then placed in a weighing test tube. The sample chamber and weighing test tube are shown in Figure 3.4. The sample chamber and weighing test tube are then evacuated and refilled with dry air that has been passed through a bed of $CaCl_2$. The stopper is then placed on the weighing test tube and all weighings are made with the sample chamber inside the stoppered weighing test tube. The weighing is then done on an analytical balance which could be read to the nearest 0.1 mg. The interior of the balance contained

$CaCl_2$ in order to maintain a dry air atmosphere. Readings were taken every ten minutes until two consecutive readings were equal within 0.1 mg.

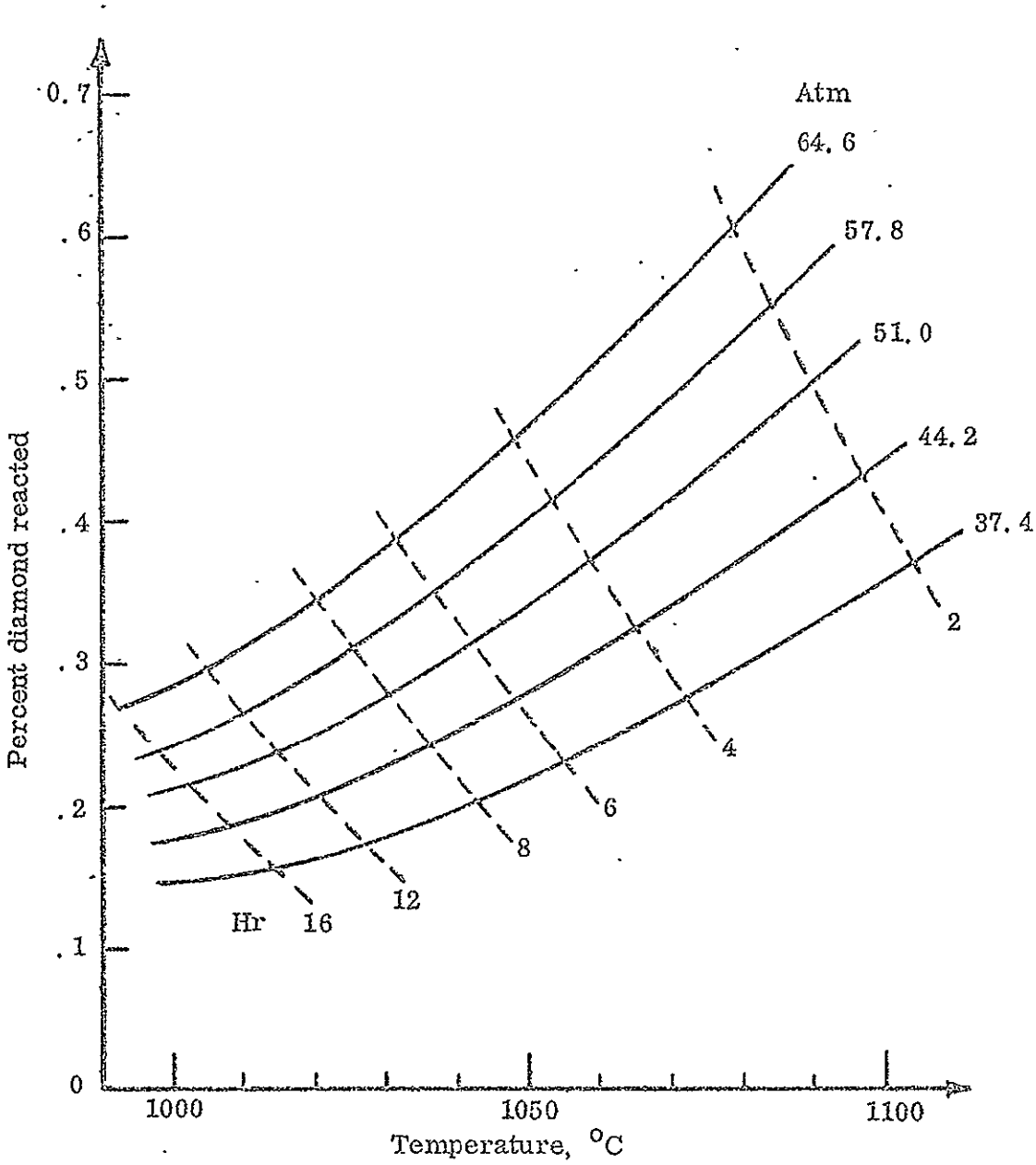

Figure 3.1. Percent diamond removed during 99.99 percent removal of graphite.

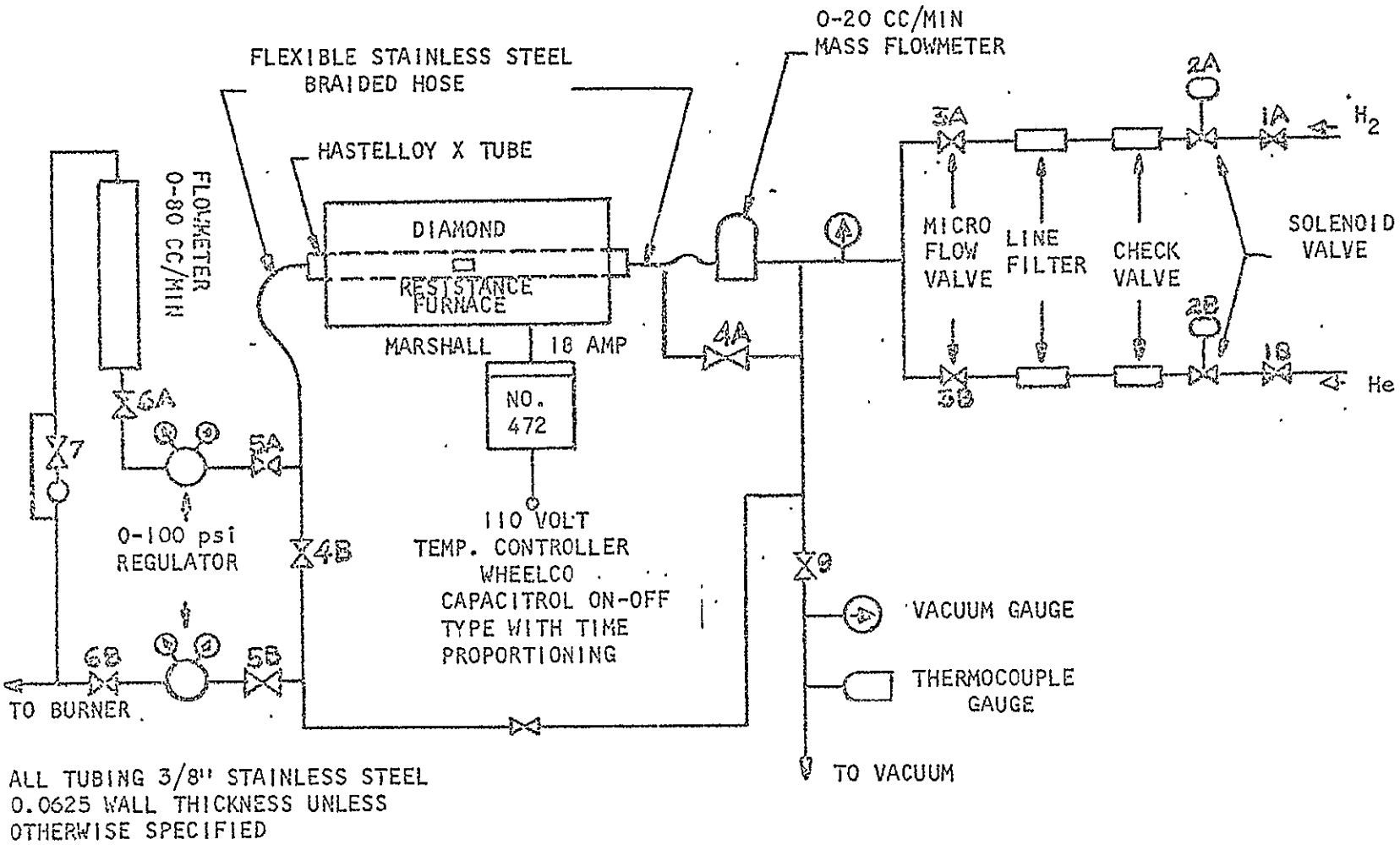

Figure 3. 2. Flow diagram of apparatus for cleaning diamonds with high pressure hydrogen.

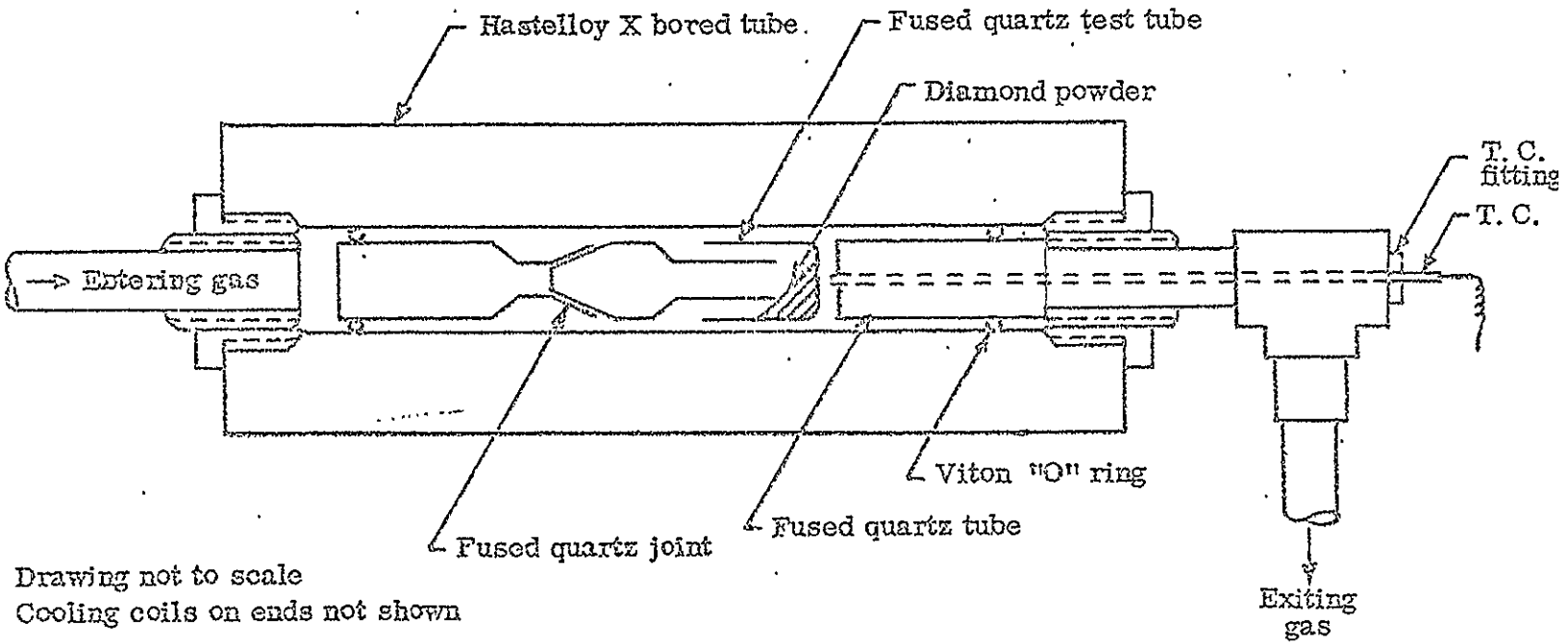

Figure 3. 3. Detail of furnace for cleaning diamonds with high pressure hydrogen.

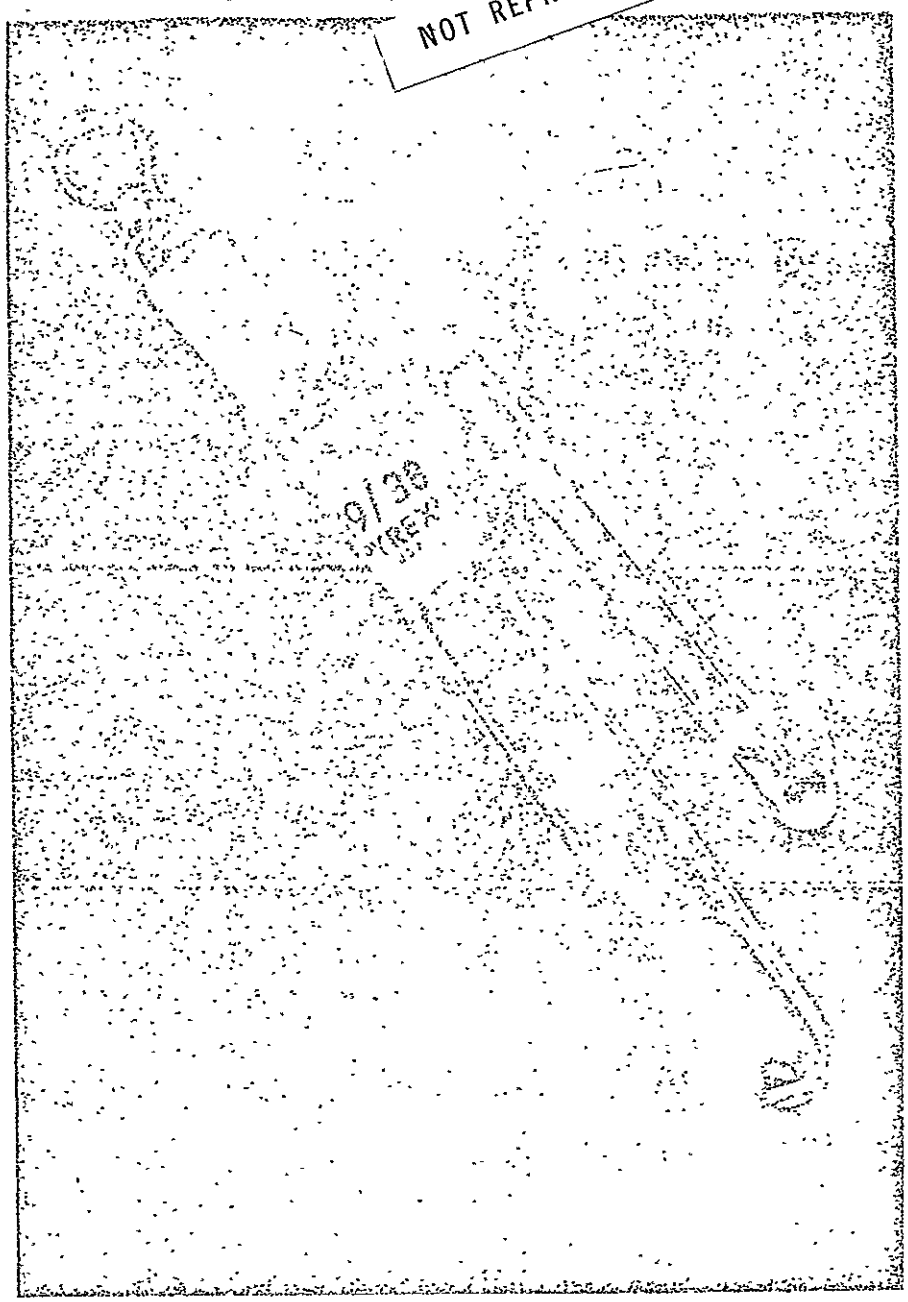

Figure 3.4. Photograph of sample chamber and stoppered test tube.

CHAPTER IV

DIAMOND DOPING SYSTEM AND PROCEDURE

4.1 The Doping Gas Mixture

A mixture of diborane in methane was used as the doping gas. The diborane/methane mixture was obtained from the Matheson Company and the chemical analysis of the mixture is given in Table 4.1. The diborane content was 0.83 volume percent. The primary impurities were ethane, carbon dioxide, propylene, hydrogen, nitrogen, and pentane with contents of 0.62, 0.12, 0.05, 0.03, 0.02, and 0.02 percent, respectively. The balance of the mixture was methane.

4.2 The Doping System

The system used for diamond doping is basically the same as that used by H. Will[2] for diamond deposition experiments. The major differences arise due to the problems associated with handling diborane. A schematic representation of the system is shown in Figure 4.1. A photograph of the deposition furnace is shown in Figure 4.2. Since this system was originally designed for epitaxial growth of diamond and the pressure required to optimize the growth process with various reacting gas systems had not been established, most of the apparatus was constructed of stainless steel to allow operation at pressures

less than or greater than atmospheric. The high temperature portions of the doping system were quartz.

Due to the toxicity of diborane, the entire doping apparatus was contained either in a hood or inside a plexiglass extension to the hood. The flow metering system, vacuum system, and deposition furnace were isolated from the main area of the laboratory by the plexiglass enclosure. Thus, diborane from any leaks or accidental breakage of the glass section of the doping apparatus would be safely vented to the hood exhaust system.

The diborane/methane mixture flowed from a compressed gas bottle through either a rotameter or mass flow meter and then through a flow orifice. A manostat maintained a constant pressure across the orifice and thus provided a constant flow to the gas mixing column. At this point the diborane/methane could be mixed with another gas such as hydrogen. However, the best diamond growth rates achieved by H. Will[1] were obtained with pure methane and it was found that dilution of the methane by hydrogen either decreased the growth rate, stopped it completely, or in many cases actually caused a weight loss of the diamond during the deposition process. Since the diborane dopant gas was premixed with methane, it was not necessary to use two separate feed systems for the diamond doping runs. After passing through the gas mixing column and a rotameter in the low pressure portion of the system, the diborane/methane mixture flowed into the quartz vacuum chamber. The details of the vacuum chamber are shown in Figure 4.3. The gas

flowed over the diamond powder in the sample chamber and exited through the mouth of the quartz test tube as shown in Figure 4.4. The gas was then exhausted through an oil diffusion pump. Before the gas was released to the hood exhaust system, it passed through a water scrubber to remove any unreacted diborane by converting it to boric acid.

The system pressure was set by adjusting needle valve 15. The pressure upstream or downstream of the quartz vacuum chamber was measured by a magnevac gage. The diamond was maintained at the required doping temperature with an electrical resistance furnace. A photograph of the furnace and the quartz vacuum chamber is shown in Figure 4.2. A reasonably flat furnace profile was obtained by adjusting the resistance across electrical shunt taps along the furnace length. The profile achieved is shown in Figure 4.5. Approximately fourteen inches in the center of the furnace was maintained at the required deposition temperature. The temperature of the diamond crystals was controlled with a Barber Coleman proportional band controller which maintained the temperature within $\pm 0.2^{\circ}$ C of the set point.

4.3 Doping Procedure

The doping procedure is similar to the diamond growth procedure used by H. Will[2] with some alterations required due to the handling of a highly toxic gas. The doping procedure is summarized below:

> Clean all quartz portions of the system in a sodium dichromate/sulfuric acid glass cleaning solution.

2. Clean and weigh the diamond sample as described in Chapter III, Preparation of Diamond for Doping.

3. With bypass valves 12 and 13 open, install the sample chamber in the quartz vacuum chamber.

4. Connect the sample chamber and vacuum chamber to the flow system, slowly evacuate the system through valve 15 with the mechanical pump and then close valve 15.

5. Open valve 14 and evacuate the flow system back to valve 10.

6. Close valve 14 and open and then close valve 10 after filling the gas mixing column with the diborane/methane mixture.

7. Repeat steps 5 and 6 twice in order to eliminate all air from the flow system between valves 5, 10, 11, and 14. (The portion of the flow system from valve 10 back to the diborane/methane tank is maintained at 10 psig with the diborane/methane gas mixture.)

8. Open valve 15 and complete the final evacuation of the quartz vacuum chamber with the oil diffusion pump.

9. Open valve 10 and adjust needle valve 11 to obtain the desired flow of diborane/methane gas over the diamond sample. (It is extremely important to assure that bypass valves 12 and 13 are open to preclude loss of diamond sample by entrainment in the diborane/methane flow.)

10. Slide the furnace which should already be at 1050° C over the quartz vacuum chamber such that the diamond sample is positioned approximately 15 inches from the inlet end of the furnace and install the thermocouple in the thermocouple wall of the vacuum chamber.

11. Close downstream bypass valve 13 in order to measure the pressure just upstream of the sample chamber during the run.

12. Adjust valve 15 to set the required pressure for the doping run at approximately 0.2 mm Hg.

13. When the desired doping time, approximately 20 hours, has elapsed, shut valves 10 and 11, open valves 13 and 15, and slide the furnace off the sample.

14. Close valve 15 when the system has been evacuated, and turn off the oil diffusion pump.

15. Open valve 14 and evacuate the system back to valves 5 and 10 with the mechanical vacuum pump.

16. Turn off the mechanical pump and open valve 16 to allow air to fill the system and then close valve 16.

17. Turn on the mechanical vacuum pump and repeat steps 15 and 16 twice thereby reducing the concentration of diborane in this section of the flow system to a safe level and then open valve 16.

18. Crack valve 11 to slowly fill the quartz vacuum chamber with air and then close valves 11 and 14.

19. Crack valve 15 and after slowly evacuating the quartz vacuum chamber close valve 15.

20. Repeat steps 18 and 19 twice to reduce the diborane concentration in the quartz vacuum chamber to a safe level.

21. Remove the diamond sample from the vacuum chamber and hydrogen clean and weigh the sample as described in Preparation of Diamond for Doping.

22. Repeat steps 3 to 21 until the desired diamond weight gain is obtained.

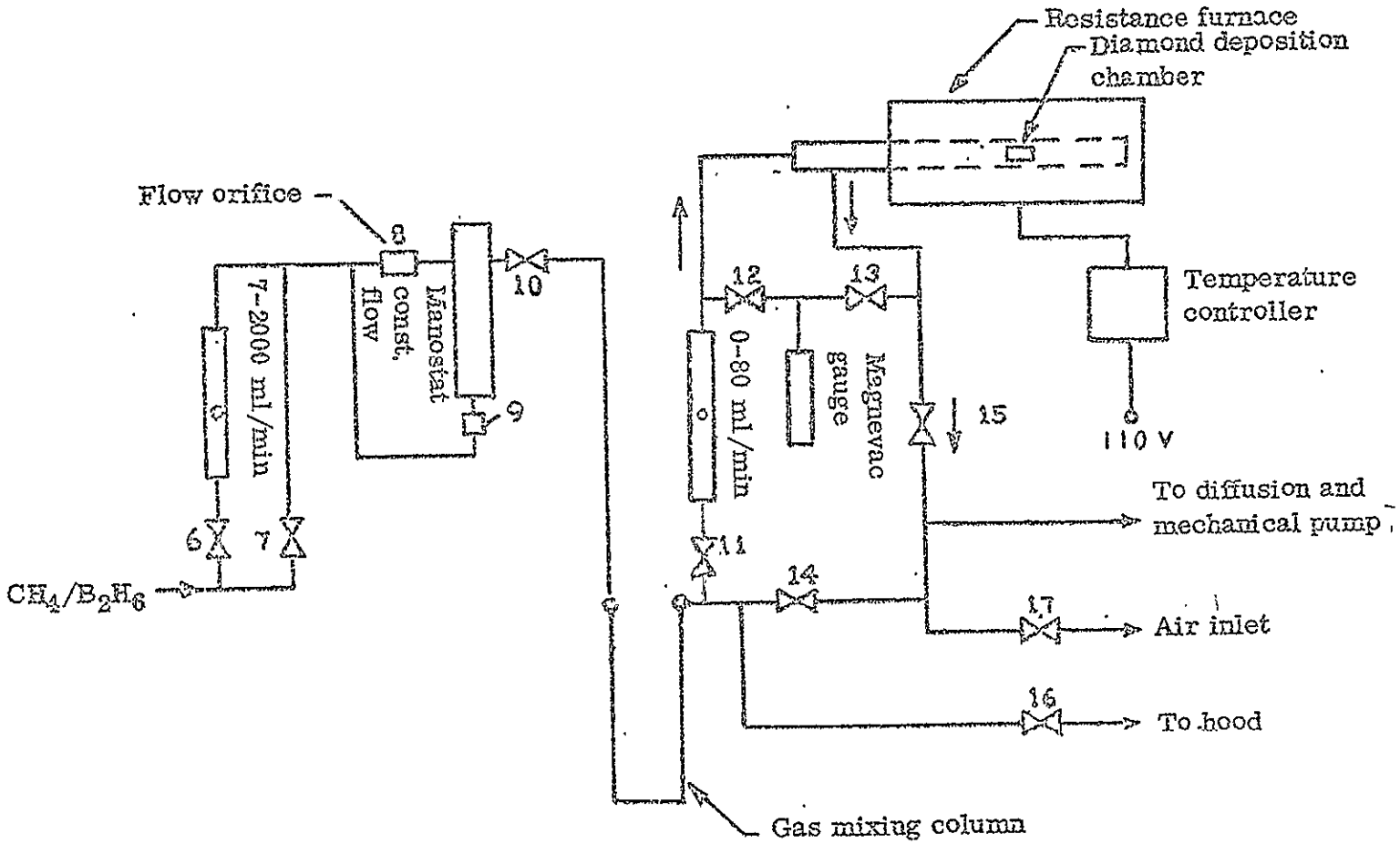

Figure 4.1. Flow system for boron doping of diamond.

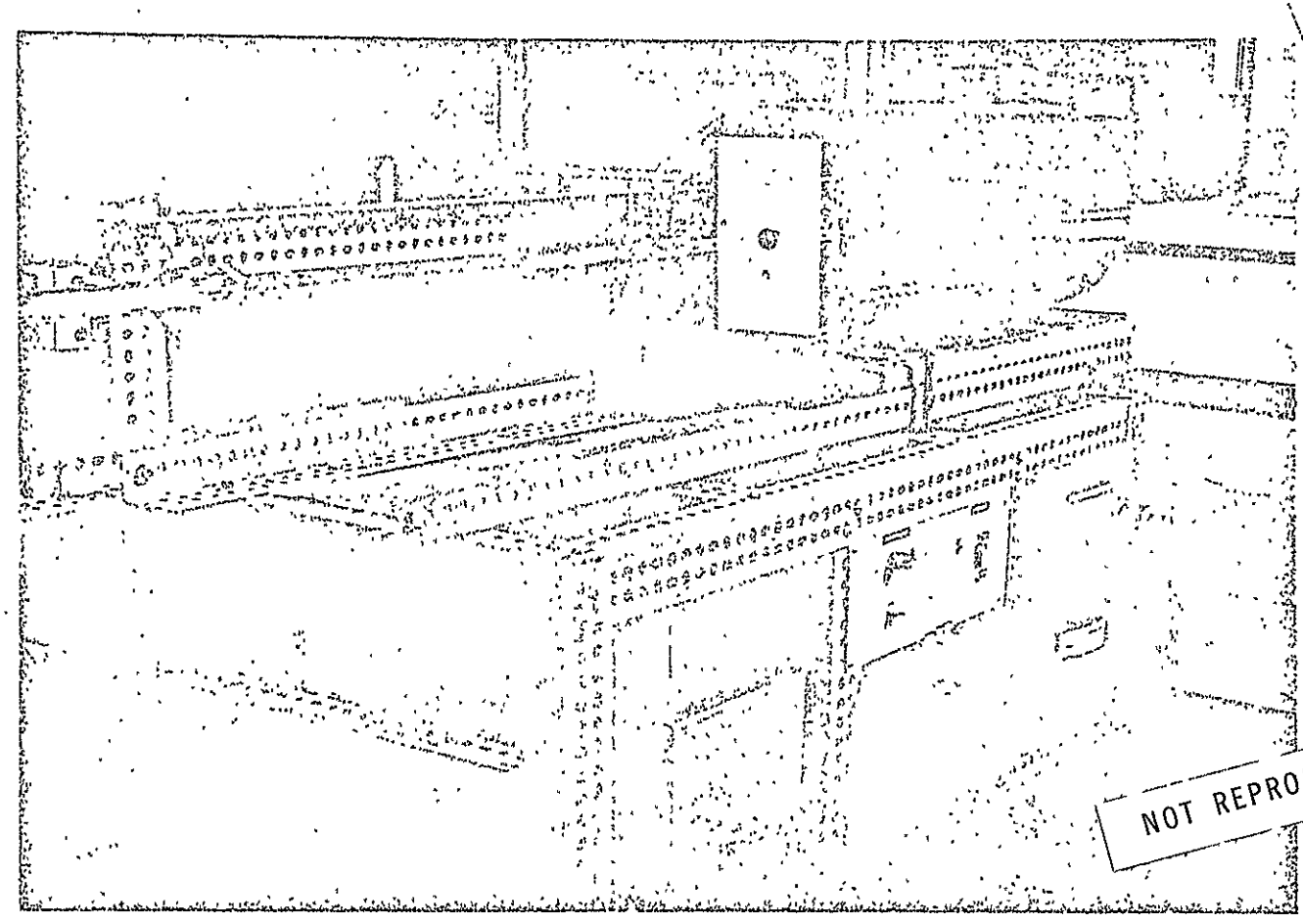

Figure 4. 2. The Quartz vacuum chamber, furnace and controller.

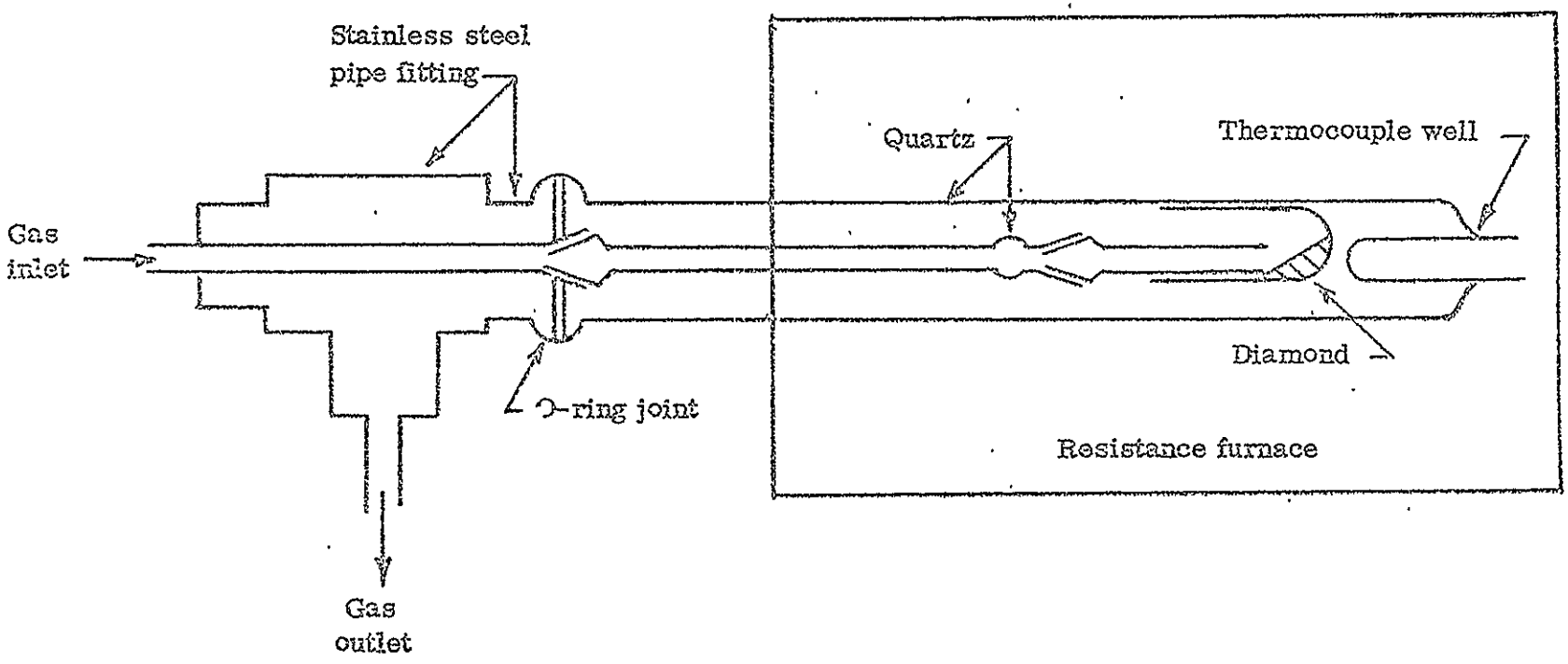

Figure 4. 3. The Quartz vacuum chamber.

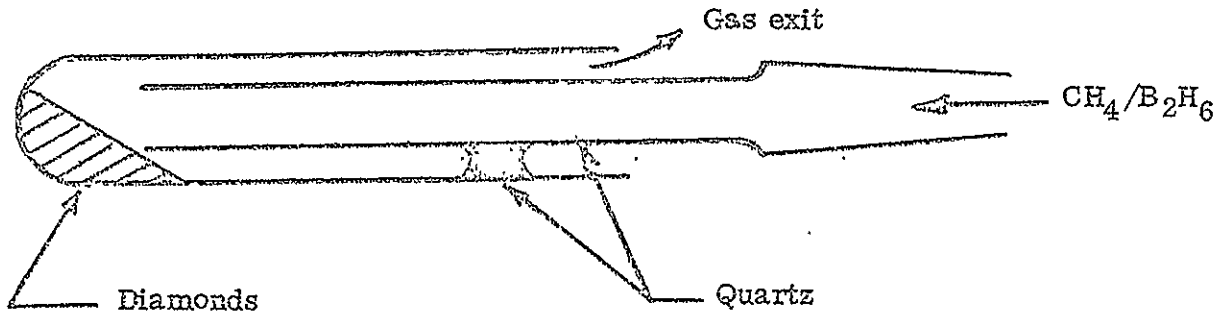

Figure 4.4. Details of diamond sample chamber.

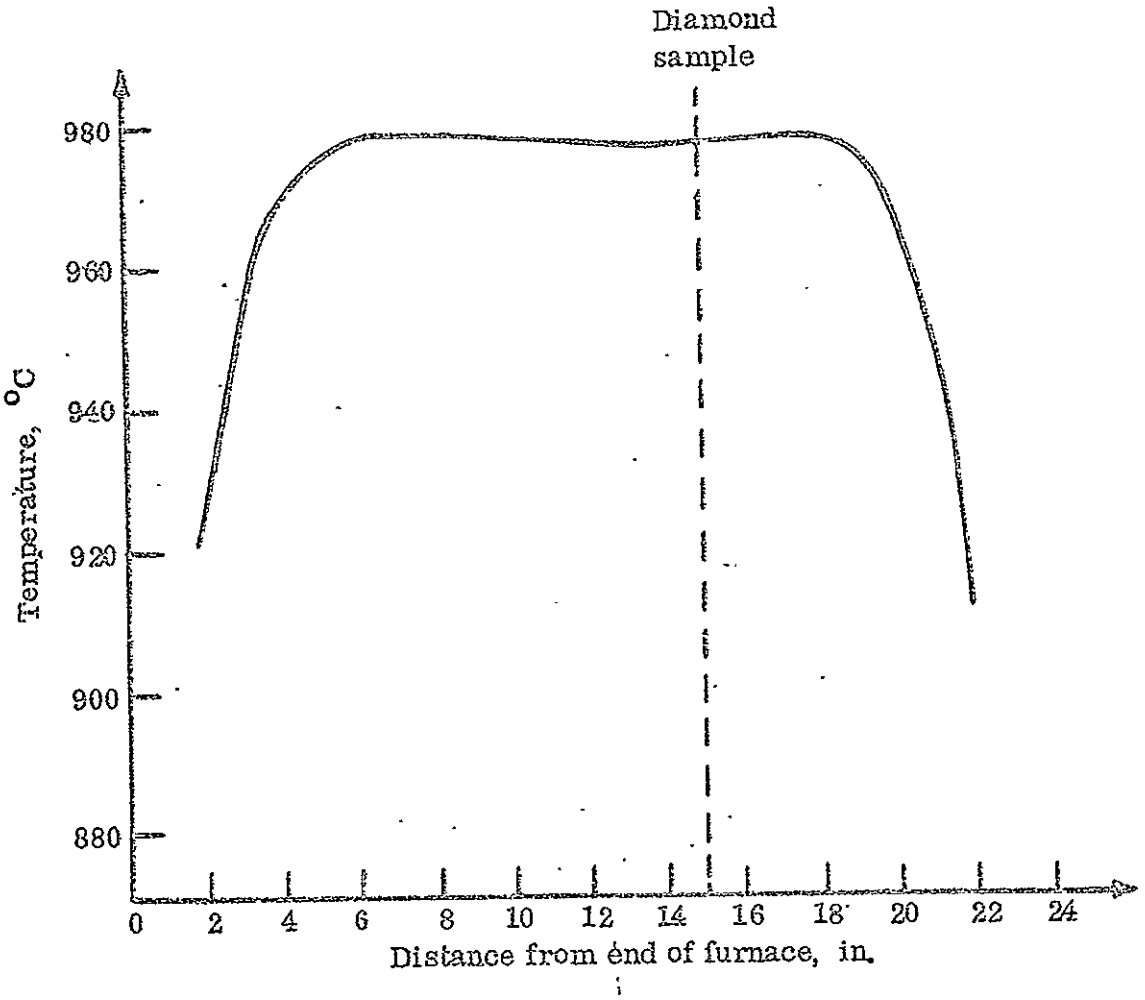

Figure 4.5. Temperature profile of the resistance furnace used in the deposition apparatus.

TABLE 4.1

Composition[a] of Gas Used for Diamond Doping

0.83% diborane

0.62% ethane

0.0013% tetraborane

1200 PPM carbon dioxide

540 PPM propane

300 PPM hydrogen

210 PPM nitrogen

200 PPM butane

<20 PPM argon

<10 PPM oxygen

<4 PPM pentaborane

balance methane

[a]Percentages are volume (mole) percent

CHAPTER V

DIAMOND DOPING EXPERIMENTS

5.1 Experimental Conditions

Based on the results of H. Will[2] for the low pressure epitaxial growth of diamond, the best diamond growth rates are obtained with pure methane at pressures below 1 Torr and a temperature of approximately 1050° C. The doping runs were performed under the conditions of temperature and pressure which produced the best diamond growth rates during the initial work of H. Will[2]. Instead of methane, however, the doping runs were performed with either a mixture of diborane in methane or diborane in hydrogen. The doping temperature was limited to 1050° C because of the resistance furnace temperature limitation. A pressure of approximately 0.20 Torr was used for all doping runs. The duration of each doping was approximately 20 hours.

5.2 Results of Doping Experiments

The pertinent information regarding the various series of doping runs is given in Table 5.1. Seven different samples were included in the doping runs. Samples 1B and 7 were obtained from KAY Industrial Diamond, whereas, samples 6B, 8A, 9 and 10 were obtained from Diamond Abrasives Corporation. The preceding diamond samples were 0 - 1

micron nominal size natural diamond powders. Sample 11 was a natural diamond macle obtained from the Van Itallie Corporation.[24] The gaseous mixture of 0.83 percent B_2H_6 by volume in methane was used for the doping runs on all samples except samples 9 and 10. The exact composition of the B_2H_6 in CH_4 mixture is given in Table 4.1. A one percent mixture of B_2H_6 in H_2 was used for the doping runs on samples 9 and 10. The graphite deposited on the diamond samples during each doping run was removed by hydrogen cleaning except for the graphite formed on sample 11 which was removed with a HNO_3/H_2SO_4 mixture.

The first series of doping runs were made on samples 1B. The initial sample weight was 0.3306g. The run times varied from 16 to 27 hours and the pressure varied from 0.17 to 0.20 Torr for the various runs. The percent weight increases varied from 2.03 to 3.39 with a cumulative weight increase of 12.89 percent for the five runs. The growth rate dropped from approximately 3 percent for each of the first two doping runs on sample 1B to slightly over 2 percent on the last three doping runs. After each hydrogen cleaning run, the color of the sample turned progressively grayer until by the end of the fifth doping run it was a very dark gray. A spectrographic analysis by Crobaugh Laboratories,[25] indicated that there was a considerable amount of tungsten contamination of the original sample and this impurity had obviously not been completely removed during the acid cleaning steps before the doping runs. The original diamond sample

had a dark gray color indicating a high level of impurity and even after acid cleaning and hydrogen cleaning in preparation for the doping runs on this sample it still remained the same color. Normally the diamond would be almost white after these cleaning operations. The continual darkening of the diamond surface after each hydrogen cleaning was therefore attributed to the reduction of a tungsten or other metal compound on the diamond surface during the hydrogen cleaning operation. This darkening of diamond samples having high tungsten contents was also noted by H. Will.[2] Due to the high impurity content no further runs were made on this batch of diamond from KAY Industrial Diamond.

Sample 6B was prepared from a batch of 0 - 1 micron natural diamond obtained from Diamond Abrasives Corporation. This batch of diamond appeared considerably cleaner than that purchased from KAY Industrial Diamond. After acid cleaning and hydrogen cleaning, this sample had only a slight off-white color. The doping run times ranged from 17 to 44 hours on this sample at pressures from 0.18 to 0.22 Torr. The percent weight increases decreased from 4.57 percent during the first doping run to a weight loss of 0.10 percent during the last run. A total weight gain of 9.86 percent was obtained on this sample. This diamond sample turned light blue after the first doping run and the blue color became more intense with succeeding runs. With the exception of the fourth doping run on sample 6B, there was a definite decrease in growth rates from one doping run to

another. Since the growth rate became negative on the sixth doping run, it was not possible to obtain a cumulative weight gain of more than 9.86 percent on this sample. Although apparent to some extent during the epitaxial diamond growth experiments of H. Will,[2] this growth rate trend was not nearly as pronounced and a cumulative weight increase of over twenty percent was readily obtained with a growth rate of two percent during the final deposition. Sample 6B was used for most of the tests described in the next chapter to determine the various properties of the doped diamond.

A second diamond batch was obtained from KAY Industrial Diamond. Sample 7 was obtained from this batch which was considerably cleaner than the first batch from which sample 1B was obtained. Four doping runs were made on sample 7. However, there were losses in the diamond sample during removal from the hydrogen cleaning furnace after the third doping run and during removal of the sample test tube from the quartz vacuum chamber during the fourth deposition. Run times and pressures were approximately the same as for the two previous diamond samples. A total of only 2.73 percent weight gain for the first two doping runs was measurable because of the sample losses during the last two runs. The blue color observed in the preceding sample was also visible in this sample after the first doping and cleaning sequence. Sample 7 was not used in any of the tests described in the next chapter since the sample test tube broke during hydrogen cleaning and some small pieces of quartz fell into the diamond sample.

Sample 8A was another sample of natural diamond supplied by Diamond Abrasive Corporation. A larger sample was used for this series of doping runs in order to have enough diamond for an accurate density measurement after obtaining the maximum weight increase possible before the growth rates dropped to zero. Six doping runs were made on this sample with run times from 20 to 23 hours and pressures from 0.19 to 0.22 Torr. A cumulative weight increase of 8.67 percent was obtained on sample 8A. Again, the growth rate after remaining essentially constant at about two percent for the first two doping runs, decreased markedly to about 0.5 percent by the sixth run. Since the growth rate was so small during the sixth doping run, this series of doping runs was terminated at this point rather than risking the loss of the sample during additional runs which would have contributed very little to the total weight gain. This sample also exhibited the same characteristic blue color as samples 6B and 7. The blue color was clearly visible after the first doping run.

Sample 9 was also diamond supplied by Diamond Abrasives Corporation. However, instead of the B_2H_6/CH_4 doping mixture that had been used for all previous doping runs, a one percent B_2H_6 in hydrogen gas mixture was used for this doping run. A run time of 22 hours at a pressure of 0.19 Torr resulted in a weight loss of 2.84 percent. Another doping run with the B_2H_6/H_2 mixture was made on sample 10. The run time in this case was 123 hours. A weight loss of 3.27 percent occurred. Neither sample 9 nor 10 exhibited any trace of blue color after the doping runs using the B_2H_6/H_2 mixture.

One doping run of 21 hours was made on sample 11, a 0.837g natural diamond macle, using the B_2H_6/CH_4 mixture. The macle was large enough to allow surface resistivity measurements to be made before and after doping. There was no measurable weight change of the diamond after doping. The graphite that had deposited on the diamond during this doping run was removed by placing the diamond in a solution consisting of one part HNO_3 to three parts H_2SO_4. Since no weight gain was measurable, acid removal of graphite was used in this case because the normal hydrogen cleaning of the diamond removes approximately 0.3 percent of the diamond.[22,23] No color change in the clear diamond was observed after the graphite was removed.

During each doping run a considerable amount of graphite was deposited on the deposition apparatus. A small amount of boron was also deposited on the deposition apparatus at the entrance to the deposition furnace. The graphite was readily removed by heating the deposition apparatus in air or by acid or hydrogen cleaning. The boron was removed with a nitric acid etch. There was no evidence of any other deposits such as boron carbide on the deposition apparatus after the doping runs.

5.3 Diamond Color Change During Doping Runs

A distinct change in the color of the diamond sample was observed during doping runs on samples 6B, 7, 8A. The color changed from a gray or off-white to light blue during doping runs on these samples. Figure 5.1 is an enlargement made from a colored slide showing the

color of sample 6B before doping and after six doping runs. The doped diamond is on the left and the bluish color of this sample is obvious. Figure 5.1 only shows the relative difference in color before and after doping because the enlargement process has intensified the actual color somewhat since even the undoped sample on the right appears to have a bluish tint. Actually, the undoped sample has a very light gray or off-white color while the doped sample is light blue. The blue color change was apparent on all doped samples after the first doping run. The color intensified slightly during additional doping runs on each sample. A similar color change was not observed on sample 1B (high level of tungsten contamination), samples 9 and 10 (doping attempted with B_2H_6 in hydrogen mixture) or sample 11 (diamond macle).

5.4 Non-doping Run

An additional diamond growth run was made during the course of this work. This run was made on natural diamond powder with methane at a pressure somewhat less than 0.01 Torr. Since this run was not a doping experiment, it will not be discussed in detail here. A complete description of the low pressure epitaxial growth experiment is presented in Appendix C.

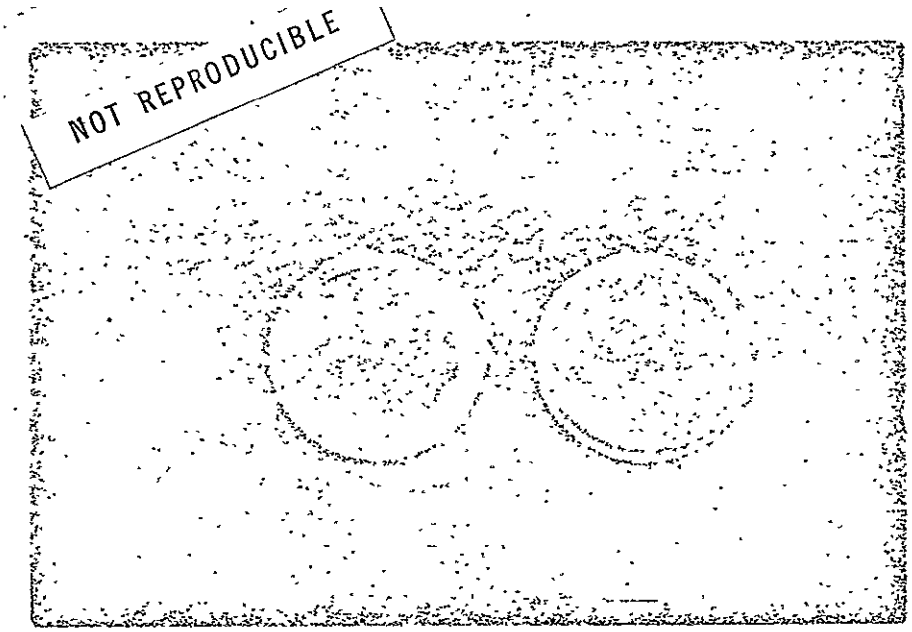

Figure 5. 1. Photograph of diamond before (right) and after (left) six boron doping runs.

TABLE 5.1

RESULTS OF DIAMOND DOPING EXPERIMENTS

Sample	Weight g	Run	Run Time hr	Temp. °C	Pressure Torr	Gross Weight Increase g	Net Weight Increase After H_2 Cleaning mg	Cumulative Weight Increase percent
1B	0.3306	1	22	1050	0.20	0.0252	0.0098	2.96
1B	.1856[a]	2	22	1050	.17	.0191	.0063	3.39
1B	.1919	3	16	1050	.18	.0145	.0039	2.03
1B	.1958	4	27	1050	.18	.0167	.0042	2.15
1B	.2000	5	21	1050	.20	.0182	.0049	2.45
6B	.4117	1	23	1050	.18	.0409	.0188	4.57
6B	.3700[a]	2	44	1050	.20	.0631	.0098	2.65
6B	.3798	3	20	1050	.22	.0349	.0034	.90
6B	.3832	4	18	1050	.18	.0270	.0050	1.30
6B	.3882	5	17	1050	.21	.0290	.0021	.54
6B	.2069	6	18	1050	.19	.0161	-.0002	-.10
7	.3399	1	21	1050	.18	.0301	.0060	1.62
7	.2532[a]	2	18	1050	.18	.0227	.0028	1.11
7	.2560	3	22	1050	.18	.0185	-------[b]	----
7	.2524	4	19	1050	.18	.0203	-------[c]	----
8A	.4200	1	20	1050	.20	.0332	.0091	2.17
8A	.4291	2	21	1050	.19	.0383	.0100	2.33

TABLE 5.1 - Continued.

Sample	Weight g	Run	Run Time hr	Temp. °C	Pressure Torr	Gross Weight Increase g	Net Weight After H_2 Increase Cleaning mg	Net Weight After H_2 Increase Cleaning percent	Cumulative Weight Increase percent
8A	0.4391	3	21	1050	0.22	0.0459	0.0083	1.89	6.39
8A	.4474	4	23	1050	.19	.0386	.0045	1.00	7.39
8A	.4519	5	20	1050	.19	.0348	.0035	.77	8.16
8A	.4554	6	20	1050	.19	.0282	.0023	.51	8.67
9	.1973	1[d]	22	1050	.19	-.0007	-.0056	-2.84	-2.84
10	.5135	1[d]	123	1050	.20	-.0053	-.0168	-3.27	-3.27
11[e]	.0937	1	21	1050	.21	0	0[f]	0	0

[a]Some sample removed for other tests.

[b]Some diamond lost during removal from H_2 cleaning furnace.

[c]Some diamond lost during the doping run due to gas entrainment.

[d]One percent B_2H_6 in hydrogen used for this run.

[e]Diamond macle used in this run.

[f]Diamond macle cleaned in 1 part red fuming HNO_3, 3 parts H_2SO_4.

CHAPTER VI

EXPERIMENTAL ANALYSIS OF DOPED DIAMOND

6.1 Chemical Etching Tests

Several chemical etching tests were run on diamond sample 6B which had undergone six doping and hydrogen cleaning cycles. Samples of this diamond were placed in aqua regia, nitric acid, and hydrofluoric acid in order to remove probably impurities that could be responsible for the blue color of the doped diamond.

A small sample of the doped diamond was placed in aqua regia for 18 hours and hydrofluoric acid for 4 hours at room temperature. There was no visible change in either the blue color or its intensity of the doped diamond. Another sample was placed in aqua regia at 90° C for one hour. There was no change in the color of the diamond sample. Samples were also placed in concentrated nitric acid for a period of 48 hours at room temperature, and in fused alkali at 450° C for 30 minutes. No change in the doped diamond sample color was observed in any of these tests and no weight losses were detected during the aqua regia, hydrofluoric acid, and fused alkali etches. These etches would have removed any surface impurity soluble in aqua regia, nitric acid, or fused alkali. Since boron is soluble in nitric acid, it is

concluded that the blue color exhibited by the doped diamond is not attributable to deposition of elemental boron.

6.2 Scanning Electron Microscopy

In an attempt to determine if a detectable structural change occurs on the diamond surface during the doping process, a scanning electron microscope was used to obtain images of the diamond surface before and after doping. Image formation with the scanning electron microscope differs from that of the conventional electron microscope inasmuch as the images are not formed directly by lenses but rather from electrical signals from the specimen surface. In the scanning electron microscope an impinging electron beam is scanned over the sample surface resulting in the emission of secondary electrons which are accelerated to a collector and amplified. The sample image is displayed on a synchronously scanned cathode ray tube based on the signals received from the secondary electron collector. Since the scanning electron microscope has a much larger depth of field than a conventional electron microscope, the diamond particles can be observed in three dimensions even at high magnification.

A Japan Electron Optics Laboratory Co., Ltd., model JSM-2 scanning electron microscope was used to obtain the polaroid photographs of the diamond samples shown in Figures6.1 through 6.3. The samples were prepared by electrically bonding "sintered" diamond pieces to the copper specimen electrodes with a conducting epoxy cement. Figure 6.1 shows samples of doped (left photograph) and undoped (right

photograph) at 30,000X magnification. In order to obtain optimum resolution, both of these samples were shadowed with a gold-palladium alloy at the same time in a rotating, tilting, vacuum shadowing apparatus. Each photograph corresponds to an area of about 3.3 microns square on the sample. Most of the particle sizes appear to be less than 0.5 microns and have irregular shapes. Surface detail is not defined sufficiently for a comparison of surface characteristics before and after doping. It was hoped that some clue could be found to explain the continuous growth rate decrease as the number of doping runs increased. Unfortunately, the small size of the particles and resolution limit of the scanning electron microscope for these samples precluded the analysis of surface changes during doping.

Since it should not be necessary with conducting specimens to evaporate a metallic coating on the surface,[26] it was decided to obtain photographs of unshadowed doped and undoped diamond samples to determine, if possible, a qualitative difference in conductivity of the two samples. The samples of doped and undoped diamond were mounted together on the same sample holder as shown in Figure 6.2. The undoped "sintered" chunk is at the lower right hand corner of the left photograph which has been magnified 100X. The images are seen as if the observer were looking down the primary electron beam with the sample illuminated by a light from the direction of the collector, in this case from the right side. The photograph on the right is a 500X magnification of the center portion of the previous photograph

with the undoped diamond sample again to the right of the doped sample. The magnification was then increased to 30,000X and photographs were taken individually of these two sintered pieces of doped and undoped diamond and the results are shown in Figure 6.3 As can be seen in Figure 6.3, the conductivity of the doped diamond is reflected in the better resolution obtainable in the photograph on the left. The photograph of the undoped sample is not sharp and the resolution is definitely not as good as for the doped sample. This is due to the fact that the undoped diamond is basically a non-conducting material, and the impinging electrons are not readily conducted away from the surface. Thus, additional electrons accumulate on the surface and tend to deflect the scanning electron beam and the image loses detail. No matter how much care was taken to focus the image, it was impossible to obtain any improvement in detail over that shown for the undoped diamond sample in Figure 6.3. So, although the scanning electron microscopy failed to show sufficient detail for an analysis of the observed decrease in growth rate as the number of doping runs increased on a sample, it did result in a qualitative demonstration of the superior conductivity of the doped diamond sample compared with the undoped sample.

6.3 X-Ray Diffraction

A Debye-Scherrer powder camera was used to obtain X-ray diffraction patterns of diamond samples before and after doping. The powder method was necessary since the diamond samples used in the

doping runs were extremely fine grained crystalline aggregates of particles with individual particle sizes of less than one micron. The interplanar lattice spacings of undoped and doped samples were obtained to determine whether or not any noticeable changes had taken place during the doping process.

The diffraction of X-rays by a lattice array of atoms follows Bragg's law. The Bragg condition for in-phase scattering is given as

$$n\lambda = 2D \sin \theta \qquad (6\text{-}1)$$

where n is the order of diffraction, λ is the X-ray wavelength, d is the lattice spacing, and θ is the glancing angle; i.e., the complement of the incidence angle. The patterns were obtained using a Debye-Scherrer powder camera in which the photographic film strip is held against the inside of a metal cylinder and coaxially encircles the sample. The collimated X-ray beam enters through the side of the cylinder, is scattered by the sample, and impinges on the photographic film along the directrices of a cone with a half angle of 2θ. The sample is rotated so that enough crystals participate in the reflection to produce a continuous line on the film rather than a number of discrete points along a circular arc. The interplanar lattice spacings are then readily calculated from the diffraction pattern recorded on the strip of film as shown in Figure 6.4. Figure 6.4 is a contact print of the original photographic film and therefore the diffraction pattern appears as bright lines rather than the dark

lines that formed the pattern on the original film. The X-ray beam entered through a hole in the left side of the film and, therefore, the small glancing angle reflections appear towards the right side of the film. In order to intensify the diffraction lines of small amounts of impurities, exposure times of forty hours were used. A chromium target in the X-ray tube provided a radiation wavelength of 2.2909 Å and a vanadium filter covering half of the photographic film was used to eliminate reflections due to β radiation.

Calculated lattice spacings and the relative intensity of the associated diffraction line for the diamond sample before and after doping are given in Table 6.1. In addition to the two intense diamond lines with calculated lattice spacings of 2.057 and 2.056 Å for the 111 planes of the doped and undoped samples respectively and 1.260 Å for the 220 planes, other weak lines are also present indicating small quantities of impurities either in the X-ray tube target material or in the diamond samples. Based on the results of the electron diffraction studies in which no impurity lines were detected, the impurities observed in the X-ray diffraction studies are most likely present in the X-ray tube target material rather than in the diamond samples. Although SiO_2 (low tridymite form) is listed as a possible impurity, the 4.08 Å lattice spacing was not detected. However, this may be due to the fact that this line is the weakest of the first three lines given for SiO_2. However, the important point to note is that no additional lines appeared after doping. Although

some of the lines in the undoped sample were not detected in the doped sample, all the lines that were observed after doping were initially present in the undoped sample. Therefore, even if the additional lines come from the sample and not the target, the formation of a new crystalline phase during doping was not detected with X-ray diffraction. Nevertheless, a search of the 1969 Inorganic Index to the Powder Diffraction File[27] was performed to indicate what the possible impurities might be. The possible impurities given in Table 6.1 are based on the lines present in the diamond sample before doping. The apparent disappearance of some of the lines after doping may be due to decompcsition or volatilization during the deposition runs. Since some error exists in measuring the position of the diffraction lines, a value within ± 0.015 Å of the calculated lattice spacing was assumed to satisfy that lattice spacing. This interval of 0.030 Å centered on the measured spacing gave good assurance that a possible impurity was not overlooked. Based on the calculated lattice spacings for the doped and undoped diamond samples, the following species were among those not detected: B, B_4C, B_2O_3, W, WC, Si, SiB_6, SiC, Ni, Si_3N_4 and Fe.

6.4 Electron Diffraction

Electron diffraction can be used to supply information regarding surface structure of diamond crystals in much the same manner that X-ray diffraction methods give crystal structure for the bulk material. The adequacy of Bragg's equation for electron diffraction

studies has been verified by M. Ponte[28] among others who have shown Bragg's law to hold within the experimental error of their results. The major difference is that the electron penetrates only the first few hundred angstroms[29] of the diamond sample because of the ease with which electrons are inelastically scattered and absorbed by the atoms of the crystal lattice and, thus, the surface structure will determine the electron diffraction pattern.

The wavelength to be used in applying Bragg's equation is that proposed by L. deBroglie.[30] Since the electron diffraction patterns were obtained with an electron microscope operating at a potential of 100 KV, and since the velocity of 100 KV electrons is a considerable fraction of the speed of light, the wavelength associated with these electrons must be calculated using the relativistic relationship for electron mass and kinetic energy. The calculated wavelength of the 100 KV electrons used in obtaining the electron diffraction patterns of diamond is 0.03700 Å. The wavelength calculations are given in Appendix D.

The diamond samples which were used for electron diffraction tests were small powder agglomerates. Electron diffraction patterns of the doped and undoped diamond were obtained by positioning the diamond powder samples in a JEM-7A electron microscope such that the electron beam impinged at the outer edge of the sample. Thus, a reflection diffraction pattern was obtained and recorded on a photographic plate. These patterns are actually Bragg powder patterns,

but since the electron wavelength is small, many additonal rings can be obtained with electron diffraction than with X-ray diffraction. The sample could not be rotated in the electron beam since the portion of the sample giving the clearest diffraction pattern was not in the center of the sample holder and thus inaccurate patterns would have been obtained. However, since the sample was a fine powder, a sufficient number of crystals were aligned at the correct angle to give a Bragg reflection and the diffraction pattern could be accurately analyzed to determine lattice plane spacings even though some of the rings were comprised only of isolated points.

Photographs of the electron diffraction patterns for diamond samples before and after doping are shown in Figures 6.5 and 6.6. At least fourteen rings were clearly visible for each sample and the results of the calculation of lattice plane spacings are given in Tables 1.2 and 6.3 for undoped and doped diamond, respectively. The experimental lattice plane spacings for the doped and undoped samples agree very well with theoretical lattice plane spacings for diamond. The observed and expected relative line intensities for doped and undoped diamond are also given in Tables 6.2 and 6.3. The observed relative intensities are qualitative observations obtained from visual examination of the diffraction powder patterns on the photographic plates. The expected line intensities[27] are given for the five most intense lines of diamond. The observed relative line intensities for the doped and undoped diamond samples agree qualitatively with the expected values. No lines other

than those of diamond were found and the same lines appeared for the doped and undoped diamond diffraction patterns. The apparent extra line at a diffraction angle of approximately 1.02 degrees is probably a second order reflection from the 111 plane. Within the experimental error it appears at just twice the angle observed for the primary diffraction from the diamond (111) plane.

The theoretical lattice plane spacings and relative line intensities[27] for boron carbide are given in Table 6.4. None of the boron carbide lattice spacings was observed in the electron diffraction patterns of doped or undoped diamond. The observed lattice spacings determined from X-ray powder patterns on a new allotropic form of carbon[31,32] are given in Table 6.5. This new form of carbon is referred to as "white carbon" or "chaoite" and it has been suggested that this material may have a density close to that of diamond. The X-ray powder pattern data for this new form of carbon was therefore compared with lattice spacing data for diamond to determine if the observed weight gain during the doping runs could be attributed to this new solid phase. It is apparent from Tables 6.3 and 6.5 that none of the lattice spacings for "white carbon" was observed in the electron diffraction patterns of the diamond sample that had undergone six boron doping runs. Since "white carbon" is formed in the laboratory during sublimation of pyrolytic graphite at a temperature of approximately 2550° K, it does not seem possible that is could account for the weight increase in the diamond sample observed during

either the epitaxial diamond growth runs of H. Will[2] or during these boron doping experiments.

It is obvious that based on the results of the electron diffraction study of doped and undoped diamond, the growth during doping cannot be attributed to deposition of boron carbide or any other crystalline solid other than diamond. Since the possibility of boron being incorporated in the diamond in a regular pattern during growth is remote, it would not be anticipated that additional diffraction lines would be observed for boron in the doped diamond.

6.5 Chemical Analysis of Doped and Undoped Diamond

Two samples of diamond were submitted to Ledoux and Company[33] for emission spectrochemical analysis. The results of this analysis are given in Table 6.6. Sample 6-0 was diamond which had been acid cleaned but had not undergone any boron doping runs. The other sample, sample 6-6, was a portion of the acid cleaned sample that had undergone a total of six boron doping runs with an accumulated weight increase of 9.86 percent. The results of the spectrographic analysis indicate that the percent boron in the diamond sample increased tenfold from 0.001 percent in the undoped diamond to 0.01 percent after six doping runs. Silicon content also increased from 0.006 percent before doping to 0.02 percent after the six doping runs. On the other hand, the concentration of phosphorous decreased from 0.005 percent to 0.0002 percent during the series of boron doping runs. No other elements were detected by spectrographic analysis.

If it is assumed that the increase in boron content is confined to the region represented by the 9.86 percent weight increase of the diamond sample, then the increase in boron content represents an average boron concentration of approximately 1010 ppm in the new diamond growth. This result is based on the assumption that diffusion of the boron from the new growth layer into the original diamond seed crystal had not occurred during successive boron doping and hydrogen cleaning cycles. Actually, the deposited boron most likely diffuses to some extent into the original seed crystal and if it is assumed that the boron is distributed uniformly throughout the entire diamond sample after doping, then the average boron concentration would be approximately 100 ppm. The boron concentration in the new diamond growth is therefore probably intermediate between the two calculated extremes of 1010 and 100 ppm.

The increase in silicon content after the boron doping runs may be attributable to the presence of gaseous silicon from the chemical dissociation of the quartz deposition apparatus. However, it is more likely the result of silica particles in the diamond sample due either to mechanical abrasion between the diamond and the quartz diamond sample holder or to gradual devitrification of the sample holder during the extended time at temperatures in excess of 1030° C. It was observed that the structure of the quartz sample holder apparently changed over a period of time at doping and hydrogen cleaning temperatures. The sample holder, which was initially clear, gradually acquired a frosted appearance and in time fracture of the sample holder

occurred due to thermal or mechanical stresses. The frosted appearance was due primarily to an apparent roughening of the outer surface of the quartz sample holder. Weighings made before and after the complete sequence of boron doping and hydrogen cleaning cycles indicated that weight of the sample holder had decreased by approximately 0.0062 g. This may be attributed primarily to mechanical abrasion between the rough outer surface of the holder and the inner surface of the Hastelloy X tube during insertion of the doped sample into the hydrogen cleaning furnace after each boron doping run. However, it is probable that the inner surface of the sample holder also experienced some roughening and therefore, mechanical abrasion by the diamond sample or by the metal spatula used to remove the doped diamond from the sample holder could be responsible for the observed increase in silicon content.

The decrease in phosphorous content during the boron doping runs would be expected due to the high vapor pressure of phosphorous and phosphorous compounds at temperatures maintained during the boron doping and hydrogen cleaning runs.

6.6 Density Measurments

The density of diamond at 25° C is given in the literature[34] as 3.51477 to 3.51554 g/cm^3 with an average density of 3.51532 g/cm^3 for the thirty-five samples investigated. The theoretical density of diamond based on lattice constant data varies from 3.51407 to

3.51531 depending on the particular value of the diamond lattice constant used in the calculation.

Boron, boron carbide, boric oxide, and boron nitride have densities[35] of 2.34 to 2.37, 2.52, 2.45 to 2.47, and 2.25 g/cm^3, respectively. Since a considerable difference in density exists between these species and diamond, a density measurement on the doped sample can be used to determine if the cumulative weight increase during the doping runs can be attributed solely to the deposition of the above species on the virgin diamond. The possibility of the weight increase being graphite is discussed in reference 2 where chemical etching, density measurements, X-ray and electron diffraction, microwave absorption, and electron spin resonance tests demonstrated that the growth was not graphite but new diamond. Theoretical composite densities of the doped samples were calculated assuming that the 8.98 percent weight increase during doping was attributable to the deposition of the boron species mentioned above. The results are given in Table 6.7. Although it has previously been demonstrated that the growth is not due to graphite deposition,[2] the theoretical composite density after deposition assuming the weight increase during growth was due to graphite is also shown in Table 6.7 for comparison. The theoretical composite densities range from 3.049 to 3.395 g/cm^3 assuming the weight increase during the doping runs due to low density graphite and boron carbide, respectively. Therefore, if density measurements on the doped samples

show that the growth cannot be attributed to boron carbide growth, then the other boron species can also be eliminated since the density of boron carbide is greater than any of the other species.

Theoretical composite densities, assuming that the weight increase during growth was due to other than boron containing species, were also calculated. Theoretical diamond sample densities of 3.416, 3.486, and 3.508 g/cm^3 were calculated assuming the weight increase during doping could be attributed to quartz, silicon carbide, and silicon nitride, respectively.

The density of the virgin diamond powder before doping and the density of the same diamond after six doping and hydrogen cleaning runs were measured. The doped sample used for the density measurements had accumulated an 8.98 percent weight increase during doping. The density of the doped sample could then be compared to the density of the original diamond and to the theoretical composite densities given in Table 6.7.

The experimental procedure used to determine the density of the undoped and doped diamond samples was basically the same as the pycnometer method described in reference 2. A known weight of diamond was placed in a 2 cm^3 pyrex pycnometer, the void volume of which had been reduced to approximately 1 cm^3 by the addition of pyrex beads in order to improve the accuracy of the measurements. The cover liquid in all cases was orthoxylene which had been boiled before each density measurement to remove any dissolved gases. Orthoxylene was chosen as the cover liquid because its density was well known as a

function of temperature, it wetted the diamond well and filled the voids readily, and it had a low volatility which lended itself to this type of measurement. After it had been boiled, the cover liquid was transferred under vacuum to the pycnometer to prevent absorption of gases during transfer. A vacuum was also maintained on the filled pycnomerer until all air trapped in the diamond sample had been displaced, orthoxylene completely filled all the voids, and bubble nucleation on the diamond powder had ceased. The pycnometer was filled to a precise level, maintained at that level, and weighed until a steady state condition was obtained, thus, assuring that the cover liquid had reached room temperature and any residual cover liquid on the outside of the pycnometer had evaporated. With the weight and density of the cover liquid required to fill the pycnometer containing the diamond sample, the known volume of the pycnometer, and the weight of the diamond, the density of the sample was readily calculated. Corrections were made for the expansion of glass, the buoyancy affect of air on the brass weights, and the variation of the density of the cover liquid with temperature.

Six density measurements were made on both the undoped diamond and the doped sample. The weight of diamond used was different for each run and the pycnometers used were interchanged to eliminate the possibility of differences due solely to a variation in pycnometers. The data are shown in Table 6.8. The density measurements of the undoped diamond samples varied from 3.487 to 3.518 g/cm^3 with an average density of 3.502 g/cm^3, whereas, the density measurements of

the doped samples gave values from 3.490 to 3.515 g/cm^3 with an average density of 3.504 g/cm^3 for the six determinations. The standard deviations for the measurements was 0.012 and 0.010, respectively, for the undoped and doped samples. It is therefore obvious that within the accuracy of these measurements the density of the diamond remains essentially unchanged by doping. The fact that the density of the virgin diamond is not exactly equal to the theoretical density based on lattice constants is probably due primarily to the fact that it is very difficult to eliminate all trapped air pockets and small nucleated bubbles in the diamond sample when the cover liquid is added to the pycnometer. Defects and impurities in the diamond could also contribute to the difference between the theoretical and experimental densities of the undoped diamond. The important point, however, is that there is essentially no difference in the measured densities of the doped and undoped diamond samples.

With the exception of silicon nitride, the Student's t-distribution can be used to show that the weight increase during doping is not due to deposition of boron carbide or any of the other species in Table 6.9. The variable, t, is given in reference 4 as:

$$t = \frac{(\bar{X} - \mu)\sqrt{n - 1}}{S}$$

where

$\bar{X}$ is the mean density of the doped diamond samples

μ is the true density of the doped diamond

S is the standard deviation of the doped diamond samples

n is the number of samples

n-1 is the degrees of freedom

Based on the mean density of 3.504 g/cm^3 and a standard deviation of 0.010 g/cm^3 for the six density determinations on the doped diamond sample, a single measurement of density will therefore fall within the range 3.492 to 3.516 g/cm^3 with a confidence level of 95 percent. The density measurements indicate that the growth of diamond has occurred and that the weight increases can not be attributed to the formation of B, B_4C, B_2O_3, BN, SiO_2, or SiC. Silicon nitride, however, can not be eliminated on the basis of density measurements alone since its density of 3.44 g/cm^3 is very close to that of diamond. The statistical analysis is conservative since no corrections have been made to account for the fact that the experimental method for determining the density of diamond gives values slightly lower than the known density. Presumably, the experimental densities for the other species measured by this method would also be slightly lower than the theoretical values.

6.7 Seebeck Coefficient

When a temperature gradient is applied across a semiconducting material, a difference in voltage is also induced across the material. The voltage developed is known as the Seebeck voltage and the proportionality constant between temperature differential and induced voltage is called the Seebeck coefficient. For small temperature

gradients across the sample, the electromotive force generated is proportional to the temperature difference across the material. Mathematically the relation is,[36]

$$S = \lim_{T_2 \to T_1} \frac{V(T_1,T_2)}{T_2 - T_1} \tag{6-2}$$

where S is the Seebeck coefficient, $V(T_1,T_2)$ is the induced electromotive force, and $T_2 - T_1$ is the applied temperature difference across the thermoelectric material. When the Seebeck coefficient of doped diamond was measured experimentally it was measured relative to a standard material, in this case copper, and the experimental Seebeck coefficient was therefore a relative Seebeck coefficient. The absolute Seebeck coefficient of the doped diamond can be determined by subtracting the absolute Seebeck coefficient of copper from the measured relative Seebeck coefficient of the doped diamond.[37] Thus

$$S_D(T) = S_{DC}(T) - S_C(T) \tag{6-3}$$

where $S_D(T)$ and $S_C(T)$ are the absolute Seebeck coefficients of the doped diamond and copper respectively, and $S_{DC}(T)$ is the relative Seebeck coefficient of diamond with respect to copper. Since the absolute Seebeck coefficient of copper[38] is less than $2\mu V/^oC$ over the temperature range for which the Seebeck coefficient was experimentally determined for doped diamond, the absolute and relative Seebeck coefficients are essentially equal and only the relative Seebeck coefficients are presented.

The basic features of the experimental apparatus used to measure the relative Seebeck coefficient of the doped diamond and boron carbide powder samples are shown schematically in Figure 6.7. The samples were placed between two copper electrodes fabricated from a solid copper rod. A piece of copper tubing was brazed to the upper electrode in order to form a container for dry ice. Since the quantity of doped diamond samples was limited, the upper electrode was machined down to 1/4 inch diameter at the cold electrode-sample junction in order to preclude inadvertent direct contact of the two electrodes during Seebeck coefficient measurements. The two electrodes and powder sample were placed in a teflon cylinder in order to insulate the apparatus from externally induced static charges. The weight of the upper electrode on the powder sample insured the thermal and electrical contact with the sample. Temperature gradients across the sample were obtained by placing dry ice in the open end of the tube brazed to the upper (cold) electrode. The high thermal resistance of the powder sample provided an adequate temperature gradient to be established across the sample for Seebeck coefficient measurements. Cooling of the upper electrode with dry ice rather than heating the lower electrode was chosen as the method of obtaining temperature gradients across the samples because early attempts to measure the Seebeck coefficient using an electrically heated hot plate to provide the required gradient proved unsatisfactory due to the fluctuating voltages induced by the surface of

the hot plate. The temperature gradient across the sample was slowly changed by incremental additions of dry ice and a steady-state condition was maintained while emf and temperature differences were measured. Inasmuch as the samples were loose powders, it was not possible to obtain emf and temperature differences directly from the sample and these measurements were therefore obtained from the two electrodes in direct contact with the samples. The temperatures near the junctions were measured with a Leeds and Northrup potentiometer using thermocouples that were electrically insulated from the copper electrodes with an insulating ceramic cement. The induced voltages across the sample were measured with Keithley model 610 electrometer, with the positive lead from the electrometer attached to the cold electrode.

The sign of the Seebeck coefficient can be used to determine whether the sample is n-type or p-type. If the material is p-type, the average flux of positive holes from the hot junction is higher than that which is entering this region and thus there is a net flux of positive holes to the cooler junction. By convention, the sign of the Seebeck voltage is the sign of the cold junction. Therefore, a positive Seebeck voltage indicates a p-type material.

The experimental results for the Seebeck coefficient of doped diamond (one doping run, 4.97 percent weight gain) are given in Table 6.9. The temperature of the cold junction was decreased from room temperature to -25.5° C by the addition of dry ice to the brazed

copper tubing section of the cold electrode. The "hot" junction temperature remained more nearly constant, decreasing only 12.8° C, thus, temperature differences as large as 35.5° C and Seebeck voltages as large as 0.0105 volts were obtained. Relative Seebeck coefficients were calculated by dividing the measured Seebeck voltage by the temperature difference between the "hot" and cold junctions. Calculated values of the Seebeck coefficient for diamond which had undergone one doping run varied from 254 to 334 $\mu V/^{\circ}C$ with an average of 296 $\mu V/^{\circ}C$ for the 14 different measurements of Seebeck coefficient. The sign of the Seebeck voltage indicated that this diamond behaved as a p-type material.

The Seebeck coefficients for diamond which had undergone six doping runs, (9.86 percent weight gain) are given in Table 6.10. The data were obtained over approximately the same range of temperature gradients as that for the sample which had only one doping run but the maximum Seebeck voltage measured was only 0.005 volts. The corresponding relative Seebeck coefficients varied from a minimum of 86 to a maximum of 135 $\mu V/^{\circ}C$. The average relative Seebeck coefficient for the 11 measurements was 120 $\mu V/^{\circ}C$, considerably lower than the relative Seebeck coefficient of the less heavily doped diamond sample. Based on the sign of the Seebeck voltage, this diamond sample is also a p-type material.

The measured Seebeck coefficients of the boron doped diamond are probably somewhat low due to sample inhomogeneity and IR voltage loss caused by circulating currents within the sample.

Table 6.11 gives the results of the Seebeck coefficient of a sample of abrasive grade boron carbide obtained from the Carborundum Corporation.[39] This material is also p-type based on the sign of the induced Seebeck voltage with an average value of 48 $\mu V/^{o}C$ for the relative Seebeck coefficient based on five measurements on this sample. This value of the Seebeck coefficient is considerably lower than that obtained for either of the two doped diamond samples, and it does not appear likely that boron carbide deposition on the diamond surface during doping could account for the measured Seebeck coefficients of the doped diamond. V. Neshpor and V. Nitikin[40] have reported a p-type Seebeck coefficient of 216 $\mu V/^{o}C$ for samples of boron carbide. The difference between this value and that for the abrasive grade boron carbide obtained from the Carborundum Corporation is probably due to differences in sample porosity and chemical composition. The Russian samples contained excess boron and had densities very close to the theoretical density of boron carbide. The Carborundum Corporation samples were abrasive grade powders as were the diamond samples.

An attempt was also made to measure the Seebeck coefficient of undoped diamond. However, the resistivity of the undoped diamond was so high that measurement of its Seebeck coefficient was impossible.

Based on the observed magnitude of the Seebeck coefficient of the doped diamond samples, it is apparent that the diamond which had

undergone six doping runs was more heavily doped than that which had only been doped once, since the largest Seebeck coefficients are associated with low carrier concentrations. Only the lower doping level, however, gives a Seebeck coefficient that is in the range that maximizes the figure of merit for a thermoelectric material, i.e., a Seebeck coefficient between 200 and 300 $\mu V/^{o}C$. Since the concentration of carriers that maximizes the figure of merit is approximately 10^{18} to 10^{21} per cm^3 depending on the effective mass of the carrier,[41] the carrier concentration in the diamond sample that had been doped once can be estimated at about this level. This conclusion is supported by the results of the chemical analysis which indicate a carrier concentration of approximately 10^{19} to 10^{20} boron atoms per cm^3 for the diamond sample which had undergone six doping runs. The carrier concentration of the more highly doped sample will be correspondingly higher. Since carrier concentrations preferred for transistor and rectifier applications are considerably less than that apparently obtained for just one diamond doping run, it appears that the production of boron doped diamond devices should be quite simple based on the doping levels obtained on the diamond powders.

The B_2H_6-CH_4 mixture used in the diamond doping runs was highly concentrated with the dopant gas. The concentration of B_2H_6 in CH_4 was approximately 0.83 percent by volume. As shown in Appendix A, this concentration of B_2H_6 in CH_4 should yield solid boron at the conditions of temperature and pressure used for the boron doping runs.

6.8 Induced Electron Emission

The technique of induced electron emission,[42,43,44] (IEE) was used in an attempt to determine if boron had been incorporated in the diamond lattice during the doping process and to determine the nature of the chemical bond between the boron and carbon atoms. In this process, the sample is bombarded with X-rays and the energy distribution of the emitted electrons is measured. Both the energy of the emitted electrons and the rate of induced electron emission are determined. The energy level at which the electrons are generated is indicative of the electron binding energy of a particular element in the chemical structure; whereas, the electron emission rate is related to the quantity of the element present in the sample.

The use of X-ray photoelectron spectroscopy as a technique for chemical structure was first demonstrated by K. Siegbahn[42] in 1957. Recently, J. C. Helmer and N. H. Weichert[43,44] of Varian Associates[45] have described a new type of X-ray photoelectron spectrometer having improved sensitivity. In this spectrometer, the X-ray generated photoelectrons are retarded to a low energy of 100 eV by the application of a retarding voltage between the sample and the source slit of the spectrometer before entering the energy analyzer. A spectrum is obtained by superimposing a sweep voltage on the initial retarding voltage. This improved instrument, the Induced Electron Emission Spectrometer, was used for these tests.

Since the application of IEE looked promising for analysis of doped semiconductors in which dopant concentration could be extremely small, several samples were submitted to Varian Associates for IEE spectrometer analysis. Of the samples initially submitted, the following were analyzed by this method: a sample of diamond which had undergone six doping cycles with the B_2H_6/CH_4 mixture, a sample consisting of a mixture of $B(OH)_3$ and B_4C, and a sample of B_4C. The $B(OH)_3$ and B_4C samples were submitted as references to determine the electron binding energy level associated with boron bonding in these two compounds. The electron binding energy associated with the boron bond in the diamond lattice could then be compared with these reference levels. Moreover, since the electron counting rate is proportional to the quantity of boron present, a comparison of the counting rates for these three samples can be used to determine the approximate boron doping level in the sample.

The results are presented in Figures 6.8 through 6.10 which show the induced electron emission spectra associated with 1s boron electrons in doped diamond, a mixture of $B(OH)_3$ and B_4C, and B_4C, respectively. The sweep voltage is recorded along the abscissa and the electron counting rate is plotted as the ordinate. Figure 6.8 indicates that the maximum electron counting rate in the doped diamond sample occurs at a sweep voltage of 1189.5 corresponding to an electron binding energy of approximately 191.5 volts. Another very weak boron peak also appears to be present at a sweep

voltage of about 1195.5 volts. The IEE spectrum for boron in the mixed sample of $B(OH)_3$ and B_4C is given in Figure 6.9. Two boron peaks are observed, one at 1188.6 volts, corresponding to $B(OH)_3$ and the other at approximately 1195.5 volts, attributed to B_4C. The IEE spectrum for B_4C is presented in Figure 6.10.

The results of the initial IEE study indicate that a rather high level of boron doping at the diamond surface has been achieved since the amplitude of the IEE signal for boron in the doped diamond is approximately eight percent of that for the boron reference compounds. Moreover, based on the observed sweep voltages at which the maximum counting rates were obtained, it appears that the boron bonding energy in the doped diamond lattice, at least that near the diamond surface, is closer to the energy of the bond in $B(OH)_3$ than to the bond in B_4C. The sample depth analyzed by this method is approximately 100 Å.[46] Since the IEE technique measures surface properties, it is possible that the strong boron signal of the doped diamond at 1189.5 volts is due to oxidation of the surface boron resulting from exposure of the surface boron atoms to air after doping.[47] The weak signal from the doped diamond sample at a sweep voltage of approximately 1195.5 volts may indicate the presence of the covalent boron bond beneath the diamond surface similar to that in B_4C.

It should be noted that the boron-carbon bonding energy in diamond is unknown. It may, in fact, be closer to the energy of the boron bonding energy in $B(OH)_3$.

6.9 Electron Spin Resonance

Electron spin resonance (ESR) data were obtained at room temperature for diamond samples before and after boron doping in order to determine if an increase in paramagnetic centers were produced in the doping process. A Varian E-3 electron spin resonance spectrometer was used to obtain these data. If boron had been incorporated in the diamond lattice as a p-type impurity, then it should be theoretically possible to detect this by examining the electron spin resonance spectra of the diamond sample before and after the boron doping runs.

The electron spin resonance technique[48] is based on the fact that the motion of a spinning electron generates a magnetic field. If a constant external DC magnetic field is applied, the spin axis of the electron precesses around the lines of force of the applied magnetic field. Although this effect alone cannot be detected, the application of a RF field at right angles to the DC field results in transitions from a low to a high energy state. The RF energy absorbed in this process is related to the DC field by

$$h\nu = \beta g H \qquad (6\text{-}4)$$

where h = Planck's constant, ν = frequency of the absorbed radiation, β = Bohr magneton (0.92752×10^{-20} erg/gauss), g = spectroscopic splitting factor, and H = DC field strength. To obtain the ESR

line, the DC field is modulated and swept over a range centered at the level associated with the absorbed RF energy. The output from the crystal detector is fed to a phase sensitive rectifier and integrator in order to produce the first derivative of the absorption curve which is recorded as the electron spin resonance line. The area under the electron spin resonance curve is therefore proportional to the total number of paramagnetic centers in the sample.

The electron spin resonance lines for diamond sample 6B before doping and after one and five doping runs is shown in Figure 6.11. This sample had been annealed for 125 hours at 1038^{o} C. For comparison, the ESR line for the reference (0.1% pitch in KCl) is shown in Figure 6.12. Each ESR in Figure 6.11 was obtained with a diamond sample of approximately 0.058 g, a 200 gauss scan field centered at a DC field strength of 3388 gauss, a receiver gain of 2000, 40 milliwatts of microwave power, and a microwave frequency of approximately $9.57X10^{9}$ hertz. The ESR lines for the doped and undoped samples show the typical room temperature ESR lines that have been observed for diamond powder.[2,49,50] For each of the diamond samples, three resonance peaks were observed in the diamond spectra; a central maximum resonance, a much less intense resonance approximately 32 gauss from the central resonance, and a very weak resonance approximately 65 gauss from the central resonance. The areas under the ESR lines of Figure 6.11 correspond to approximately 3.34, 3.38, and $2.00X10^{17}$ unpaired electron spins per gram of

sample 6B before boron doping, after one boron doping, and after five boron doping runs, respectively. This is considerably less than would be expected based on the results of the Seebeck measurements and chemical analysis. This may be due to compensation by defects or nitrogen. Both the maximum deflection of the ESR curve and the area under the line showed slight increases after one boron doping run but then decreased significantly after five doping runs. In Figure 6.11, the width of each resonance line between maximum and minimum points on the derivative curve was approximately 3 gauss in all cases.

As can be seen in Figure 6.13, the ESR spectra intensity is a strong function of the annealing time at temperatures used for the boron doping runs and hydrogen cleaning cycles (the ESR of the strong-pitch reference is given in Figure 6.14). This effect was deduced from ESR spectra obtained on early boron doping attempts. The effect of annealing mechanically crushed diamond on ESR data has also been observed by others.[49,50] Since the magnitude of this effect can completely mask changes in the ESR line due solely to the boron doping, an experiment was performed to determine the time required to completely anneal a diamond sample in the hydrogen cleaning furnace before proceeding with doping. The data of Figures 6.13 and 6.14 were obtained at essentially the same spectrometer settings as used to obtain the data in Figures 6.11 and 6.12 with the only important difference being a receiver gain of 1250 instead of 2000. A 0.110 g sample was used for the annealing experiments. The

results indicate that the paramagnetic spin centers have been reduced by 72 percent to $2.68X10^{17}$ spins per gram after 5.5 hours and by 78 percent to $2.68X10^{17}$ spins per gram after 100 hours at 1038^{o} C. Therefore, the annealing process is essentially complete after 5.5 hours and little change could be expected after 100 hours of annealing. Based on these results, sample 6B was annealed at 1038^{o} C for 125 hours before starting the boron doping runs.

Comparing the ESR data for sample 6B after one doping run with that obtained on the sample before doping, indicates the possibility that boron doping of the diamond could be responsible for the slight increase in paramagnetic spins observed after the first boron doping run. However, the subsequent decrease in area under the ESR line after five doping runs cannot be explained unless the annealing process is still in effect even after approximately 150 hours at temperatures in excess of 1030^{o} C.

6.10 Fluorescence

A sample of diamond which had undergone six boron doping runs was exposed to ultraviolet radiation to determine if fluorescent emission could be observed. The ultraviolet source was a 550 watt Hanovia Type A medium pressure mercury lamp. The wavelengths and relative energies of the radiation from this lamp are given in Table 6.12. The ultraviolet source was placed approximately four inches above the diamond sample and visual observation was made in a dark room. Since the valence band and the conduction band of a

perfect diamond are separated by an energy gap of approximately 5.6 eV, corresponding to the absorption edge at 2200 Å, the ultraviolet radiation wavelength used in this experiment is slightly higher than that required to excite fluorescent emission from a perfect diamond. However, it was anticipated that the doping process had introduced an electronic excitation level with a separation of considerably less than 5.6 eV. No fluorescence was detected.

Another attempt to measure fluorescence from the doped diamond sample was made using a Hitachi MPF-2A fluorescence spectrophotometer. The sample was first observed visually for fluorescence as the excitation wavelength was scanned from 2000 to 7000 Å. No fluorescence was observed. The sample was then exposed to several discrete excitation wavelengths while the sample emission was scanned from approximately 3000 to 7000 Å for each excitation wavelength. The few, weak emission peaks observed were investigated further by setting the emission wavelength corresponding to the peak and scanning the excitation wavelength from 2000 to 7000 Å. A Hitachi QPD-33 was used to record the emission spectra generated for both the doped and undoped diamond samples. An investigation of the spectra revealed no significant fluorescence peaks, and the spectra for the doped and undoped diamond samples were essentially identical.

We have no ready explanation for the lack of fluorescence. Other workers[51] have found that fluorescence is not always observed

in semiconducting diamond. Perhaps the presence of other impurities such as nitrogen are necessary for fluorescence.

6.11 Optical Measurements

The Hitachi MPF-2A fluorescence spectrophotometer, which was used in the fluorescence tests described in the previous section, was also used to measure the reflectance of undoped diamond, boron doped diamond, boron, and boron carbide samples. Each powder sample was exposed to incident radiation over a range of wavelengths from 2400 to 7000 Å. To obtain a particular reflectance measurement, the incident wavelength and the wavelength sensed by the photomultiplier were made identical. This process was repeated at 200 Å increments from 2400 to 7000 Å. The spectrophotometer sensitivity was initially adjusted at each wavelength to maintain the spectrum of the undoped diamond within the limits of the recorder. This sensitivity setting schedule was then maintained for reflectance measurements on the other three samples in order to simplify spectrum comparisons.

The results of this investigation are given in Table 6.13 and Figure 6.15. The relative reflectance given in Table 6.13 is the reflected energy sensed by the photomultiplier tube for the sensitivity level employed. In order to compare the reflected energy of the four samples, the doped diamond, boron, and boron carbide relative reflectances were normalized with respect to the relative reflectance of undoped diamond at each wavelength. The results show that the doped diamond sample reflects less energy than the undoped

diamond sample at wavelengths less than 4000 Å and greater than 5600 Å. Both the boron and boron carbide samples reflect less energy than the undoped diamond sample over the range of wavelengths investigated. Furthermore, the normalized relative reflectance spectra of the boron and boron carbide samples are quite different from the boron doped diamond spectrum. This can be more readily seen in Figure 6.15. Whereas the doped diamond spectrum increases rapidly at short wavelengths the opposite trend is observed for the boron and boron carbide smaples. Furthermore, the normalized doped diamond spectrum decreases after reaching a maximum at approximately 4600 Å while boron and boron carbide spectra maintain essentially a constant value after reaching their maximum level.

The results of these reflectance measurements are consistent with the blue color of the diamond observed after boron doping since the doped diamond sample apparently absorbs more of the orange and red wavelengths than does the undoped diamond sample. The blue color of six type IIb diamonds investigated by C. Clark et al[52] has also been shown to result from absorption which increases from the orange, through the red, and into the near infra-red portions of the spectrum. Furthermore, the boron and boron carbide spectra are sufficiently different from the doped diamond spectrum to indicate that the blue color resulting from the boron doping process cannot be attributed to surface boron or boron carbide.

The increased absorption of the doped diamond in the ultraviolet can tentatively be attributed to a shift of the absorption edge to slightly higher wavelenths by the presence of the acceptor level. Unfortunately, it was not possible to make measurements at wavelengths less than the absorption edge of undoped diamond (2200 Å or 5.6 eV) to test this hypothesis. Another useful measurement would be to measure the photoconductivity of the doped diamond over the ultraviolet, visible and near infrared regions to obtain information regarding the energy levels existing within the energy gap of the boron doped diamond.

The optical absorption measurements may be perturbed by the effect of particle size on the light scattering efficiency. The magnitude of the effect may be estimated by comparing the intensity of scattered light of the undoped and doped samples in the region of the spectrum where no absorption occurs, i.e., in the blue-green region at about 4500 Å. From Table 6.13 one can see that the doped sample scatters slightly more light, at most 6 percent more. This indicates that particle size effects are probably rather small and that the observed differences in intensity are caused by absorption.

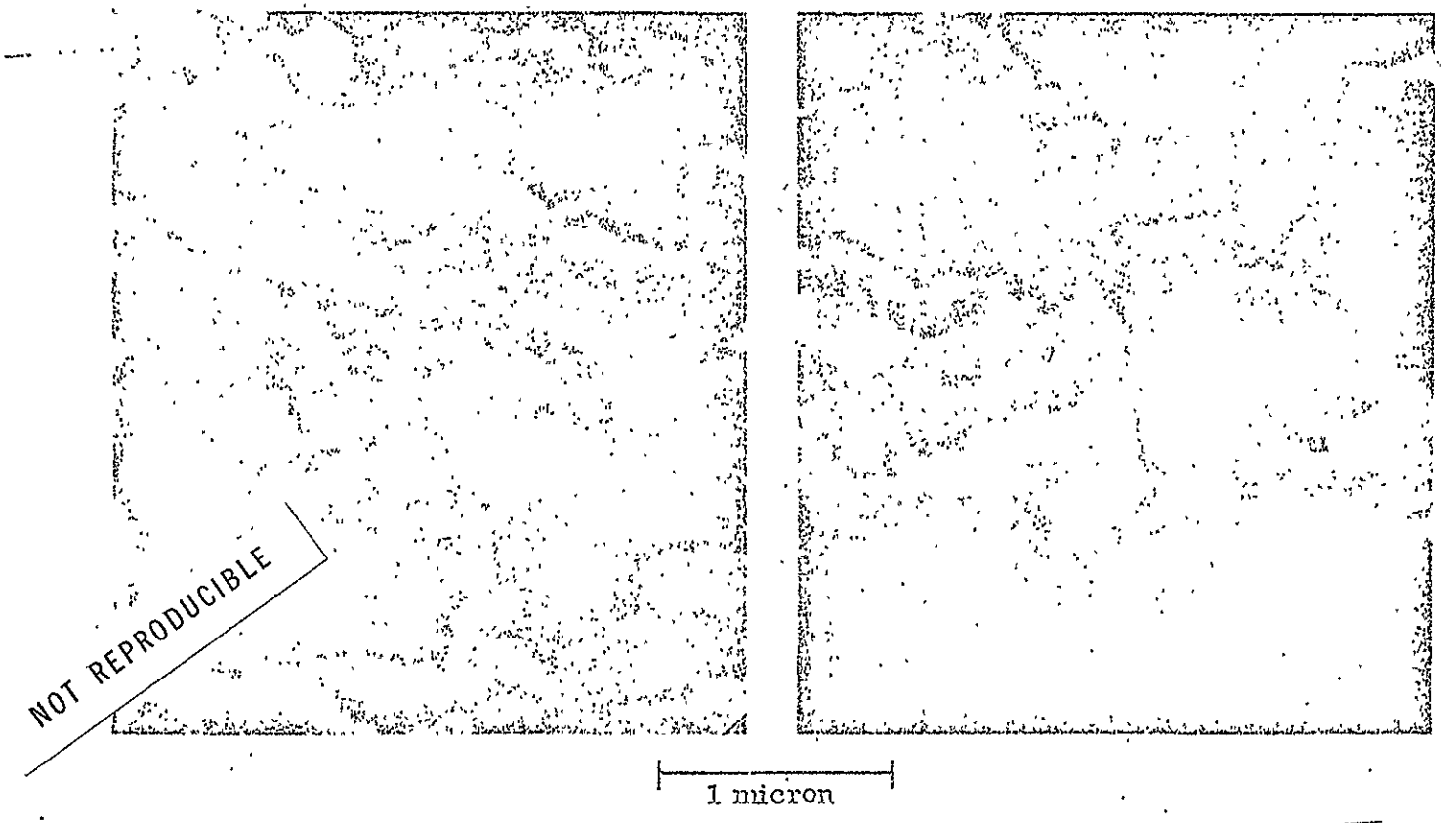

(a) Doped diamond shadowed with Au-Pd alloy. 30, 000X

(b) Undoped diamond shadowed with Au-Pd alloy. 30, 000X

Figure 6. 1. Scanning electron microscope photographs of shadowed doped and undoped diamond at 30, 000X magnification.

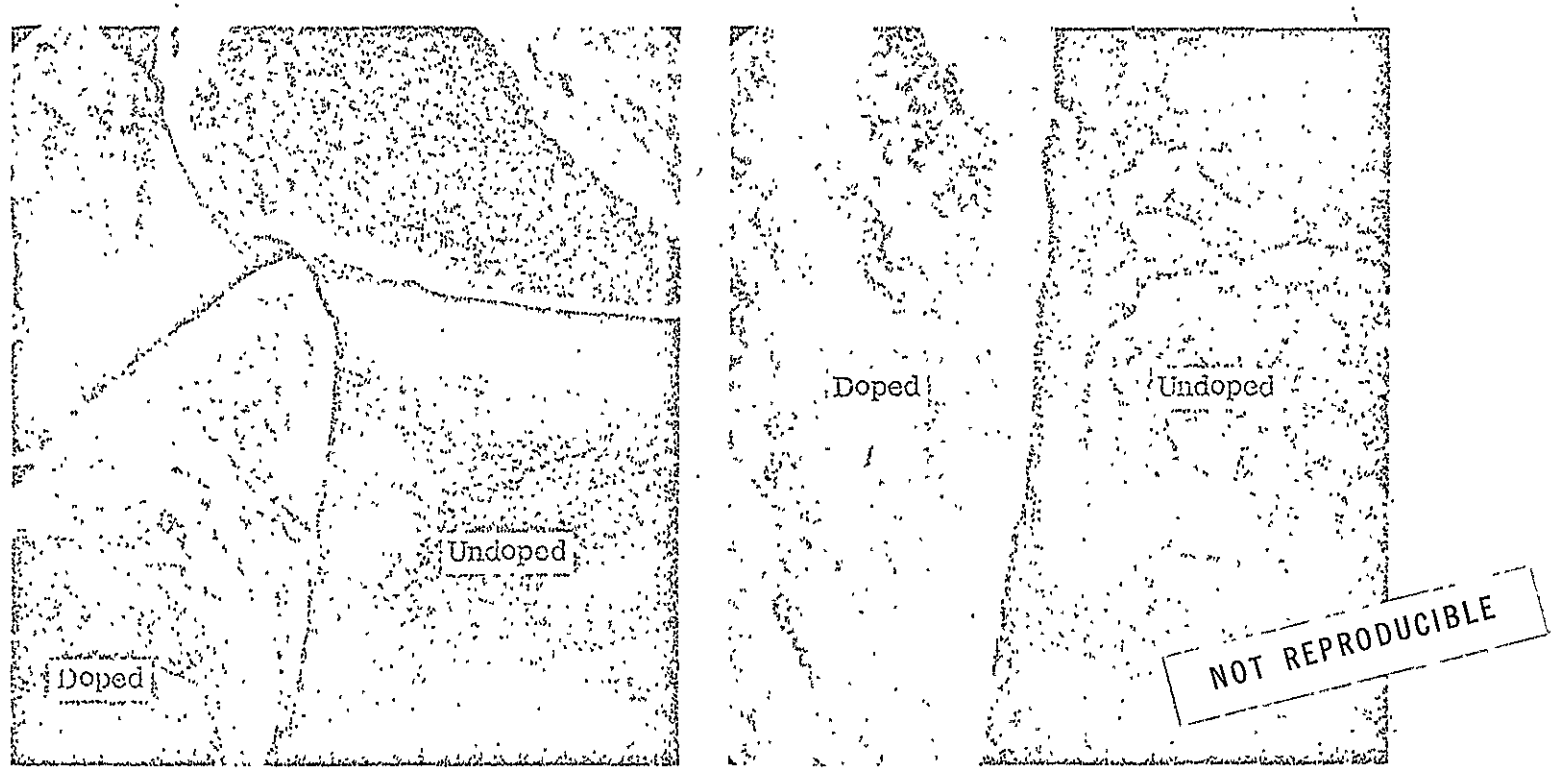

(a) Doped and undoped diamond; no shadowing. 100X

(b) Doped and undoped diamond; no shadowing. 500X

Figure 6. 2. Scanning electron microscope photographs of unshadowed doped and undoped diamond.

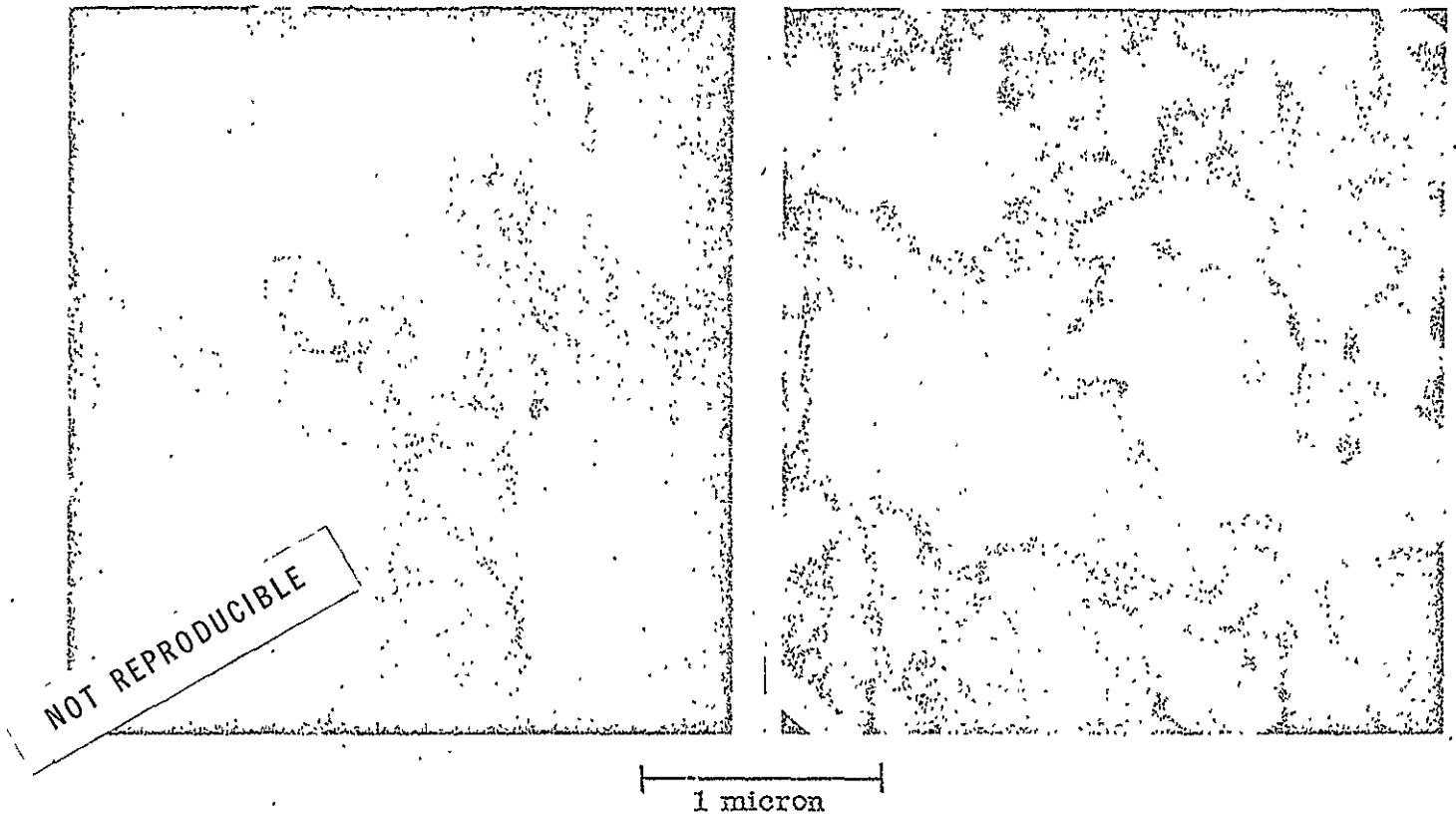

(a) Doped diamond; no shadowing. 30, 000X (b) Undoped diamond; no shadowing. 30, 000X

Figure 6. 3. Scanning electron microscope photographs of unshadowed doped and undoped diamond at 30, 000X magnification.

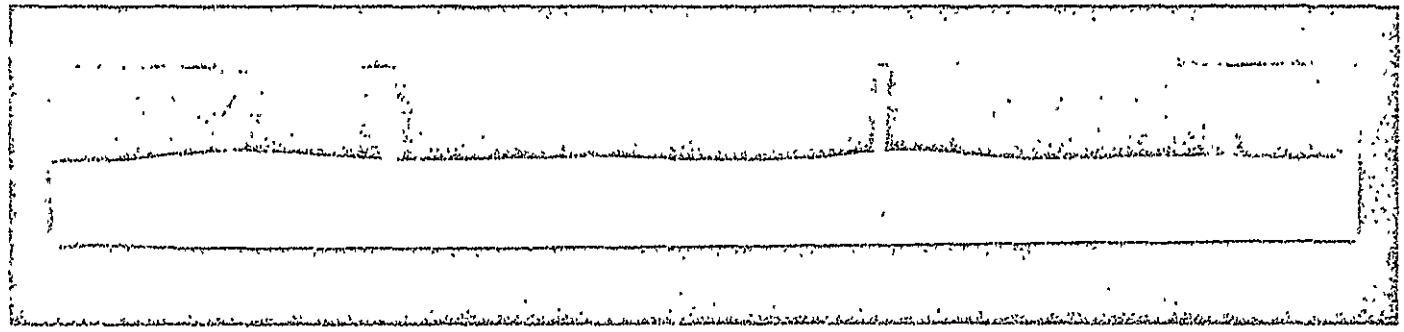

(a) Undoped diamond.

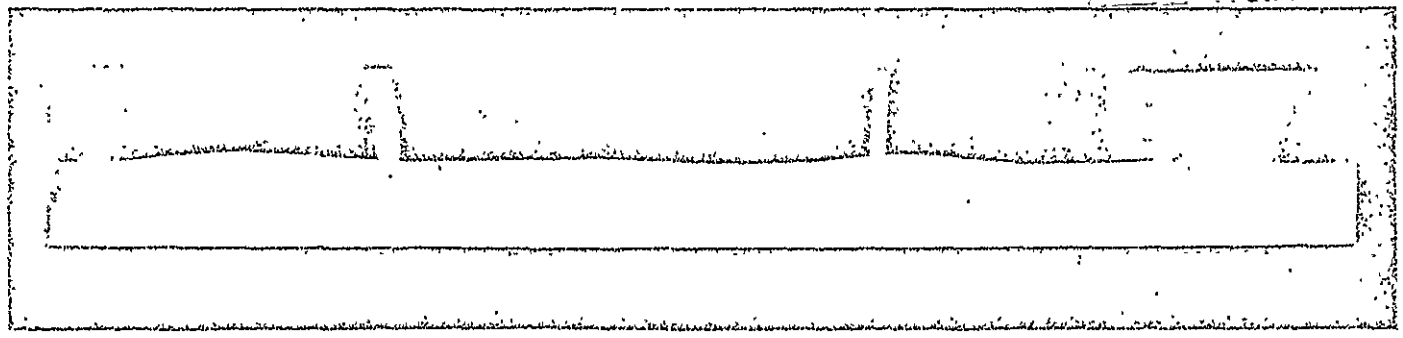

(b) Doped diamond.

Figure 6.4. X-ray diffraction powder pattern of diamond before and after doping.

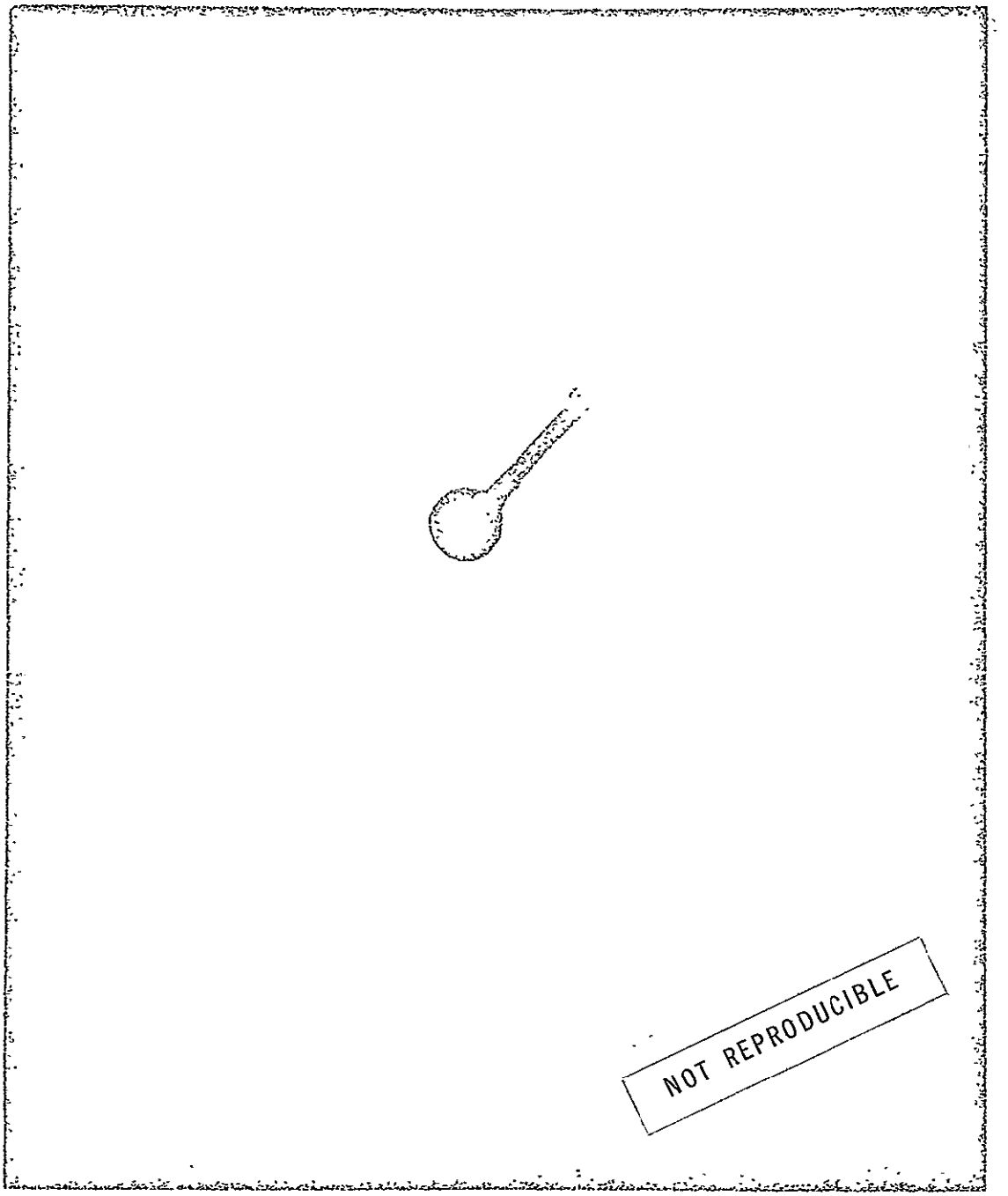

Figure 6.5. Electron diffraction pattern of undoped diamond.

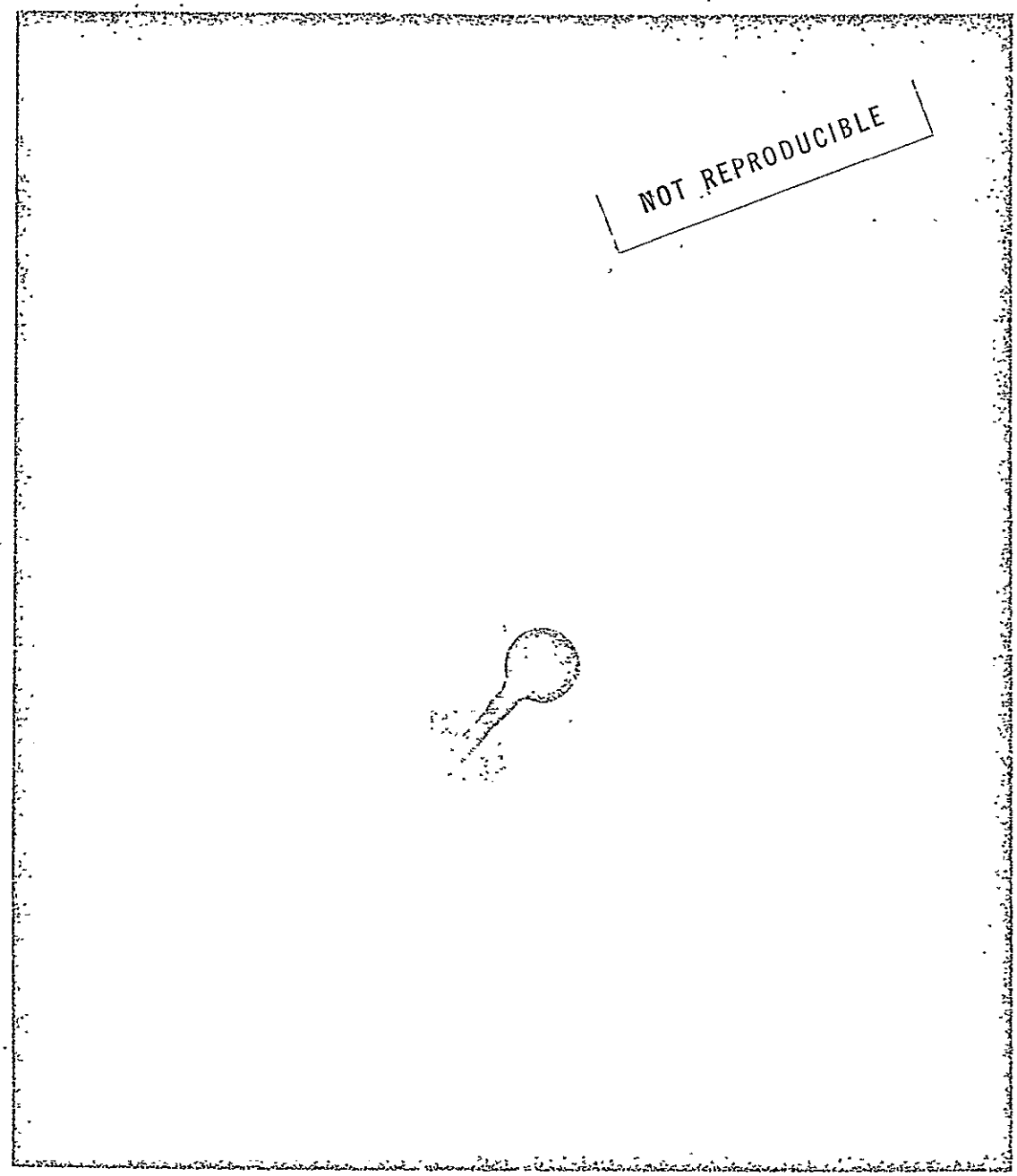

Figure 6. 6. Diffraction pattern of doped diamond.

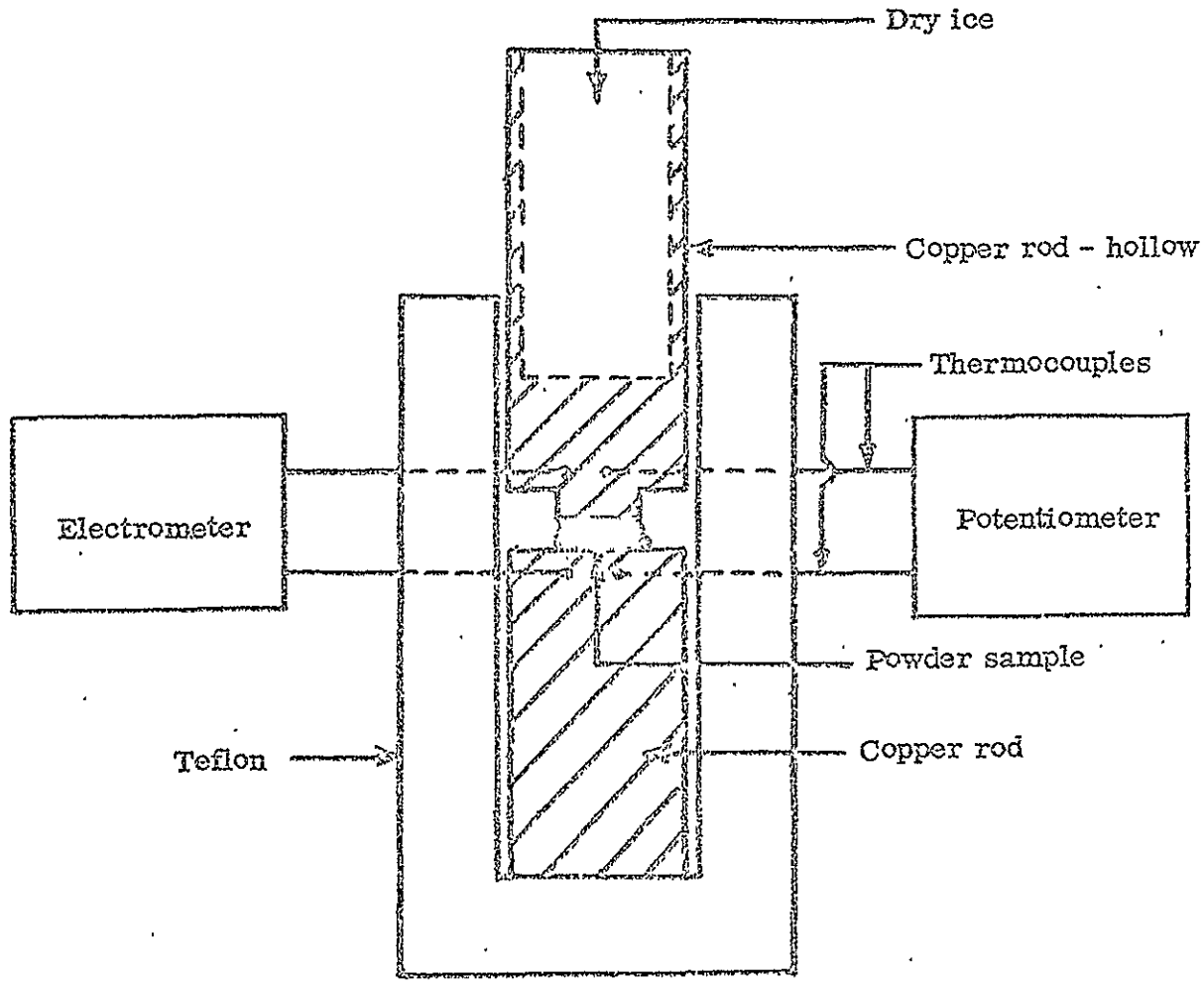

Figure 6.7. Schematic of experimental Seebeck coefficient apparatus.

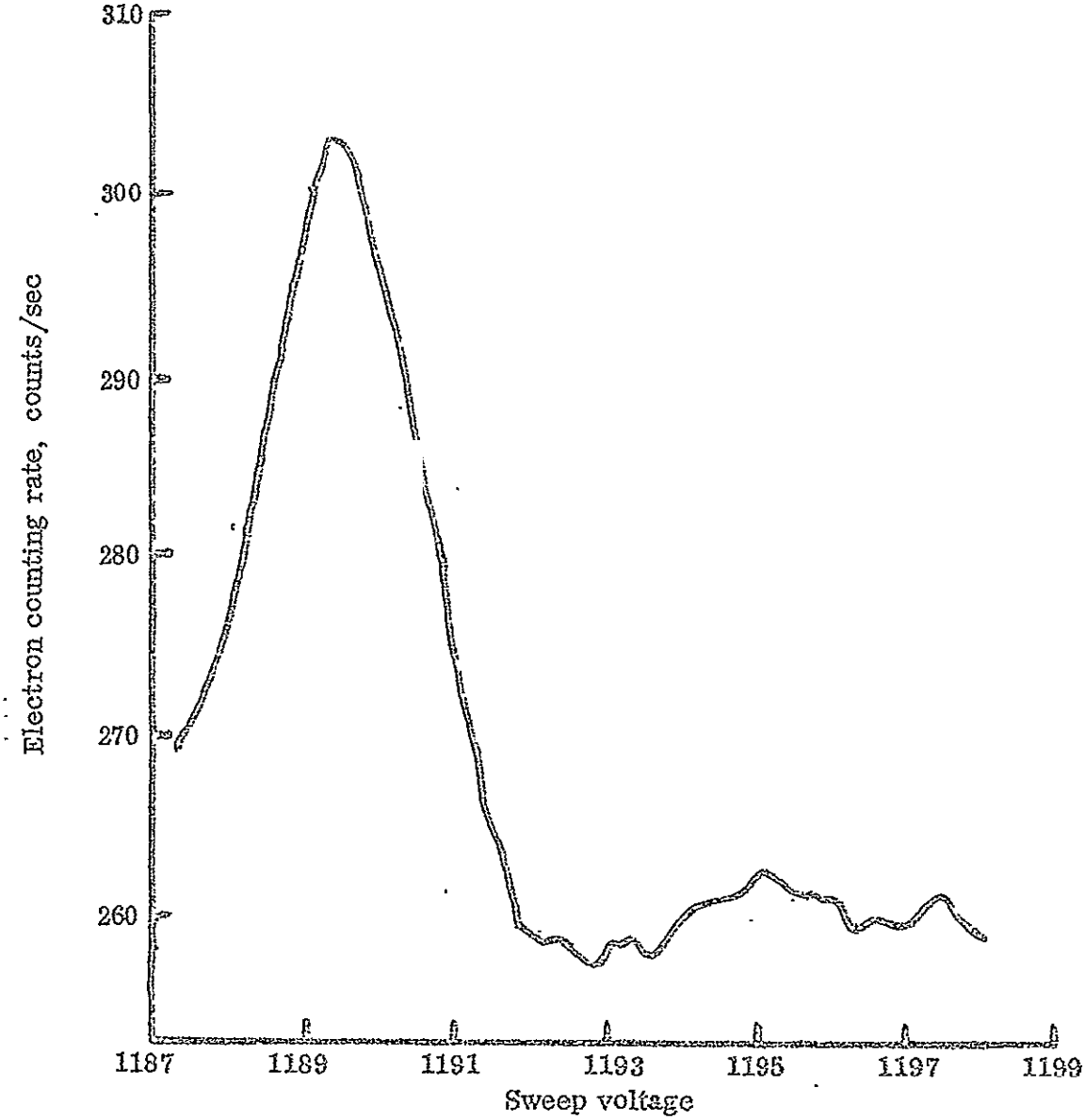

Figure 6.8. IEE boron spectrum for doped diamond.

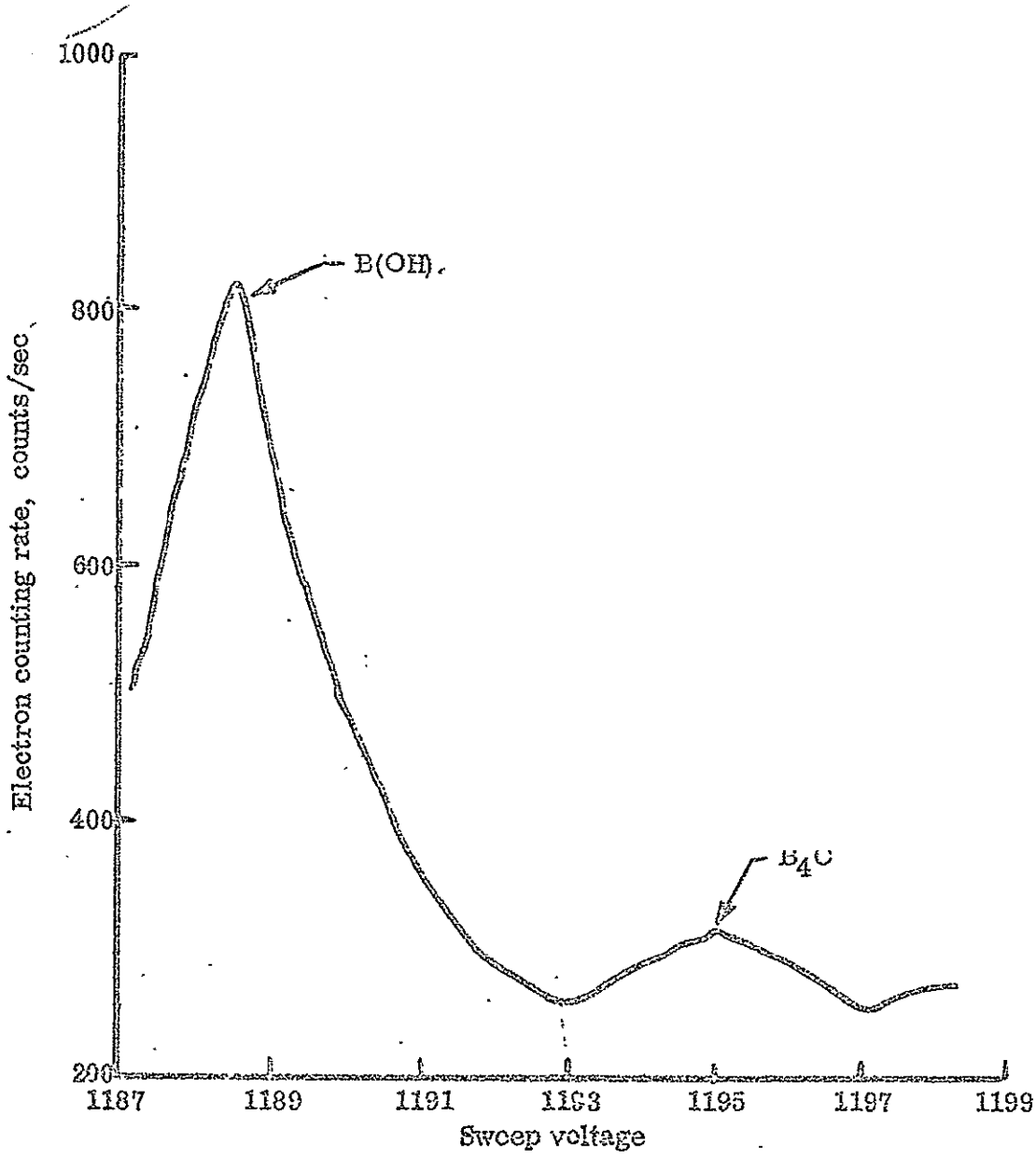

Figure 6.9. IEE boron spectrum for mixture of $B(OH)_3$ and B_4C.

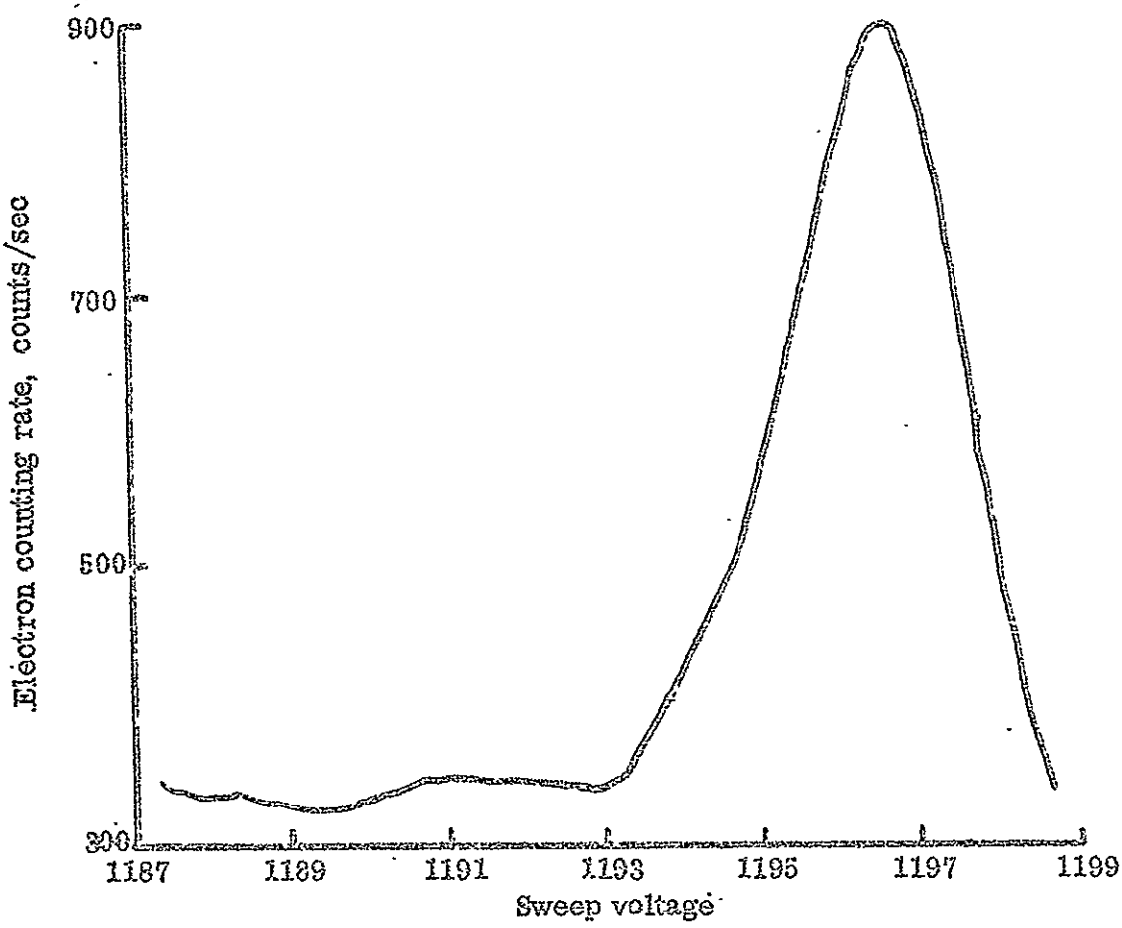

Figure 6.10. IEE boron spectrum for B_4C.

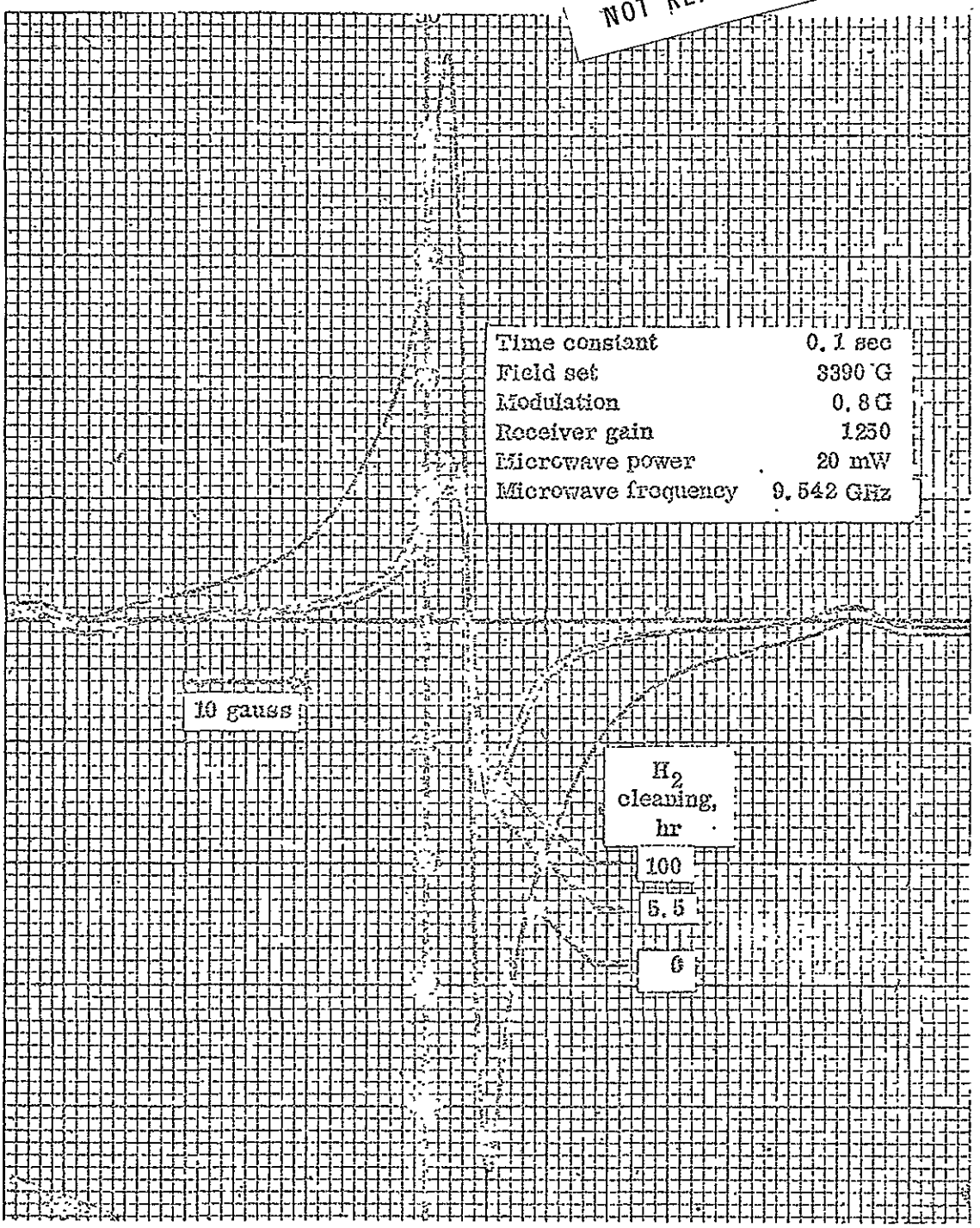

Figure 6.11. Electron spin resonance of annealed diamond (sample 5).

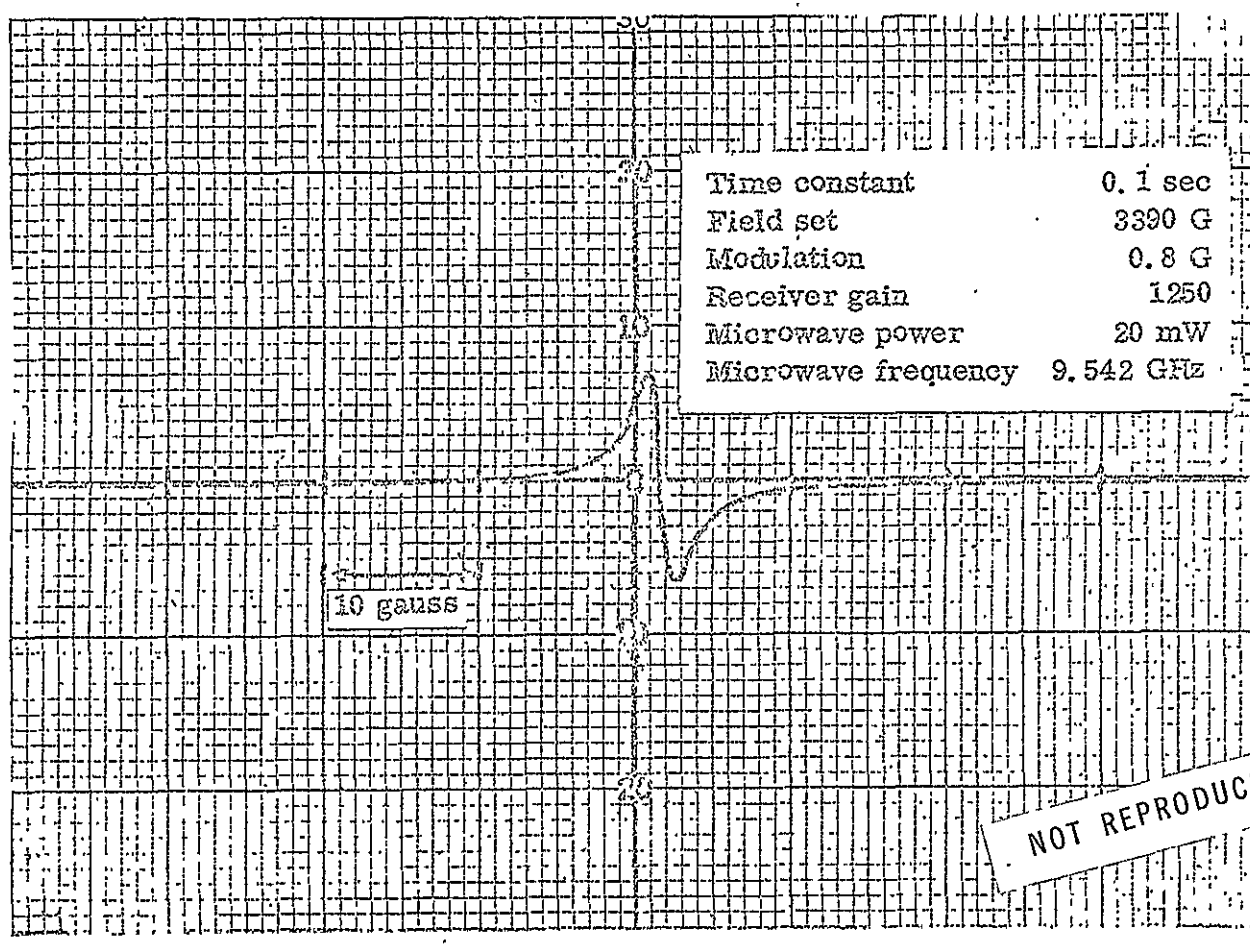

Figure 6.12. Electron spin resonance of strong-pitch reference (0.1% pitch in KCl).

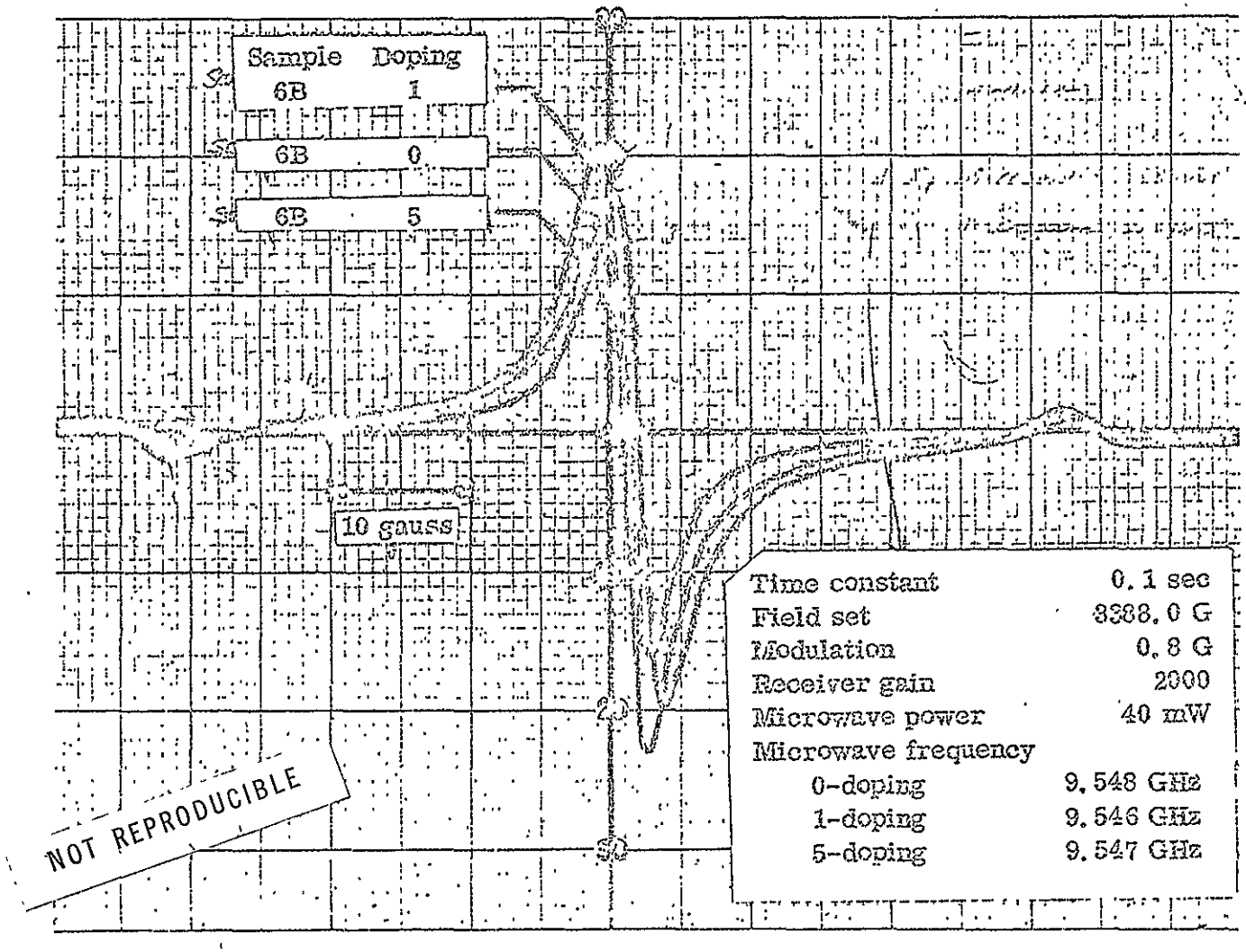

Figure 6.13. Electron spin resonance of doped and undoped diamond (sample 6B).

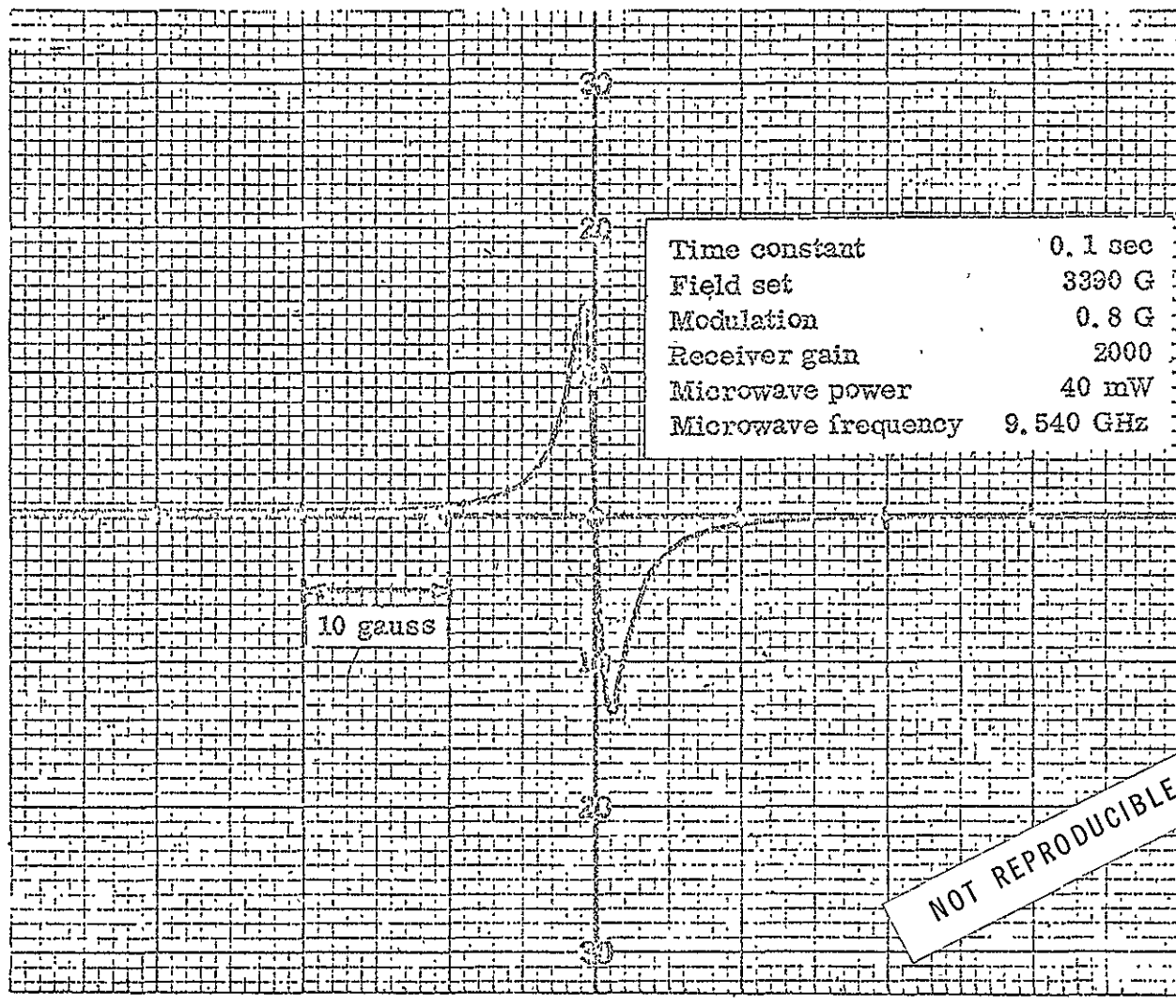

Figure 6.14. Electron spin resonance of strong-pitch reference (0.1% pitch in KCl).

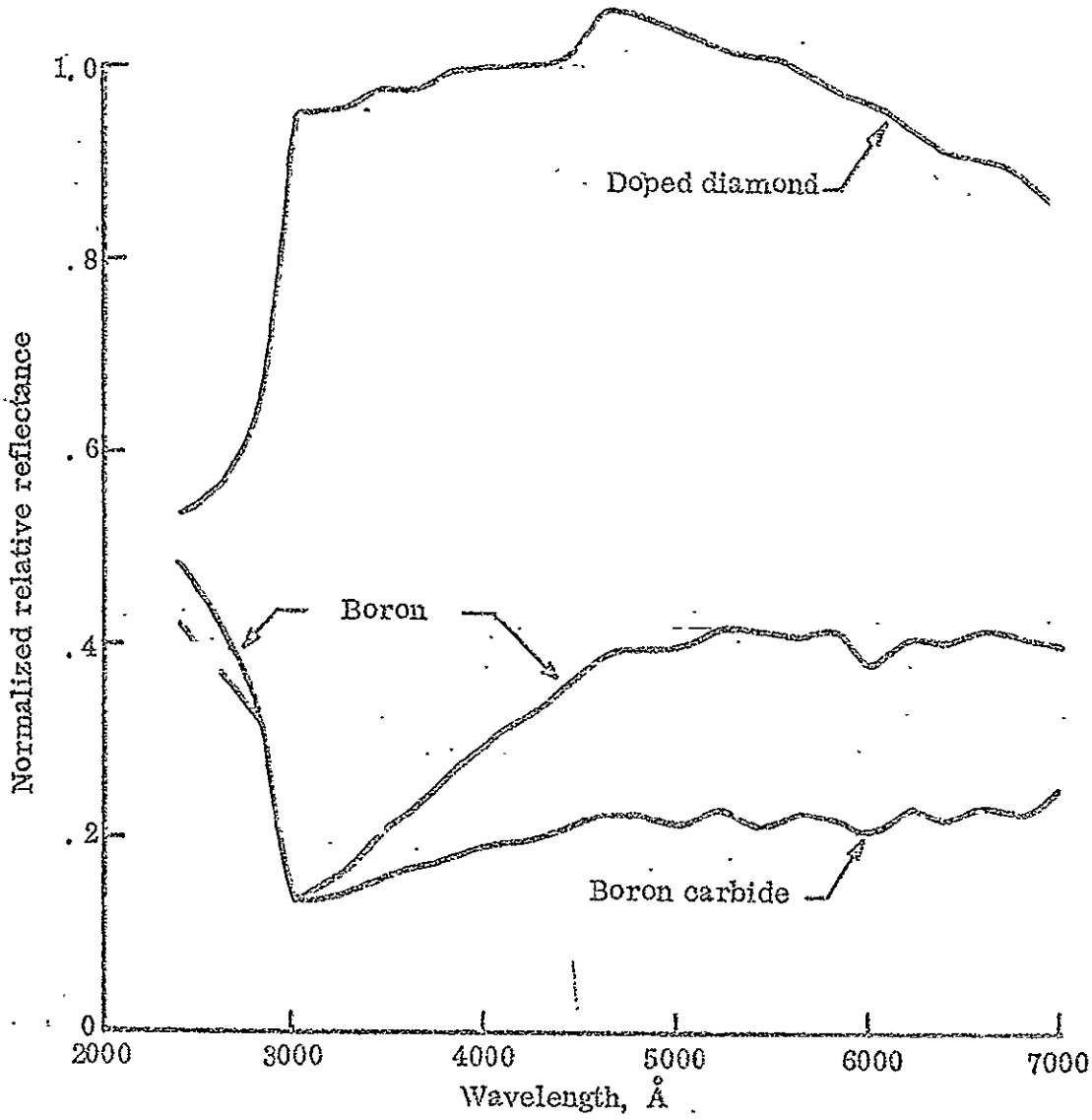

Figure 6.15. Normalized relative reflectance of boron doped diamond, boron, and boron carbide as a function of wavelength.

TABLE 6.1

X-RAY DIFFRACTION DATA

Lattice Spacing (Å)		Relative Intensity	Possible Impurities
Undoped	Doped		
5.867	Not detected	Weak	Not identified
4.310	4.314	Very weak	SiO_2
3.813	3.801	Very weak	SiO_2
3.685	3.672	Weak	Not identified
3.195	3.180	Weak	$Li_2B_2O_4$
3.035	Not detected	Weak	$Cu_3(Ge,Fe)S_4$, $BaSnO_4$
2.905	Not detected	Weak	$Li_2B_2O_4$, $BaSnO_4$
2.313	2.317	Weak	Cr
2.056	2.057	Very strong	Diamond, $BaSnO_4$, NiFe, Co_3V, Cr
1.938	1.947	Very weak	Not identified
1.924	1.915	Very weak	Co_3V
1.863	1.873	Very weak	$Cu_3(Ge,Fe)S_4$, Cr
1.782	Not detected	Weak	NiFe, Co_3V
1.711	1.708	Very weak	Not identified
1.592	1.594	Very weak	$Li_2B_2O_4$, $Cu(Ge,Fe)S_4$
1.537	Not detected	Very weak	Not identified
1.521	Not detected	Weak	Not identified
1.449	Not detected	Very weak	Not identified
1.324	1.338	Weak	Not identified
1.301	1.295	Very weak	Not identified
1.279	Not detected	Very weak	Cr
1.260	1.260	Very strong	Diamond, NiFe
1.234	1.228	Very weak	Cr

TABLE 6.2

ELECTRON DIFFRACTION DETERMINATION OF LATTICE SPACINGS FOR UNDOPED DIAMOND

Indices (h k l)	Angular Diffraction of Electron Beam, θ (degrees)	Lattice Plane Spacing (Angstroms) and Relative Line Intensities			
		Experimental		Theoretical	
		Spacing	Intensity[a]	Spacing	Intensity
111	0.5127	2.067	v.s.	2.060	100
220	.8397	1.262	s	1.262	27
311	.9854	1.976	s	1.076	16
111	1.0208	1.038	v.w.	(b)	
400	1.1885	.892	v.w.	0.892	7
331	1.3021	.814	w	.819	15
422	1.4598	.726	w	.728	
511, 333	1.5457	.686	w	.687	
440	1.6779	.632	v.w.	.631	
531	1.7616	.602	v.w.	.603	
620	1.8761	.565	v.w.	.564	
533	1.9509	.543	v.w.	.544	
444	Not detected			.515	
711, 551	2.1136	.502	v.w.	.500	
642	2.2147	.479	v.w.	.477	
731, 553	2.2806	.465	v.w.	.465	

(a) Abbreviations: v.s., very strong; s, strong; w, weak; v.w., very weak.

(b) This line is believed to be a weak second order reflection from the 111 plane.

TABLE 6.3

ELECTRON DIFFRACTION DETERMINATION OF LATTICE SPACINGS FOR DOPED DIAMOND

Indices (h k l)	Angular Diffraction of Electron Beam, θ (degrees)	Lattice Plane Spacing (Angstroms) and Relative Line Intensities			
		Experimental		Theoretical	
		Spacing	Intensity[a]	Spacing	Intensity
111	0.5114	2.073	v.s.	2.060	100
220	.8383	1.264	s	1.262	27
311	.9852	1.076	s	1.076	16
111	1.0269	1.032	v.w.	(b)	
400	1.1847	.894	v.w.	0.892	7
331	1.2986	.816	w	.819	15
422	1.4585	.727	w	.728	
511, 333	1.5460	.686	w	.687	
440	1.6817	.630	v.w.	.631	
531	1.7561	.604	v.w.	.603	
620	1.8785	.564	v.w.	.564	
533	1.9484	.544	v.w.	.544	
444	Not Detected			.515	
711, 551	2.1188	.500	v.w.	.500	
642	2.2192	.478	v.w.	.477	
731, 553	2.2737	.466	v.w.	.465	

[a] Abbreviations: v.s., very strong; s, strong; w, weak; v.w., very weak.

[b] This line is believed to be a weak second order reflection from the 111 planes.

TABLE 6:4

THEORETICAL LATTICE SPACINGS FOR BORON CARBID

Indices (h k l)	Lattice Plane Spacing (Angstroms)	Relative Line Intensity
101	4.49	30
003	4.02	40
012	3.79	70
110	2.81	30
104	2.57	80
021	2.38	100
113	2.30	10
006	2.02	10
211	1.82	10
205	1.714	30
116	1.637	10
107	1.628	10
303	1.505	20
125	1.463	30
018	1.446	30
027	1.407	30
220	1.403	30
009	1.345	20
131	1.342	20
223	1.326	20
208	1.286	10
306	1.261	20
042	1.191	10

TABLE 6.5

OBSERVED LATTICE SPACINGS FOR WHITE CARBON

Lattice Spacing (Angstroms)	Relative Intensity[a]
4.47	v.v.s.
4.26	v.v.s.
4.12	v.s.
3.71	m
3.22	m
3.03	s
2.94	w
2.55	s
2.46	m
2.28	s
2.24	m
2.10	m
1.983	w
1.910	w
1.496	w
1.370	w
1.289	w
1.26	w
1.197	m
1.184	m
1.080	w
0.8642	w

[a] Abbreviations: v.v.s., very, very strong; v.s., very strong; s, strong; m, medium; w, weak

TABLE 6.6

CHEMICAL ANALYSIS OF DOPED AND UNDOPED DIAMOND

Ledoux & Company
INC. 1880

CABLE ADDRESS "LLDOUX TEANECK"
TWX 201 833 0676

359 Alfred Avenue, Teaneck, New Jersey 07666 • Telephones: 201 837 7160
212 947 0955

INDEPENDENT CONTROL, AND RESEARCH CHEMISTRY, INSTRUMENTAL AND CHEMICAL ANALYSIS • SAMPLING, WEIGHING, SHIPPERS' REPRESENTATION, BENEFICIATION, AND STORAGE OF ORES AND METALS

KH REPORT OF ANALYSIS

No. 905202

October 26, 1970

Our analysis of the sample of DIAMOND POWDER Date Received: 9/21/70

From Case Western University

Marked: Samples: 6-0 (undoped Diamond Powder) and 6-6 (doped Diamond Powder)
P.O.-F-22252

and submitted to us, shows:

BY SPECTROGRAPHIC ANALYSIS

	#6-0	—	#6-6
BORON	0.001%		0.01%
SILICON	0.006%		0.02%
PHOSPHORUS	0.005%		0.0002%

Note: Other elements not detected

* * *

To Case Western University

LEDOUX & COMPANY

FORM 5A COH 6-70 P. E.

TABLE 6.7

THEORETICAL COMPOSITE DENSITY OF DOPED SAMPLE ASSUMING 8.98 PERCENT WEIGHT INCREASE IS DUE TO DEPOSITION OF VARIOUS SPECIES

Species	Species density g/cm^3	Theoretical Density of Doped Sample Assuming Growth Attributed to a Given Species
Surface boron	2.34 - 2.37	3.364 - 3.369
Boron carbide	2.52	3.395
Boric oxide	2.45 - 2.47	3.383 - 3.387
Boron nitride	2.25	3.346
Graphite	1.3 - 2.265	3.049 - 3.349
Quartz	2.60	3.416
Silicon carbide	3.20	3.486
Silicon nitride	3.43	3.508

TABLE 6.8

MEASURED DENSITY OF DIAMOND BEFORE AND AFTER DOPING

Run No.	Density (g/cm^3)		Pycnometer
	Undoped	Doped	
1	3.510	3.515	72
2	3.507	3.511	72
3	3.498	3.499	72
4	3.487	3.490	6
5	3.492	3.495	6
6	3.518	3.511	6

TABLE 6.9

SEEBECK COEFFICIENT FOR BORON DOPED DIAMOND AFTER ONE DOPING RUN
(4.57 PERCENT WEIGHT GAIN)

Temperature (°C)		Temperature Differential °C	Seebeck Voltage, +V(volts)	Relative Seebeck Coefficient (μV/°C)
Cold Junction	Hot Junction			
22.8	22.8	0	0	---
13.9	22.8	8.9	0.0023	258
10.0	22.2	12.2	.0031	254
7.5	20.3	12.8	.0037	289
5.0	19.5	14.5	.0042	290
3.3	18.9	15.6	.0052	334
0	18.3	18.3	.0057	311
-2.8	18.3	21.1	.0064	306
-5.5	17.8	23.3	.0068	292
-8.1	16.6	24.7	.0072	291
-10.6	14.4	25.0	.0077	308
-13.3	12.8	26.1	.0082	314
-16.1	12.8	28.9	.0087	301
-21.6	10.6	32.2	.0095	295
-25.5	10.0	35.5	.0105	296

ave = 296 μV/°C

TABLE 6.10

SEEBECK COEFFICIENT FOR BORON DOPED DIAMOND AFTER SIX DOPING RUNS
(9.86 PERCENT WEIGHT GAIN)

Temperature (°C)		Temperature Differential °C	Seebeck Voltage, +V(volts)	Relative Seebeck Coefficient (μV/°C)
Cold Junction	Hot Junction			
22.8	22.8	0	0	---
13.9	19.7	5.8	0.0005	86
8.4	19.2	10.8	.0014	130
4.5	19.2	14.7	.0017	116
1.7	19.2	17.5	.0020	114
-3.9	19.2	23.1	.0027	117
-7.8	18.6	26.4	.0030	114
-11.1	18.3	29.4	.0037	126
-14.7	17.7	32.4	.0042	130
-15.5	17.2	32.7	.0042	128
-18.9	16.7	35.6	.0048	135
-23.3	16.7	40.0	.0050	125

ave = 296 μV/°C

TABLE 6.11

SEEBECK COEFFICIENT OF BORON CARBIDE

Temperature (°C)		Temperature Differential °C	Seebeck Voltage, +V(volts)	Relative Seebeck Coefficient (μV/°C)
Cold Junction	Hot Junction			
23.9	23.9	0	0	---
10.6	20.1	9.5	0.0004	42
-11.1	18.1	29.2	.0013	45
-14.2	17.6	31.8	.0015	47
-16.1	17.2	33.3	.0018	54
-21.6	16.4	38.0	.0020	53

TABLE 6.12

ULTRAVIOLET RADIATION[a] USED FOR FLUORESCENCE TEST

Wavelength (Å)	Relative Energy	Energy (eV)
2224	14.0	5.58
2320	8.0	5.35
2360	6.0	5.25
2380	8.6	5.21
2400	7.3	5.17
2482	8.6	5.00
2537	16.6	4.89
2571	6.0	4.82
2652-2655	15.3	4.68-4.67
2700	4.0	4.59
2753	2.7	4.50
2804	9.3	4.42
2894	6.0	4.29
2967	16.6	4.18
3022-3028	23.9	4.10
3126-3132	49.9	3.96
3341	9.3	3.71
3650-3663	100.0	3.40-3.39
4045-4078	42.2	3.07-3.04
4358	77.5	2.84
5461	93.0	2.27
5770-5790	76.5	2.15-2.14
10,140	40.6	1.22
11,287	12.6	1.10
13,673	15.3	0.91

[a]The ultraviolet radiation source was a 550 watt Hanovia, Type A medium pressure mercury lamp.

TABLE 6.13

OPTICAL MEASUREMENTS

Wavelength (Å)	Sensitivity	Relative Reflectance				Normalized[a] Relative Reflectance		
		Undoped Diamond	Doped Diamond	Boron	Boron Carbide	Doped Diamond	Boron	Boron Carbide
2400	6	36.0	14.2	17.5	15.3	0.532	0.486	0.425
2600	5	62.0	34.7	26.2	23.1	.560	.423	.373
2800	4	32.5	20.7	11.3	10.7	.637	.348	.329
3000	3	79.7	75.8	10.8	10.7	.951	.135	.134
3200	2	40.2	38.3	6.0	5.3	.953	.149	.132
3400	2	53.2	51.9	10.2	8.1	.975	.192	.152
3600	2	66.3	64.5	15.0	11.0	.973	.226	.166
3800	2	72.8	72.4	19.3	13.0	.995	.265	.178
4000	2	70.8	70.8	21.2	13.5	1.00	.299	.191
4200	2	66.7	66.9	21.7	13.1	1.00	.325	.196
4400	2	57.5	58.1	20.4	11.9	1.01	.355	.207
4600	2	57.5	61.0	22.3	12.9	1.06	.388	.224
4800	2	53.3	55.8	21.2	12.0	1.05	.398	.225
5000	2	33.0	34.2	13.1	7.0	1.04	.398	.212
5200	3	91.0	93.2	38.0	21.1	1.02	.418	.232
5400	3	71.3	72.0	29.8	15.4	1.01	.418	.216
5600	3	53.6	53.8	22.0	12.1	1.00	.410	.226
5800	3	39.9	39.0	16.6	8.9	.978	.416	.223
6000	4	75.8	73.3	32.2	17.8	.967	.377	.208
6200	4	60.7	56.8	24.8	14.1	.936	.408	.232
6400	4	31.3	28.5	12.8	6.9	.911	.408	.220
6600	5	67.3	60.9	28.0	15.7	.905	.416	.233
6800	5	36.3	32.0	14.9	8.1	.882	.410	.223
7000	6	47.7	40.7	19.0	12.0	.853	.398	.252

[a]Normalized with respect to undoped diamond.

CHAPTER VII

SUMMARY OF RESULTS

7.1 Summary of Diamond Doping Experiments

The first known attempt to grow boron doped diamond by vapor phase deposition has been accomplished by passing a gaseous mixture of 0.83 percent diborane in methane over a bed of nonconducting natural diamond seed crystals of 0 to 1 micron nominal size at 1050° C and 0.2 Torr. The growth of diamond at this temperature and pressure by vapor phase deposition using methane has been previously demonstrated.[1,2]

A consistent decrease in growth rate, resulting eventually in zero growth rates, limited the cumulative weight increase to approximately ten percent during the boron doping runs. Although this growth rate trend was also observed during the expitaxial diamond growth experiments of H. Will,[2] it was not nearly as pronounced. Since initial growth rates during the boron doping runs were as large or larger than those obtained in the epitaxial diamond growth experiments, it appears that the boron doping process alters the diamond surface in such a way as to decrease the rate of diamond growth. The mechanism responsible for this affect is not known.

However, it is probable that active surface sites are filled up as growth proceeds, making further growth more difficult.

A distinct change in color of the diamond samples was observed except for initial samples of diamond which were highly contaminated with tungsten. The diamond seed crystals, which were initially a gray or off-white color, turned light blue as a result of the boron doping experiments. The blue color appeared after one doping run and became somewhat more intense during subsequent doping runs.

7.2 Summary of Experimental Analyses

In order to evaluate the physical, chemical, and electrical properties of the blue diamonds resulting from the boron doping experiments, the following tests were performed:

1. Chemical etching tests
2. Scanning electron microscopy
3. X-ray diffraction
4. Electron diffraction
5. Chemical analysis
6. Density measurements
7. Seebeck coefficient measurements
8. Induced electron emission spectroscopy
9. Electron spin resonance
10. Fluorescence tests
11. Optical absorption measurements

A. Chemical Etching Tests

Chemical etching tests were made using aqua regia, hydrofluoric acid, nitric acid, and fused alkali. No weight change or visible change in the blue color of the doped diamond was detected after the chemical etching tests.

B. Scanning Electron Microscopy

Scanning electron microscopy was used to obtain surface details on diamond samples before and after doping in an attempt to use this information to explain the decreasing growth rates observed during the doping experiments. Although the scanning electron microscope photographs did not show sufficient detail to distinguish differences in diamond surface detail before and after doping, the superior resolution obtainable for the boron doped diamond sample qualitatively demonstrates the increased conductivity of the doped sample.

C. X-ray Diffraction

X-ray diffraction powder patterns were obtained on diamond samples before and after boron doping experiments. In addition to the two intense diamond lines, several other weak diffraction lines appear in both the undoped and doped diamond samples. The weak lines are most likely due to small quantities of impurities in the X-ray target material since no lines other than those of diamond were observed in the electron diffraction studies.

D. Electron Diffraction

Electron diffraction on diamond samples before and after the boron doping experiments revealed the first fourteen lattice plane spacings of diamond. No lines other than those of diamond were found for either the undoped or doped diamond samples. This indicates that the weak impurity lines observed in the X-ray diffraction

patterns were most likely due to impurities in the X-ray target material.

E. Chemical Analysis

Emission spectrographic analysis indicates that the boron concentration increased from 0.001 to 0.01 percent during a series of six boron doping runs. This increase in boron concentration corresponds to a boron doping level between 1010 and 100 ppm depending upon the extent of boron diffusion from the new growth layer into the original diamond seed crystal. The concentration of silicon also increased from 0.006 to 0.02 percent after six doping runs. The increase in silicon content may be due either to the chemical dissociation, devitrification, or mechanical abrasion of the quartz deposition apparatus. The concentration of phosphorus decreased from 0.005 percent before doping to 0.0002 percent after the six doping runs. No other elements were detected by spectrochemical analysis.

F. Density Measurements

The density of a diamond sample before and after six boron doping runs was measured. The average of six density measurements on undoped diamond sample was 3.502 g/cm^3, whereas the average density after six boron doping runs was 3.504 g/cm^3 indicating that the density of the diamond sample is essentially unchanged by boron doping. A statistical analysis using the Student's t-distribution excluded the possibility that the weight increases during the boron doping

experiments can be attributed to the formation of B, B_4C, B_2O_3, BN, SiO_2, or SiC at a confidence level of 95 percent. The density measurements alone do not eliminate the possibility of silicon nitride, however, since its density is very close to that of diamond.

G. Seebeck Coefficient

The Seebeck coefficient of the diamond before boron doping could not be measured due to its high resistivity. After one doping run, a Seebeck coefficient of approximately 296 $\mu V/^oC$ was observed, indicating a carrier concentration of approximately 10^{18} to 10^{21} per cm^3 depending on the effective mass of the carrier. This concentration of carriers is consistent with the observed boron weight increase determined by chemical analysis. The measured Seebeck coefficient of this sample dropped to approximately 120 $\mu V/^oC$ after six boron doping runs. The doped diamond behaved as a p-type material based on the sign of the induced Seebeck voltage. Similar measurements on a sample of boron carbide indicated that it was also a p-type material; however, its Seebeck coefficient was only 48 $\mu V/^oC$.

H. Induced Electron Emission

Induced electron emission spectroscopy was used to determine the boron content and the nature of its chemical bond in doped diamond samples. Initial doped diamond samples analyzed by this technique indicated a high level of boron doping with a bonding energy of the boron atoms near the surface approximately equal to that in B_2O_3.

Since the binding energy of B dissolved in diamond is not available from independent measurements it is not possible to say whether the surface boron atoms are oxidized or not.

I. Electron Spin Resonance

High temperature annealing effects tended to mask the changes in electron spin resonance spectra due to the boron doping process in diamond. Comparison of ESR data for an undoped sample and one that had undergone one boron doping run indicated a slight increase in paramagnetic spins after doping. However, the subsequent decrease in the ESR signal after six doping runs cannot be explained unless it is attributed to the annealing process still being in effect after approximately 150 hours at temperatures in excess of 1030° C.

J. Fluorescence

Samples of diamond before and after boron doping runs were exposed to ultraviolet and visible radiation to determine if fluorescent emission could be observed. No fluorescence was observed and there was essentially no difference between the fluorescence spectra of doped and undoped diamond samples.

K. Optical Measurements

Samples of undoped diamond, boron doped diamond, boron and boron carbide were exposed to incident radiation having wavelengths from 2400 to 7000 Å, and the reflected energy spectra were obtained.

The results show increased absorption by the doped diamond in the red end of the optical spectrum and in the ultraviolet, thus confirming the visual observation of a blue color. These tests also gave further evidence that the properties exhibited by the boron doped diamonds can not be attributed to the formation of boron or boron carbide during the doping process.

7.3 Concluding Remarks

The boron doping of nonconducting natural diamond seed crystals by vapor deposition produced blue diamonds which appeared to be p-type semiconductors based on the sign of the measured Seebeck voltage. It is believed that the blue color obtained in these experiments indicates that boron doping of diamond has occurred since boron doping by the growth or diffusion methods[11,12] also resulted in the production of blue semiconducting diamonds. Emission spectrochemical analysis of the diamond before and after doping indicates that the boron concentration increased tenfold during the boron doping runs. Carrier concentrations estimated from measured Seebeck coefficients of the doped diamonds are consistent with the boron concentration determined by chemical analysis. No impurities other than silicon and phosphorus were detected by spectrochemical analysis and no crystalline impurities were detected by X-ray and electron diffraction studies of diamond before and after doping. Furthermore, density measurements eliminate, at the 95 percent confidence level, the possibility that the weight increases obtained

during a series of boron doping runs can be attributed solely to the formation of B, B_4C, B_2O_3, BN, Si, SiO_2, or SiC. Silicon nitride, however, cannot be ruled out on this basis alone; however, the presence of silicon nitride was not detected by X-ray or electron diffraction patterns and only trace amounts of silicon were detected by spectrochemical analysis. In addition, the chemical etching tests indicate that the observed weight increases during the boron doping experiments cannot be attributed to substances soluble in aqua regia, nitric acid, or hydrofluoric acid such as B, B_2O_3, and Si_3N_4. Scanning electron microscopy qualitatively indicated the increase in conductivity resulting from the boron doping runs although an explanation for the decrease in growth rates could not be obtained by examination of the diamond surface using this technique. Optical measurements provided additional evidence that the properties observed for the boron doped diamonds cannot be attributed to the formation of boron or boron carbide during the boron doping process.

The runs using one percent B_2H_6 in H_2 at otherwise identical conditions gave no indication of doping or the formation of boron carbide from the reaction of diborane with the diamond. Furthermore, there was no evidence of the formation of boron carbide on any portions of the deposition apparatus during either the B_2H_6 in CH_4 or the B_2H_6 in H_2 doping runs. This is further confirmation that the boron is incorporated into the new structure as it is grown.

Although the data indicate that boron doped semiconducting diamond has been obtained by the boron doping experiments performed in this study, the ESR spectra and the absence of fluorescence in the boron doped samples cannot be explained at this time.

CHAPTER VIII

FUTURE WORK

The optical absorption study was limited to a minimum wavelength of 2400 Å. Additional data should be obtained for wavelengths less than 2400 Å to compare the absorption spectra of doped and undoped diamond in the region of the energy gap. Furthermore, photoconductivity measurements should be made to determine the positions of energy levels within the energy gap.

The requirement to use fine diamond powders for these boron doping experiments in order to obtain measurable growth rates, precludes analysis of the doped diamond layers by conventional methods such as resistivity and Hall effect measurements. A method must be developed to increase diamond growth rates during vapor deposition and to prevent the decreasing growth rates observed for successive doping runs. If growth rates are improved, then boron doped layers can be deposited on diamond macle surfaces. Measurements of conductivity, electron mobility, carrier concentration, and activation energy can then be readily made.

Attempts to grow n-type diamond semiconductors by vapor deposition should also be made. When the growth of n-type layers has demonstrated by this process, the formation p-n junctions can be

attempted. Selective masking procedures may lend themselves to production of p-n junctions by successive depositions of a p-type layer followed by deposition of an overlapping n-type layer.

APPENDIX A

EQUILIBRIUM CALCULATIONS

The equilibrium composition of the C-H-B system was calculated over a range of pressures, temperatures, and initial compositions in order to determine the conditions under which solid boron and diamond phases would be present. The calculations were also made to define the gas phase equilibrium composition that would exist during the boron doping experiments on diamond. The results of these calculations were used to define in a general manner the proper conditions of temperature, pressure, and composition of the reactant gases for boron doping of diamond. Equilibrium mole fractions for the C-H-B system were determined for temperatures from 1000^{o} to 1600^{o} K, pressures from 0.01 to 0.0001 atm., and initial concentrations of B_2H_6 in CH_4 from 0.01 to 0.0001 percent by volume.

All chemical equilibrium calculations were made using an existing computer program obtained from NASA.[18-21] This program is based on determining the equilibrium composition of a reacting chemical system by minimizing the total free energy. Equations for the conservation of mass, the change in free energy across reactions that define the formation of each reaction product from its elements, and Dalton's law of partial pressures comprises a set of nonlinear

Tables A-2 through A-13. This temperature range adequately spans the boron doping temperature of 1325° K that was used for all boron doping runs in this investigation. Only those species whose equilibrium mole fraction exceed $1X10^{-8}$ are given in Tables A-2 through A-13. For those mole fractions that are less than 0.1, the negative exponent of 10 associated with the mole fraction is given to the right.

The equilibrium mole fractions for a mixture of B_2H_6 in CH_4 at pressures of 0.01, 0.001, 0.000263, and 0.0001 atm. for a 0.01 percent by volume initial concentration of B_2H_6 are given in Tables A-2 through A-5, respectively. Two solid phases, boron and diamond, are present at all temperatures from 1200° to 1450° K. The primary gas phase species present under these conditions are H_2, H, CH_2, CH_4, and C_2H_2. The major boron species present in the gas phase is BH_2. The mole fractions of all gas phase species, with the exception of H_2, are less than $0.7X10^{-3}$ over the range of temperatures and pressures specified in Tables A-2 through A-13.

Tables A-6 through A-13 give chemical equilibrium data similar to that presented in Tables A-2 through A-5. However, the data in Tables A-6 through A-9 pertain to an initial B_2H_6-CH_4 gas mixture that is 0.001 percent B_2H_6 by volume while the data in Tables A-10 through A-13 refer to an initial B_2H_6 concentration of 0.0001 percent by volume. It can be seen that the gas phase equilibrium compositions in Tables A-6 through A-13 are identical to the

compositions given in Tables A-2 through A-5 for the same temperature and pressure when both solid phases are present. This result is consistent with the Gibbs phase rule.

$$F = C + 2 - P \qquad (A-1)$$

The number of components, C, in a reacting chemical mixture is normally equal to the number of chemical elements constituting the system. Only when the elements appear in a constant ratio in all the products of reaction will the number of components differ from the number of elements. Three phases exist, two solid and one gas phase, over the range of temperature, pressure, and initial composition given in Tables A-2 through A-9. Therefore, two degrees of freedom exist. Thus, whenever two solid phases are present in the C-H-B system the equilibrium composition of the gas phase is fixed for a given temperature and pressure. For an initial B_2H_6 concentration of 0.0001 percent by volume the solid boron phase is not present at temperatures above approximately 1300^{o} K for a pressure of 0.01 atmospheres. The solid boron phase is also not present at temperatures above approximately 1350^{o} K for pressures of 0.001, 0.000263, or 0.0001 atmospheres. However, the diamond phase was present at equilibrium for all pressures, temperatures, and initial B_2H_6 compositions investigated.

The temperatures, pressures, and initial compositions of the B_2H_6-CH_4 reaction mixture for which the solid boron phase is present are defined in Table A-14. It is obvious from this table that

the equilibrium calculations did not have to be extended to initial mixtures of B_2H_6-CH_4 that contained more than 0.01 percent B_2H_6 by volume since both solid phases would always be present for the temperatures and pressures of interest. The gas phase is therefore defined and is the same as that presented in Tables A-2 through A-5.

TABLE A-1

CHEMICAL SPECIES CONSIDERED IN THE C-H-B SYSTEM

H_2	(g)	$C_{10}H_1$	(g)	C_5H_4	(g)
H_1	(g)	C_1H_2	(g)	C_6H_4	(g)
C_1	(s)	C_2H_2	(g)	C_3H_5	(g)
C_1	(g)	C_3H_2	(g)	C_4H_5	(g)
C_2	(g)	C_4H_2	(g)	C_2H_6	(g)
C_3	(g)	C_5H_2	(g)	C_3H_6	(g)
C_4	(g)	C_6H_2	(g)	C_4H_6	(g)
C_5	(g)	C_7H_2	(g)	C_5H_6	(g)
C_6	(g)	C_8H_2	(g)	C_6H_6	(g)
C_7	(g)	C_9H_2	(g)	C_3H_8	(g)
C_8	(g)	$C_{10}H_2$	(g)	C_4H_8	(g)
C_9	(g)	C_1H_3	(g)	C_4H_{10}	(g)
C_{10}	(g)	C_2H_3	(g)	B_1	(s)
C_1H_1	(g)	C_3H_3	(g)	B_1	(l)
C_2H_1	(g)	C_4H_3	(g)	B_1	(g)
C_3H_1	(g)	C_5H_3	(g)	B_2	(g)
C_4H_1	(g)	C_6H_3	(g)	B_1H_1	(g)
C_5H_1	(g)	C_1H_4	(g)	B_1H_2	(g)
C_6H_1	(g)	C_2H_4	(g)	B_1H_3	(g)
C_7H_1	(g)	C_3H_4	(g)	B_2H_6	(g)
C_8H_1	(g)	C_4H_4	(g)	$B_{10}H_{14}$	(g)
C_9H_1	(g)				

TABLE A-2

EQUILIBRIUM MOLE FRACTIONS FOR THE B_2H_6-CH_4 SYSTEM AT 0.01 ATM FOR A 0.01% BY VOLUME B_2H_6 INITIAL CONCENTRATION

Chemical Species		Temperature (°K)					
		1200	1250	1300	1350	1400	1450
H_2	(g)	0.667	0.667	0.667	0.667	0.667	0.667
H	(g)	.132-05	.322-05	.737-05	.159-04	.324-04	.630-04
CH_2	(g)	<.100-07	<.100-07	<.100-07	.118-07	.282-07	.636-07
C_2H_2	(g)	.294-06	.707-06	.159-05	.336-05	.672-05	.129-04
CH_3	(g)	.215-07	.352-07	.556-07	.848-07	.126-06	.181-06
CH_4	(g)	.209-03	.144-03	.102-03	.743-04	.552-04	.420-04
C_2H_4	(g)	.365-07	.418-07	.474-07	.533-07	.594-07	.658-07
BH_2	(g)	.134-06	.292-06	.600-06	.117-05	.217-05	.385-05
BH_3	(g)	.662-07	.957-07	.134-06	.184-06	.245-06	.321-06
B	(s)	.665-04	.663-04	.660-04	.653-04	.643-04	.625-04
C	(s)	.333	.333	.333	.333	.333	.333

TABLE A-3

EQUILIBRIUM MOLE FRACTIONS FOR THE B_2H_6-CH_4 SYSTEM AT 0.001 ATM FOR A 0.01% BY VOLUME B_2H_6 INITIAL CONCENTRATION

Chemical Species		Temperature (°K)					
		1200	1250	1300	1350	1400	1450
H_2	(g)	0.667	0.667	0.667	0.667	0.667	0.667
H	(g)	.416-05	.102-04	.233-04	.502-04	.103-03	.199-03
CH_2	(g)	<.100-07	<.100-07	<.100-07	.118-07	.283-07	.636-07
C_2H_2	(g)	.294-06	.708-06	.159-05	.336-05	.673-05	.129-04
CH_3	(g)	<.100-07	.111-07	.176-07	.268-07	.397-07	.572-07
CH_4	(g)	.209-04	.144-04	.102-04	.743-05	.552-05	.419-05
C_2H_4	(g)	<.100-07	<.100-07	<.100-07	<.100-07	<.100-07	<.100-07
BH_2	(g)	.134-06	.292-06	.600-06	.117-05	.217-05	.385-05
BH_3	(g)	.209-07	.303-07	.425-07	.581-07	.776-07	.101-06
B	(s)	.665-04	.664-04	.660-04	.655-04	.644-04	.627-04
C	(s)	.333	.333	.333	.333	.333	.333

TABLE A-4

EQUILIBRIUM MOLE FRACTIONS FOR THE B_2H_6-CH_4 SYSTEM AT 0.000263 ATM
FOR A 0.01% BY VOLUME B_2H_6 INITIAL CONCENTRATION

Chemical Species		Temperature (°K)					
		1200	1250	1300	1350	1400	1450
H_2	(g)	0.667	0.667	0.667	0.667	0.667	0.667
H	(g)	.811-05	.199-04	.455-04	.979-04	.200-03	.388-03
CH_2	(g)	<.100-07	<.100-07	<.100-07	.118-07	.282-07	.636-07
C_2H_2	(g)	.294-06	.708-06	.159-05	.336-05	.673-05	.129-04
CH_3	(g)	<.100-05	<.100-07	<.100-07	.138-07	.204-07	.293-07
CH_4	(g)	.551-05	.379-05	.269-05	.195-05	.145-05	.110-05
C_2H_4	(g)	<.100-07	<.100-07	<.100-07	<.100-07	<.100-07	<.100-07
BH_2	(g)	.134-06	.292-06	.600-06	.117-05	.217-05	.385-05
BH_3	(g)	.107-07	.155-07	.218-07	.298-07	.398-07	.520-07
B	(s)	.665-04	.664-04	.661-04	.655-04	.645-04	.628-04
C	(s)	.333	.333	.333	.333	.333	.333

TABLE A-5

EQUILIBRIUM MOLE FRACTIONS FOR THE B_2H_6-CH_4 SYSTEM AT 0.0001 ATM
FOR A 0.01% BY VOLUME B_2H_6 INITIAL CONCENTRATION

Chemical Species		Temperature (°K)					
		1200	1250	1300	1350	1400	1450
H_2	(g)	0.667	0.667	0.667	0.667	0.667	0.667
H	(g)	.132-04	.322-04	.737-04	.159-03	.324-03	.630-03
CH_2	(g)	<.100-07	<.100-07	<.100-07	.118-07	.282-07	.636-07
C_2H_2	(g)	.294-06	.707-06	.159-05	.336-05	.672-05	.129-04
CH_3	(g)	<.100-07	<.100-07	<.100-07	<.100-07	.126-07	.181-07
CH_4	(g)	.209-05	.144-05	.102-05	.743-06	.552-06	.419-06
C_2H_4	(g)	<.100-07	<.100-07	<.100-07	<.100-07	<.100-07	<.100-07
BH_2	(g)	.134-06	.292-06	.600-06	.117-05	.217-05	.385-05
BH_3	(g)	<.100-07	<.100-07	.134-07	.184-07	.245-07	.320-07
B	(s)	.665-04	.661-04	.661-04	.655-04	.645-04	.628-04
C	(s)	.333	.333	.333	.333	.333	.333

TABLE A-6

EQUILIBRIUM MOLE FRACTIONS FOR THE B_2H_6-CH_4 SYSTEM AT 0.01 ATM
FOR A 0.001% BY VOLUME B_2H_6 INITIAL CONCENTRATION

Chemical Species		Temperature (°K)					
		1200	1250	1300	1350	1400	1450
H_2	(g)	0.667	0.667	0.667	0.667	0.667	0.667
H	(g)	.132-05	.322-05	.737-05	.159-04	.324-04	.630-04
CH_2	(g)	<.100-07	<.100-07	<.100-07	.118-07	.283-07	.636-07
C_2H_2	(g)	.294-06	.707-06	.159-05	.334-05	.673-05	.129-04
CH_3	(g)	.215-07	.352-07	.556-07	.848-07	.126-06	.181-06
CH_4	(g)	.209-03	.144-03	.102-03	.743-04	.552-04	.420-04
C_2H_4	(g)	.365-07	.418-07	.474-07	.533-07	.594-07	.658-07
BH_2	(g)	.134-06	.292-06	.600-06	.117-05	.217-05	.385-05
BH_3	(g)	.662-07	.957-07	.134-06	.184-06	.245-06	.321-06
B	(s)	.647-05	.628-05	.593-05	.532-05	.426-05	.313-05
C	(s)	.333	.333	.333	.333	.333	.333

TABLE A-7

EQUILIBRIUM MOLE FRACTIONS FOR THE B_2H_6-CH_4 SYSTEM AT 0.001 ATM FOR A 0.001% BY VOLUME B_2H_6 INITIAL CONCENTRATION

Chemical Species		Temperature (°K)					
		1200	1250	1300	1350	1400	1450
H_2	(g)	0.667	0.667	0.667	0.667	0.667	0.667
H	(g)	.416-05	.102-04	.233-04	.502-04	.103-03	.199-03
CH_2	(g)	<.100-07	<.100-07	<.100-07	.118-07	.283-07	.636-07
C_2H_2	(g)	.294-06	.708-06	.159-05	.336-05	.673-04	.129-04
CH_3	(g)	<.100-07	.111-07	.176-07	.268-07	.347-07	.572-07
CH_4	(g)	.209-04	.144-04	.102-04	.743-05	.552-05	.419-05
C_2H_4	(g)	<.100-07	<.100-07	<.100-07	<.100-07	<.100-07	<.100-07
BH_2	(g)	.134-06	.292-06	.600-06	.117-05	.217-05	.385-05
BH_3	(g)	.209-07	.303-07	.425-07	.581-07	.776-07	.101-06
B	(s)	.651-05	.635-05	.603-05	.544-05	.442-05	.349-05
C	(s)	.333	.333	.333	.333	.333	.333

TABLE A-8

EQUILIBRIUM MOLE FRACTIONS FOR THE B_2H_6-CH_4 SYSTEM AT 0.000263 ATM
FOR A 0.001% BY VOLUME B_2H_6 INITIAL CONCENTRATION

Chemical Species		Temperature (°K)					
		1200	1250	1300	1350	1400	1450
H_2	(g)	0.667	0.667	0.667	0.667	0.667	0.667
H	(g)	.811-05	.199-04	.455-04	.979-04	.200-03	.388-03
CH_2	(g)	<.100-07	<.100-07	<.100-07	.118-07	.282-07	.636-07
C_2H_2	(g)	.294-06	.708-06	.159-05	.336-05	.673-05	.129-04
CH_3	(g)	<.100-07	<.100-07	<.100-07	.138-07	.204-07	.293-07
CH_4	(g)	.551-05	.379-05	.269-05	.195-05	.145-05	.110-05
C_2H_4	(g)	<.100-07	<.100-07	<.100-07	<.100-07	<.100-07	<.100-07
BH_2	(g)	.134-06	.292-06	.600-06	.117-05	.217-05	.385-05
BH_3	(g)	.107-07	.155-07	.218-07	.298-07	.398-07	.520-07
B	(s)	.652-05	.636-05	.605-05	.547-05	.446-05	.276-05
C	(s)	.333	.333	.333	.333	.333	.333

TABLE A-9

EQUILIBRIUM MOLE FRACTIONS FOR THE B_2H_6-CH_4 SYSTEM AT 0.0001 ATM FOR A 0.001% BY VOLUME B_2H_6 INITIAL CONCENTRATION

Chemical Species		Temperature (°K)					
		1200	1250	1300	1350	1400	1450
H_2	(g)	0.667	0.667	0.667	0.667	0.667	0.667
H	(g)	.132-04	.322-04	.737-04	.159-03	.324-03	.630-03
CH_2	(g)	<.100-07	<.100-07	<.100-07	.118-07	.282-07	.636-07
C_2H_2	(g)	.294-06	.707-06	.159-05	.336-05	.672-05	.129-04
CH_3	(g)	<.100-07	<.100-07	<.100-07	<.100-07	.126-07	.181-07
CH_4	(g)	.209-05	.144-05	.102-05	.743-06	.552-06	.419-06
C_2H_4	(g)	<.100-07	<.100-07	<.100-07	<.100-07	<.100-07	<.100-07
BH_2	(g)	.134-06	.292-06	.600-06	.117-05	.217-05	.385-05
BH_3	(g)	<.100-07	<.100-07	.134-07	.184-07	.245-07	.320-07
B	(s)	.653-05	.637-05	.605-06	.548-05	.447-05	.278-05
C	(s)	.333	.333	.333	.333	.333	.333

TABLE A-10

EQUILIBRIUM MOLE FRACTIONS FOR THE B_2H_6-CH_4 SYSTEM AT 0.01 ATM FOR A 0.0001% BY VOLUME B_2H_6 INITIAL CONCENTRATION

Chemical Species		Temperature (°K)					
		1200	1250	1300	1350	1400	1450
H_2	(g)	0.667	0.667	0.667	0.667	0.667	0.667
H	(g)	.132-05	.322-05	.737-05	.159-04	.324-04	.630-04
CH_2	(g)	<.100-07	<.100-07	<.100-07	.118-07	.282-07	.636-07
C_2H_2	(g)	.294-06	.707-06	.159-05	.336-05	.672-05	.129-04
CH_3	(g)	.215-07	.352-07	.556-07	.848-07	.126-06	.181-06
CH_4	(g)	.209-03	.144-03	.102-03	.743-04	.552-04	.420-04
C_2H_4	(g)	.365-07	.418-07	.474-07	.533-07	.594-07	.658-07
BH_2	(g)	.134-06	.292-06	.545-06	.576-06	.599-06	.616-06
BH_3	(g)	.662-07	.957-07	.122-06	.906-07	.678-07	.512-07
B	(s)	.467-06	.362-06	.000	.000	.000	.000
C	(s)	.333	.333	.333	.333	.333	.333

TABLE A-11

EQUILIBRIUM MOLE FRACTIONS FOR THE B_2H_6-CH_4 SYSTEM AT 0.001 ATM
FOR A 0.0001% BY VOLUME B_2H_6 INITIAL CONCENTRATION

Chemical Species		Temperature (°K)					
		1200	1250	1300	1350	1400	1450
H_2	(g)	0.667	0.667	0.667	0.667	0.667	0.667
H	(g)	.416-05	.102-04	.233-04	.502-04	.103-03	.199-03
CH_2	(g)	<.100-07	<.100-07	<.100-07	.118-07	.283-07	.636-07
C_2H_2	(g)	.294-06	.708-06	.159-05	.336-05	.673-05	.129-04
CH_3	(g)	.100-07	.111-07	.176-07	.268-07	.397-07	.572-07
CH_4	(g)	.209-04	.144-04	.102-04	.743-05	.552-05	.419-05
C_2H_4	(g)	<.100-07	<.100-07	<.100-07	<.100-07	<.100-07	<.100-07
BH_2	(g)	.134-06	.292-06	.600-06	.635-06	.644-06	.650-06
BH_3	(g)	.209-07	.303-07	.425-07	.316-07	.230-07	.171-07
B	(s)	.512-06	.345-06	.245-07	.000	.000	.000
C	(s)	.333	.333	.333	.333	.333	.333

TABLE A-12

EQUILIBRIUM MOLE FRACTIONS FOR THE B_2H_6-CH_4 SYSTEM AT 0.000263 ATM FOR A 0.0001% BY VOLUME B_2H_6 INITIAL CONCENTRATION

Chemical Species		Temperature (°K)					
		1200	1250	1300	1350	1400	1450
H_2	(g)	0.667	0.667	0.667	0.667	0.667	0.667
H	(g)	.811-05	.199-04	.455-04	.979-04	.200-03	.388-03
CH_2	(g)	<.100-07	<.100-07	<.100-07	.118-07	.282-07	.636-07
C_2H_2	(g)	.294-06	.708-06	.159-05	.336-05	.673-05	.129-04
CH_3	(g)	<.100-07	<.100-07	<.100-07	.138-07	.204-07	.293-07
CH_4	(g)	.551-05	.379-05	.269-05	.195-05	.145-05	.110-05
C_2H_4	(g)	<.100-07	<.100-07	<.100-07	<.100-07	<.100-07	<.100-07
BH_2	(g)	.134-06	.292-06	.600-06	.650-06	.655-06	.658-06
BH_3	(g)	.107-07	.155-07	.218-07	.166-07	.120-07	<.100-07
B	(s)	.522-06	.359-06	.463-07	.000	.000	.000
C	(s)	.333	.333	.333	.333	.333	.333

TABLE A-13

EQUILIBRIUM MOLE FRACTIONS FOR THE B_2H_6-CH_4 SYSTEM AT 0.0001 ATM FOR A 0.0001% BY VOLUME B_2H_6 INITIAL CONCENTRATION

Chemical Species		Temperature (°K)					
		1200	1250	1300	1350	1400	1450
H_2	(g)	0.667	0.667	0.667	0.667	0.667	0.667
H	(g)	.132-04	.322-04	.737-04	.159-03	.324-03	.630-03
CH_2	(g)	<.100-07	<.100-07	<.100-07	.118-07	.282-07	.636-04
C_2H_2	(g)	.294-06	.707-06	.159-05	.336-05	.672-05	.129-04
CH_3	(g)	<.100-07	<.100-07	<.100-07	<.100-07	.126-07	.181-07
CH_4	(g)	.209-05	.144-05	.102-05	.743-06	.552-06	.419-06
C_2H_4	(g)	<.100-07	<.100-07	<.100-07	<.100-07	<.100-07	<.100-07
BH_2	(g)	.134-06	.292-06	.600-06	.656-06	.659-06	.667-06
BH_3	(g)	<.100-07	<.100-07	.134-07	.103-07	<.100-07	<.100-07
B	(s)	.527-06	.365-06	.554-07	.000	.000	.000
C	(s)	.333	.333	.333	.333	.333	.333

TABLE A-10

EQUILIBRIUM MOLE FRACTIONS FOR THE B_2H_6-CH_4 SYSTEM AT 0.01 ATM FOR A 0.0001% BY VOLUME B_2H_6 INITIAL CONCENTRATION

Chemical Species		Temperature (°K)					
		1200	1250	1300	1350	1400	1450
H_2	(g)	0.667	0.667	0.667	0.667	0.667	0.667
H	(g)	.132-05	.322-05	.737-05	.159-04	.324-04	.630-04
CH_2	(g)	<.100-07	<.100-07	<.100-07	.118-07	.282-07	.636-07
C_2H_2	(g)	.294-06	.707-06	.159-05	.336-05	.672-05	.129-04
CH_3	(g)	.215-07	.352-07	.556-07	.848-07	.126-06	.181-06
CH_4	(g)	.209-03	.144-03	.102-03	.743-04	.552-04	.420-04
C_2H_4	(g)	.365-07	.418-07	.474-07	.533-07	.594-07	.658-07
BH_2	(g)	.134-06	.292-06	.545-06	.576-06	.599-06	.616-06
BH_3	(g)	.662-07	.957-07	.122-06	.906-07	.678-07	.512-07
B	(s)	.467-06	.362-06	.000	.000	.000	.000
C	(s)	.333	.333	.333	.333	.333	.333

TABLE A-11

EQUILIBRIUM MOLE FRACTIONS FOR THE B_2H_6-CH_4 SYSTEM AT 0.001 ATM FOR A 0.0001% BY VOLUME B_2H_6 INITIAL CONCENTRATION

Chemical Species		Temperature (°K)					
		1200	1250	1300	1350	1400	1450
H_2	(g)	0.667	0.667	0.667	0.667	0.667	0.667
H	(g)	.416-05	.102-04	.233-04	.502-04	.103-03	.199-03
CH_2	(g)	<.100-07	<.100-07	<.100-07	.118-07	.283-07	.636-07
C_2H_2	(g)	.294-06	.708-06	.159-05	.336-05	.673-05	.129-04
CH_3	(g)	.100-07	.111-07	.176-07	.268-07	.397-07	.572-07
CH_4	(g)	.209-04	.144-04	.102-04	.743-05	.552-05	.419-05
C_2H_4	(g)	<.100-07	<.100-07	<.100-07	<.100-07	<.100-07	<.100-07
BH_2	(g)	.134-06	.292-06	.600-06	.635-06	.644-06	.650-06
BH_3	(g)	.209-07	.303-07	.425-07	.316-07	.230-07	.171-07
B	(s)	.512-06	.345-06	.245-07	.000	.000	.000
C	(s)	.333	.333	.333	.333	.333	.333

TABLE A-12

EQUILIBRIUM MOLE FRACTIONS FOR THE B_2H_6-CH_4 SYSTEM AT 0.000263 ATM FOR A 0.0001% BY VOLUME B_2H_6 INITIAL CONCENTRATION

Chemical Species		Temperature (°K)					
		1200	1250	1300	1350	1400	1450
H_2	(g)	0.667	0.667	0.667	0.667	0.667	0.667
H	(g)	.811-05	.199-04	.455-04	.979-04	.200-03	.388-03
CH_2	(g)	<.100-07	<.100-07	<.100-07	.118-07	.282-07	.636-07
C_2H_2	(g)	.294-06	.708-06	.159-05	.336-05	.673-05	.129-04
CH_3	(g)	<.100-07	<.100-07	<.100-07	.138-07	.204-07	.293-07
CH_4	(g)	.551-05	.379-05	.269-05	.195-05	.145-05	.110-05
C_2H_4	(g)	<.100-07	<.100-07	<.100-07	<.100-07	<.100-07	<.100-07
BH_2	(g)	.134-06	.292-06	.600-06	.650-06	.655-06	.658-06
BH_3	(g)	.107-07	.155-07	.218-07	.166-07	.120-07	<.100-07
B	(s)	.522-06	.359-06	.463-07	.000	.000	.000
C	(s)	.333	.333	.333	.333	.333	.333

TABLE A-13

EQUILIBRIUM MOLE FRACTIONS FOR THE B_2H_6-CH_4 SYSTEM AT 0.0001 ATM FOR A 0.0001% BY VOLUME B_2H_6 INITIAL CONCENTRATION

Chemical Species		Temperature (°K)					
		1200	1250	1300	1350	1400	1450
H_2	(g)	0.667	0.667	0.667	0.667	0.667	0.667
H	(g)	.132-04	.322-04	.737-04	.159-03	.324-03	.630-03
CH_2	(g)	<.100-07	<.100-07	<.100-07	.118-07	.282-07	.636-04
C_2H_2	(g)	.294-06	.707-06	.159-05	.336-05	.672-05	.129-04
CH_3	(g)	<.100-07	<.100-07	<.100-07	<.100-07	.126-07	.181-07
CH_4	(g)	.209-05	.144-05	.102-05	.743-06	.552-06	.419-06
C_2H_4	(g)	<.100-07	<.100-07	<.100-07	<.100-07	<.100-07	<.100-07
BH_2	(g)	.134-06	.292-06	.600-06	.656-06	.659-06	.667-06
BH_3	(g)	<.100-07	<.100-07	.134-07	.103-07	<.100-07	<.100-07
B	(s)	.527-06	.365-06	.554-07	.000	.000	.000
C	(s)	.333	.333	.333	.333	.333	.333

TABLE A-14

SUMMARY OF CONDITIONS FOR WHICH THE SOLID BORON PHASE IS PRESENT

Percent B_2H_6 in Original B_2H_6-CH Reaction Mixture	Pressure (atm)	Temperature Below Which Solid Boron Phase is Present (°K)
0.01	0.01	1600
.01	.001	1600
.01	.000263	1600
.01	.0001	1600
.001	.01	1450
.001	.001	1450
.001	.000263	1500
.001	.0001	1500
.0001	.01	1250
.0001	.001	1300
.0001	.000263	1300
.0001	.0001	1300

APPENDIX B

OPERATION OF HYDROGEN CLEANING FURNACE

Start-Up Procedure

1. Shut all valves, EXCEPT valves 4A, B.
2. Put sample in furnace and tighten fittings.
3. Attach hose to vacuum pump and turn on pump.
4. Slightly open valve 9 until system is evacuated in a few hours.
5. Open H_2 tank; set regulator at 100 PSIG; set safe auto-fill switch to "fill"; open valves 1A, 2A.
6. Shut off vacuum pump and pressurize system with H_2 to atmospheric pressure with valve 3A and then close valve 3A.
7. Open valve 5A by 1/2 turn; close valve 9; slowly open valve 3A by 5 turns.
8. Slowly pressurize system to 600 PSIG at 50 PSIG intervals and set downstream pressure regulators to 10 PSIG.
9. Set timer; plug Helium solenoid valve and controller into timed outlet; plug in furnace variac (set at 75); set controller to required temperature and turn on (controller will remain off until turned on by timer); set safe auto-fill switch to "auto safe"; shut safety valve 2A.
10. Turn on cooling water; shut valve 1A; set H_2 regulator to approximately 150 PSIG above previous setting; shut off H_2 tank.

Run Procedure

1. If system is at temperature, turn on H_2 tank; open safety valve 2A and wait 1/2 hour.
2. Light fisher burner and turn on valve 6A.
3. Set flow with valve 7; close bypass valves 4A, B. (Maintain flow at less than 10 cc/min.)

Shut down Procedure

1. Open bypass valves 4A, B; close safety valve 2A; shut off contoller; unplug variac; put helium purge solenoid on timer (set to turn off 5-6 hours after controller is shut off); slowly vent system with valve 7.

2. After venting, close all valves, EXCEPT bypass valves 4A, B; turn off H_2 tank; shut off fisher burner.
3. Start vacuum pump and slightly open valve 9. (Cool down and evacuate system overnight.)

Removal of Sample from Furnace

1. Unplug helium purge solenoid valve; open valve 9 all the way.
2. Open helium tank (regulator set at 100 PSIG); open valves 1B, 2B; set safe auto-fill switch to "fill"; turn off vacuum pump.
3. Slowly fill system with helium using valve 3B; at atmospheric pressure close valve 3B; close valve 9; remove hose from vacuum pump; slowly open valve 9; close valves 1B, 2B.
4. Unload furnace.
5. Exhaust H_2 from H_2 regulator into hood. (Make sure valves 5A, B, 9, 4B are closed; open helium and H_2 tanks; open valves 4A, 1A, B, 2A, B; connect metal hose to line going to hood; open valve 3B by 15 turns; open valve 3A by 2 turns; set H_2 regulator at 100 PSIG; close valves 3A, B, 1A, B, 2A, B.)

APPENDIX C

LOW PRESSURE EPITAXIAL DIAMOND GROWTH

An epitaxial diamond growth run was also made in addition to the doping runs discussed previously. This experiment was a low pressure deposition using methane in an attempt to improve the diamond deposition rate by precluding the formation of graphite.

One of the terminating steps in the diamond growth process is the formation of graphite on the diamond surface during deposition. When graphite covers the diamond surfaces, no further growth occurs since graphite is the stable carbon phase at the temperatures and pressures that have been used for low pressure epitaxial diamond growth. If graphite formation during the diamond growth process can be precluded, substantial increases in growth may be obtained. The deposition process would be greatly simplified since a run would not have to be terminated for hydrogen removal of graphite and could therefore continue until the required weight gain had been obtained. Lowering the pressure at which the deposition is performed, should theoretically tend to eliminate or reduce graphite formation during the diamond growth process. This effect was observed during the diamond deposition experiments of H. Will.[2] As the system pressure was

reduced below 1 Torr, the amount of graphite deposited during deposition decreased. The lowest pressure used by H. Will[2] was 0.15 Torr. In an attempt to eliminate graphite formation completely during the epitaxial growth of diamond, a deposition was made on 0.2664g of 0-1 micron natural diamond powder at a pressure of approximately 0.01 Torr. The pressure just upstream of the quartz vacuum chamber was 0.015 Torr and the pressure downstream of the chamber was less than 0.002 Torr. The pressure at the diamond sample was therefore somewhat less than 0.01 Torr. The deposition proceeded for 23 hours at 1050° C. There was a noticeable decrease in the amount of graphite deposited on the diamond and on the quartz portions of the deposition chamber during this run compared with the doping runs and the earlier deposition experiments of H. Will.[2] The diamond was dark gray instead of the usual black color after this deposition. The gross weight increase of the diamond plus the deposition sample test tube was 0.0090 g. The sample was hydrogen cleaned to remove graphite. A weight loss of 0.0048 g occurred during the hydrogen cleaning. Based on the work of W. Stanko,[22,23] a weight loss of approximately 0.3 percent of the diamond sample (i.e., 0.8 mg) can be expected during hydrogen cleaning. Therefore, approximately 56 percent of the gross weight increase during this deposition was new diamond. This is considerably larger than the usual 25 to 30 percent of the gross weight gain that is new diamond.

APPENDIX D

CALCULATION OF WAVELENGTH ASSOCIATED WITH A 100 KV ELECTRON

The deBroglie wavelength associated with an electron which has been accelerated through a 100 KV potential field can be calculated by equating the energy gained by the electron, its kinetic energy, to the work done on the electron.

Equating the force on the electron to its time rate of change of momentum gives

$$F = \frac{d(mv)}{dt} = m \frac{dv}{dt} + v \frac{dm}{dt} \qquad \text{(D-1)}$$

The work done on the electron over an infinitesimal distance dx is

$$Fdx = m\ dv \frac{dx}{dt} + v\ dm \frac{dx}{dt} \qquad \text{(D-2)}$$

or

$$Fdx = mv\ dv + v^2 dm \qquad \text{(D-3)}$$

For the non-relativistic case, $dm = 0$ and integration of equation (D-3) leads to a kinetic energy of $1/2\ mv^2$. However, the assumption that dm equals zero cannot be made for a 100 KV electron, since its velocity is a considerable fraction of the velocity of light. The electron mass and velocity in equation (D-3) are related by the following equation:

$$m = \frac{m_o}{\sqrt{1 - v^2/c^2}} \qquad \text{(D-4)}$$

where: m_o = electron rest mass ($9.109X10^{-28}$ g)

C = velocity of light ($2.997925X10^{10}$ cm/sec)

Substitution of equation (D-4) into equation (D-3) gives

$$Fdx = \frac{m_o}{\sqrt{1 - v^2/C^2}} vdv + \left(C^2 - C^2 \frac{m_o^2}{m^2}\right) dm \qquad (D-5)$$

Integration of equation (D-5) results in

$$Fx = mC^2 + K \qquad (D-6)$$

The boundary condition that when $x = 0$, $m = m_o$ gives a value of $-m_oC^2$ for the integration constant in equation (D-6). The kinetic energy of the electron is therefore:

$$K.E. = mC^2 - m_oC^2 \qquad (D-7)$$

The mass and velocity of a 100 KV electron can be readily calculated from equation (D-7).

$$100{,}000 \text{ eV}\left(1.6021X10^{-12} \frac{\text{ergs}}{\text{eV}}\right) = \left(2.997925X10^{10} \frac{\text{cm}}{\text{sec}}\right)^2 (m - m_o)$$

$$m = 10.892X10^{-28} \text{ g}$$

The electron velocity is then found from equation (D-4).

$$v = 1.644X10^{10} \frac{\text{cm}}{\text{sec}}$$

The deBroglie wavelength of 100 KV electron which was used in the calculation of lattice constants from the doped and undoped diamond electron diffraction patterns can then be calculated from the following equation

$$\lambda_D = \frac{h}{mv} = 0.03700 \text{ Å}$$

where: λ_D = deBroglie wavelength

h = Planck's constant (6.62554×10^{-27} erg-sec)

REFERENCES

1. W. G. Eversole: Canadian Patent No. 628567, October 3, 1961, see also U.S. Patent No. 3030187 and 3030188, April 17, 1962.

2. J. C. Angus, H. Will, and W. Stanko: J. Appl. Phys. 39, 2915 (1968).

3. D. V. Fedoseev and D. V. Spitzin: Doklady Akad. Nauk SSSR 181, 1094 (1968).

4. Berman: Physical Properties of Diamonds. (Oxford University Press, London, England, 1956.)

5. Robertson, Fox, and Martin: Trans. Roy Soc. (London) A263, 463 (1934).

6. W. Kaiser and W. L. Bond, Phys. Rev. 115, 857 (1959).

7. J. F. H. Custers: Physica 10, 489, (1952).

8. I. G. Austin and R. Wolfe: Proc. Phys. Soc. (London) B69, 329 (1956).

9. J. J. Brophy: Phys. Rev. 99, 1336 (1955).

10. P. T. Wedepohl: Proc. Phys. Soc. (London) B70, 177 (1957).

11. R. H. Wentorf, Jr. and H. P. Bovenkerk: J. Chem. Phys., 36, 1987 (1962).

12. C. M. Huggins and P. Cannon: Nature, 829, June 2, 1962.

13. R. H. Wentorf, Jr. and K. A. Darrow: Phys. Rev., 137, A1614 (1965).

14. V. S. Vavilov, M. I. Guseva, E. A. Konotova, V. V. Krasnopevtsev, V. F. Sergienko and V. V. Tutov: Soviet Physics - Solid State, 8, 1560 (1966).

15. R. O. Carlson: Trans. AIME, 245, 483 (1969).

16. E. C. Lightowlers and A. T. Collins: Phys. Rev. 151, 685 (1966).

17. A. T. Collins and A. W. S. Williams: Diamond Research 1971 p. 23.

18. Sanford Gordon, Frank J. Zeleznik, and Vearl N. Huff: A General Method for Automatic Computation of Equilibrium Compositions and Theoretical Rocket Performance of Propellants. NASA TN D-132, October, 1959.

19. Frank J. Zeleznik and Sanford Gordon: An Analytical Investigation of Three General Methods of Calculating Chemical-Equilibrium Compositions. NASA TN D-473, September 1960.

20. Frank J. Zeleznik and Sanford Gordon: A General IBM 704 or 7090 Computer Program for Computation of General Chemical Equilibrium Compositions, Rocket Performance, and Chapman-Jouget Detonations. NASA TN D-1454, October 1962.

21. Sanford Gordon and Frank Zeleznik: A General IBM 704 or 7090 Computer Program for Computation of Chemical Equilibrium Compositions, Rocket Performance, and Chapman-Jouget Detonations - Supplement I. NASA TN D-1737, October 1963.

22. W. Stanko, M. S. Thesis, Case Institute of Technology, June 1966.

23. W. Stanko and J. Angus: Journal of Chemical and Engineering Data, 14, 223 (1969).

24. Vanitallie Corporation, 70 W. 40th St., New York, N.Y.

25. Crobaugh Laboratories, 3800 Perkins Avenue, Cleveland, O.

26. W. C. Nixon: Comtemp. Phys., vol. 10, no. 1, p. 71 (1969).

27. Inorganic Index to the Powder Diffraction File. (American Society for Testing Materials, 1969.)

28. M. Ponte: Ann. de Phys., 13, 395 (1930).

29. B. D. Callity: Elements of X-ray Diffraction. (Addison-Wesley Publisher, 1956) p. 487.

30. L. de Broglie: Ann. Phys., 3, 22 (1925).

A. El. Goresy and G. Donnay: Science, vol. 161, June 28, 1968.

32. A. Greenville Whittaker and P. L. Kintner: Science, vol. 165, August 8, 1969.

33. Ledoux and Company, 359 Alfred Avenue, Teaneck, New Jersey.

34. R. Mykolajewycz, J. Hainajs and A. Smakula: J. Appl. Phys., 35, 1773 (1964).

35. Handbook of Chemistry and Physics, 40th Edition, (The Chemical Rubber Co., 1968)

36. R. Heikes and R. Ure, Jr.: Thermoelectricity: Science and Engineering (Interscience Publishers, 1961) p. 312.

37. Ibid, p. 313.

38 Ibid, p. 314.

39. Carborundum Corporation, Niagra Falls, New York.

40. V. S. Neshpor and V. P. Nitikin: Porosh Met 8, 62 (1968).

41. R. Heikes and R. Ure, Jr.: Op. Cit., p. 344.

42. K. Siegbahn, et al: ESCA, Atomic, Molecular and Solid State Structure Studied by Means of Electron Spectroscopy, Almquist and Wicksells Boktryckeri AB, Uppsala 1967.

43. J. C. Helmer and N. H. Weichert: Enhancement of Sensitivity in ESCA Spectrometers. Appl. Phys. Letters 13, 266 (1968).

44. J. C. Helmer and N. H. Weichert: Induced Electron Emission Spectroscopy. Record of 10th Symposium on Electron, Ion and Laser Beam Technology. (L. Marton, ed.) San Francisco Press.

45. Varian and Associates, 611 Hansen Way, Palo Alto, California.

46. Personal Communication with Dr. J. C. Helmer of Varian and Associates.

47. J. W. Mellor: A Comprehensive Treatise on Inorganic and Theoretical Chemistry. (Longmans, Green and Company, 1946), vol. V, p. 49.

48. Terence L. Squires: An Introduction to Electron Spin Resonance. (Academic Press) 1964.

49. M. J. A. Smith and B. R. Angel: Phil Mag. (6B) 15, 783 (1967).

50. M. D. Bell and W. J. Leivo: J. Appl. Phys., vol. 38, no. 1 (1967).

51. Personal Communication with Dr. Thomas J. Clark.

52. C. D. Clark, R. W. Ditchburn, and H. B. Dyer: Proc. Roy. Soc. A234, 363 (1956).

53. Dow Chemical Company. JANAF Thermochemical Tables.

54. R. E. Duff and S. H. Bauer: The Equilibrium Composition of the C/H System at Elevated Temperatures (Los Alamos Scientific Laboratory, N. Mexico) rep. LA-2556, June 196.